COLLECTED PAPERS on Off-shell Science

Vol. 40

January 2025 – December 2025

Motoichi OHTSU[1,2]

1 Chief Director
(General Incorporated Association)
Research Origin for Dressed Photon
2 Prof. Emeritus, The University of Tokyo
and Tokyo Institute of Technology

MEMBERS

[I] RESEARCH ORIGIN FOR DRESSED PHOTON (RODreP) *

Chief Director

Motoichi OHTSU** (Dr. Eng.)

Directors

Masayuki NAYA (Dr. Eng.)
Hirofumi SAKUMA (Ph. D.)

Auditor

Satoshi SUGIURA

Advisors

Izumi OJIMA (Dr. Sci.)
Junji MIYAHARA (Dr. Eng.)
Masuo FUKUI (Dr. Eng.)
Naoya TATE (Dr. Eng.)

Visiting Scientists

Hayato SAIGO (Dr. Sci.) (Nagahama Inst. Bio-Sci. and Tech.)
Itsuki BANNO (Univ. Yamanashi)
Suguru SANGU (Dr. Eng.) (Ricoh Co. Ltd.)
Etsuo SEGAWA (Dr. Eng.) (Yokohama National Univ.)
Seiken SAITO (Dr. Sci.) (Kogakuin Univ.)
Kazuya OKAMURA (Dr. Sci.) (Chubu Univ.)
(also, Senior Researcher, RODreP)

Secretary

Mari KAZAMA

(*)（General Incorporated Association）Research Origin for Dressed Photon
(RODreP)
Phone: 090-1603-0562
E-mail: ohtsu@rodrep.or.jp
URL: https://rodrep.or.jp/
(Labs.)
c/o Bdg.1, Yokohama Research Center, NICHIA Corp.
3-13-19 Moriya-cho, Kanagawa-ku, Yokohama-shi, Kanagawa 221-0022, Japan
(Executive office)
Adthree Publishing Co., Ltd.
4-27-37 Higashi-Nakano, Nakano-ku, Tokyo164-0003, Japan
The 3rd Floor, Sunrise Bldg. II, 5-20 Shin-Ogawa-cho, Shinjuku-ku, Tokyo 162-0814, Japan

（一般社団法人）ドレスト光子研究起点
Phone: 090-1603-0562
E-mail: ohtsu@rodrep.or.jp
URL: https://rodrep.or.jp/
（研究所）
〒221-0022　神奈川県横浜市神奈川区守屋町 3－13－19
日亜化学工業（株）　横浜研究所　1 号館 1 階
（事務局）
〒162-0814　東京都新宿区新小川町 5-20　サンライズビルⅡ ３F
株式会社アドスリー

(**) Professor Emeritus, The University of Tokyo and Tokyo Institute of Technology
東京大学名誉教授、東京工業大学名誉教授

VIDEO LECTURES

[1] 大津元一、「ドレスト光子フォノンの移動速度」
(2025 年 9 月)

その１　https://www.youtube.com/watch?v=SRwIQeOImjg
その２　https://www.youtube.com/watch?v=gj_fQElRncM

[2] 大津元一、「ドレスト光子フォノンの明歩道と暗歩道」
(2025 年 3 月)

その１　https://www.youtube.com/watch?v=SRwIQeOImjg
その２　https://www.youtube.com/watch?v=gj_fQElRncM

LIST OF PAPERS

[(pp. XX-XX); pages in this issue of the COLLECTED PAPERS**]**

[I] ORIGINAL PAPERS

[1] H. Du, T. Kadowaki, N. Tate, Y. Oki, M. Ohtsu, and K. Hayashi, "Wavelength- and polarization-dependent enhancement of the magneto-optical effect with Al-doped 4H-SiC," *Opt. Lett*., **50** (2025) pp.6237-6240.

[II] PRESENTATIONS IN INTERNATIONAL CONFERENCES

[1] M. Ohtsu, "Embarking on Off-shell Science Guided by Dressed Photons," Conference Handbook of the 15th Asia-Pacific Conference on Near-Field Optics (APNFO15), 18-21 August, 2025, Bali, Indonesia, paper number Plenary-05, p.24 **[Plenary lecture]**

[III] REVIEW PAPERS

N.A.

[IV] PREPRINT DEPOSITORIES

[IV-1] OFF-SHELL ARCHIVE

[Original papers]

[1] M. Ohtsu, E. Segawa, K. Yuki, and S. Saito, "Non-adiabatic relaxation process that lies behind the adiabatic relaxation of dressed-photon–phonon transfer," *Off-shell Archive* (December, 2025) Offshell: 2512O.001.v1.
DOI : 10.14939/2512O.001.v1
https://rodrep.or.jp/en/off-shell/original_2512O.001.v1.html

[2] M. Ohtsu, E. Segawa, K. Yuki, S. Saito, and S. Sangu, "Speed of dressed-photon–phonon transfer among a small number of particles," *Off-shell Archive* (September, 2025) Offshell: 2509O.001.v1. **DOI** : 10.14939/2509O.001.v1
https://rodrep.or.jp/en/off-shell/original_2509O.001.v1.html

[3] M. Ohtsu, E. Segawa, K. Yuki, and S. Saito, "Bright and dark walks for dressed-photon-phonon transfer," *Off-shell Archive* (January, 2025)

Offshell: 2501O.001.v1.
DOI 10.14939/2501O.001.v1,
https://rodrep.or.jp/en/off-shell/original_2501O.001.v1.html

[Review papers]

[1] M. Ohtsu, "Quantum walk and random walk behaviors of dressed-photon–phonon transfers," *Off-shell Archive* (October, 2025) Offshell: 2510O.001.v1.
DOI 10.14939/2510R.001.v1,
https://rodrep.or.jp/en/off-shell/review_2510R.001.v1.html

[V] PUBLISHED BOOKS

[1] M. Ohtsu, *Off-Shell Science Guided by Dressed Photons, Part 1* (Design Egg, Tokyo, Japan) 153 pages, ISBN978-4-8150-4995-9.

[2] M. Ohtsu, *Off-Shell Science Guided by Dressed Photons, Part 2* (Design Egg, Tokyo, Japan) 154 pages, ISBN978-4-8150-4996-6.

[3] M. Ohtsu, *Mathematical Science of Dressed Photons* (Design Egg, Tokyo, Japan) 153 pages, ISBN978-4-8150-4934-8.
【大津元一、「ドレスト光子の数理 - オフシェル科学への展開 -」 （デザインエッグ社、東京） 153 ページ、ISBN978-4-8150-4934-8】

[4] M. Ohtsu, and H. Sakuma, Dressed Photons to Revolutionize Modern Physics - Exploring Longitudinal Electromagnetic Waves and Off-shell Quantum Fields - (Springer Nature, Switzerland, 2025) 118 pages.

[VI] PRESENTATIONS IN DOMESTIC CONFERENCES

[1] H. Du, T. Kadowaki, N. Tate, Y. Oki, K. Hayashi, and M. Ohtsu," Rewritable polarization rotation effect based on the photoelectrically-induced dopant drift phenomenon" Abstracts of Optics & Photonics Japan 2025, December 9 – 11, 2025 (Tokushima Pref. Culture Hall), paper number 11aC2.
【杜昊澤、門脇拓也、竪直也、興雄司、林健司、大津元一、「光電誘起ドーパントドリフト現象に基づくリライタブル偏光回転効果」、Optics & Photonics Japan 2025予稿集（2025年12月9−11日：徳島あわぎんホール）講演番号11aC2】

[2] I. Banno, "What Causal Laws does the Internal Electromagnetic Field Follow?" Abstracts of the 86th Jpn. Soc. Appl. Phys. Autumn Meeting, September 7-10, 2025 (Meijo University and Online meeting), paper number 10p-N204-1.

【坂野斎、「内在電磁場はどのような因果律に従うのか？」、第86回応用物理学秋季学術講演会予稿集（2025年9月7−10日：名城大学天白キャンパス＆オンライン）講演番号10p-N204-1】

[3] I. Banno, “Nonlinear and Non-adiabatic Effect of the Internal Vector Potential and Photon-Breeding Devices,” Abstracts of the 86th Jpn. Soc. Appl. Phys. Autumn Meeting, September 7-10, 2025 (Meijo University and Online meeting), paper number 10p-N204-2.
【坂野斎、「内在ベクトルポテンシャルの非線形非断熱効果とフォトンブリーディングデバイス」、第86回応用物理学秋季学術講演会予稿集（2025年9月7−10日：名城大学天白キャンパス＆オンライン）講演番号10p-N204-2】

[4] H. Sakuma, “Overview on the newly developed theory of dressed photon,” Abstracts of the 86th Jpn. Soc. Appl. Phys. Autumn Meeting, September 7-10, 2025 (Meijo University and Online meeting), paper number 10p-N204-3.
【佐久間弘文、「ここ数年で構築されたドレスト光子新理論の振り返り」、第86回応用物理学秋季学術講演会予稿集（2025年9月7−10日：名城大学天白キャンパス＆オンライン）講演番号10p-N204-3】

[5] H. Saigo, “Off-shell Sciences as Categorification of On-shell Sciences,” Abstracts of the 86th Jpn. Soc. Appl. Phys. Autumn Meeting, September 7-10, 2025 (Meijo University and Online meeting), paper number 10p-N204-4.
【西郷甲矢人、「オンシェル科学の圏化としてのオフシェル科学」、第86回応用物理学秋季学術講演会予稿集（2025年9月7−10日：名城大学天白キャンパス＆オンライン）講演番号10p-N204-4】

[6] K. Okamura, “Bohr’s complementarity and quantum measurement theory,” Abstracts of the 86th Jpn. Soc. Appl. Phys. Autumn Meeting, September 7-10, 2025 (Meijo University and Online meeting), paper number 10p-N204-5.
【岡村和弥、「ボーアの相補性と量子測定理論」、第86回応用物理学秋季学術講演会予稿集（2025年9月7−10日：名城大学天白キャンパス＆オンライン）講演番号10p-N204-5】

[7] S. Saito, “The wave function of a quantum walk on the regular tree,” Abstracts of the 86th Jpn. Soc. Appl. Phys. Autumn Meeting, September 7-10, 2025 (Meijo University and Online meeting), paper number 10p-N204-6.
【齋藤 正顕、「正則木上の量子ウォークの波動関数」、第86回応用物理学秋季学術講演会予稿集（2025年9月7−10日：名城大学天白キャンパス＆オンライン）講演番号10p-N204-6】

[8] T. Kakegawa and E. Segawa, “Quantum walks and edge coloring of graphs by rotation,” Abstracts of the 86th Jpn. Soc. Appl. Phys. Autumn Meeting, September 7-10, 2025 (Meijo University and Online meeting), paper number 10p-N204-7.

【掛川拓巳、瀬川悦生、「量子ウォークとローテーションによるグラフの辺彩色」、第86回応用物理学秋季学術講演会予稿集（2025年9月7−10日：名城大学天白キャンパス＆オンライン）講演番号10p-N204-7】

[9] Y. Iida and E. Segawa, “Scattering of Quantum Walk in Blowup Graph,” Abstracts of the 86th Jpn. Soc. Appl. Phys. Autumn Meeting, September 7-10, 2025 (Meijo University and Online meeting), paper number 10p-N204-8.
【飯田佳之、瀬川悦生、「膨張グラフ上の量子ウォークと散乱」、第86回応用物理学秋季学術講演会予稿集（2025年9月7−10日：名城大学天白キャンパス＆オンライン）講演番号10p-N204-8】

[10] M. Ohtsu, E. Segawa, K.Yuki, S. Saito, and S. Sangu, “Correlation among channels of dressed-photon-phonon transfer,” Abstracts of the 86th Jpn. Soc. Appl. Phys. Autumn Meeting, September 7-10, 2025 (Meijo University and Online meeting), paper number 10p-N204-9.
【大津元一、瀬川悦生、結城謙太、齋藤正顕、三宮俊、「ドレスト光子フォノンの移動チャンネル間の相関」、第86回応用物理学秋季学術講演会予稿集（2025年9月7−10日：名城大学天白キャンパス＆オンライン）講演番号10p-N204-9】

[11] S. Sangu, “Visualization of Spatiotemporal Dynamics of Highly-Excited States of Dressed Photons,” Abstracts of the 86th Jpn. Soc. Appl. Phys. Autumn Meeting, September 7-10, 2025 (Meijo University and Online meeting), paper number 10p-N204-10.
【三宮俊、「ドレスト光子高励起状態の時空間ダイナミクスの可視化」、第86回応用物理学秋季学術講演会予稿集（2025年9月7−10日：名城大学天白キャンパス＆オンライン）講演番号10p-N204-10】

[12] I. Banno, “Current-induced Non-equlibrium Structure V,” Abstracts of the 72nd Jpn. Soc. Appl. Phys. Spring Meeting, March 14-17, 2025
(Tokyo University of Science and Online meeting), paper number 16p-K508-1.
【坂野 斎、「流れが誘導する平衡から遠い量子構造 V」、第72回応用物理学春季学術講演会予稿集（2025年3月14-17日：東京理科大学野田キャンパス＆オンライン）講演番号16p-K508-1】

[13] H. Sakuma, “On the dressed photon field connecting micro-macro duality,” Abstracts of the 72nd Jpn. Soc. Appl. Phys. Spring Meeting, March 14-17, 2025
(Tokyo University of Science and Online meeting), paper number 16p-K508-2.
【佐久間 弘文、「ミクロ・マクロ双対理論と一般相対論を繋げるドレスト光子場について」、第72回応用物理学春季学術講演会予稿集（2025年3月14-17日：東京理科大学野田キャンパス＆オンライン）講演番号16p-K508-2】

[14] H. Saigo, “Process, Causality and Noncommutative Probability: From Categorical

Structures to Off-shell Sciences," Abstracts of the 72nd Jpn. Soc. Appl. Phys. Spring Meeting, March 14-17, 2025
(Tokyo University of Science and Online meeting), paper number 16p-K508-3.
【西郷 甲矢人、「過程・因果・非可換確率：圏構造からオフシェル科学へ」、第72回応用物理学春季学術講演会予稿集（2025年3月14-17日：東京理科大学野田キャンパス＆オンライン）講演番号16p-K508-3】

[15] K. Okamura, "On Bohr's complementarity and quantum instrument," Abstracts of the 72nd Jpn. Soc. Appl. Phys. Spring Meeting, March 14-17, 2025
(Tokyo University of Science and Online meeting), paper number 16p-K508-4.
【岡村 和弥、「ボーアの相補性と量子インストルメントについて」、第72回応用物理学春季学術講演会予稿集（2025年3月14-17日：東京理科大学野田キャンパス＆オンライン）講演番号16p-K508-4】

[16] M. Ohtsu, E. Segawa, K. Yuki, and S. Saito, "Bright and dark walks for dressed-photon-phonon transfer," Abstracts of the 72nd Jpn. Soc. Appl. Phys. Spring Meeting, March 14-17, 2025
(Tokyo University of Science and Online meeting), paper number 16p-K508-5.
【大津 元一, 瀬川悦生, 結城謙太, 齋藤正顕、「ドレスト光子フォノンの移動の明歩道と暗歩道」、第72回応用物理学春季学術講演会予稿集（2025年3月14-17日：東京理科大学野田キャンパス＆オンライン）講演番号16p-K508-5】

[17] S. Sangu, "Retention and Dissipation Control of Dressed Photons by Energy Detuning," Abstracts of the 72nd Jpn. Soc. Appl. Phys. Spring Meeting, March 14-17, 2025
(Tokyo University of Science and Online meeting), paper number 16p-K508-6.
【三宮 俊、「エネルギー離調によるドレスト光子の停留および散逸制御」、第72回応用物理学春季学術講演会予稿集（2025年3月14-17日：東京理科大学野田キャンパス＆オンライン）講演番号16p-K508-6】

[18] M. Ohtsu, "Autonomous transfer of dressed photons and its principle," Abstracts of the 45th annual meeting of the Laser Society of Japan, January 21-24, 2025 (The International Conference Center Hiroshima, Hiroshima)
paper number S03-23p-Ⅳ-04.
【大津元一、「ドレスト光子の自律的移動とその原理」、レーザー学会学術講演会第45回年次大会予稿集（2025年1月21日−24日）、(広島国際会議場、広島) 講演番号S03-23p-Ⅳ-04】
[Invited presentation]

[19] E. Segawa and M. Ohtsu, "Relation between autonomous paths of dressed photon and geometric structures of networks induced dressed quantum walk simulation," Abstracts of the 45th annual meeting of the Laser Society of Japan, January 21-24, 2025 (The International Conference Center Hiroshima, Hiroshima)

paper number S03-23p-Ⅳ-05.
【瀬川悦生、大津元一、「ドレスト光子の量子ウォークシミュレーションによる自律的移動経路とネットワークの幾何的構造の関係」、レーザー学会学術講演会第45回年次大会予稿集（2025年1月21日−24日）、（広島国際会議場、広島）講演番号S03-23p-Ⅳ-05】
[Invited presentation]

[20] S. Sangu, “Control of dressed-photon excited states by geometrical structures,” Abstracts of the 45th annual meeting of the Laser Society of Japan, January 21-24, 2025 (The International Conference Center Hiroshima, Hiroshima)
paper number S03-23p-Ⅳ-06.
【三宮俊、「幾何学的構造によるドレスト光子励起状態の制御」、レーザー学会学術講演会第45回年次大会予稿集（2025年1月21日−24日）、（広島国際会議場、広島）講演番号S03-23p-Ⅳ-06】
[Invited presentation]

CUMULATIVE LIST: Off-shell Archive

2025

42 Non-adiabatic relaxation process that lies behind the adiabatic relaxation of dressed-photon–phonon transfer

Authors M.Ohtsu, E.Segawa, K.Yuki and S.Saito
DOI 10.14939/2512O.001.v1
URL https://rodrep.or.jp/en/off-shell/original_2512O.001.v1.html
Date 2025.12.12

41 Quantum walk and random walk behaviors of dressed-photon–phonon transfers

Authors M.Ohtsu
DOI 10.14939/2510R.001.v1
URL https://rodrep.or.jp/en/off-shell/review_2510R.001.v1.html
Date 2025.10.27

40 Speed of dressed-photon–phonon transfer among a small number of particles

Authors M.Ohtsu, E.Segawa, K.Yuki, S.Saito and S.Sangu
DOI 10.14939/2509O.001.v1
URL https://rodrep.or.jp/en/off-shell/original_2509O.001.v1.html
Date 2025.09.12

39 Bright and dark walks for dressed-photon–phonon transfer

Authors M.Ohtsu, E.Segawa, K.Yuki, and S.Saito
DOI 10.14939/2501O.001.v1
URL https://rodrep.or.jp/en/off-shell/original_2501O.001.v1.html
Date 2025.01.06

2024

38 Quantum walk analyses of the off-shell scientific features of

dressed-photon–phonon transfers among a small number of nanometer-sized particles

Authors M.Ohtsu, E.Segawa, K.Yuki, and S.Saito
DOI 10.14939/2407O.001.v1
URL https://rodrep.or.jp/en/off-shell/original_2407O.001.v1.html
Date 2024.07.26

37 Optimum dissipation for governing the autonomous transfer of dressed photons

Authors M.Ohtsu, E.Segawa, K.Yuki, and S.Saito
DOI 10.14939/2405O.001.v1
URL https://rodrep.or.jp/en/off-shell/original_2405O.001.v1.html
Date 2024.05.27

36 Off-shell scientific nature of dressed photon energy transfer and dissipation

Authors M.Ohtsu
DOI 10.14939/2404R.001.v1
URL https://rodrep.or.jp/en/off-shell/review_2404R.001.v1.html
Date 2024.04.10

2023

35 Analyses of photon breeding with respect to photon spin by using a three-dimensional quantum walk model

Authors M.Ohtsu, E.Segawa, K.Yuki, and S.Saito
DOI 10.14939/2311O.001.v1
URL https://rodrep.or.jp/en/off-shell/original_2311O.001.v1.html
Date 2023.11.13

34 A quantum walk model with energy dissipation for a dressed-photon–phonon confined by an impurity atom-pair in a crystal

Authors M.Ohtsu, E.Segawa, K.Yuki, and S.Saito
DOI 10.14939/2304O.001.v1
URL https://rodrep.or.jp/en/off-shell/original_2304O.001.v1.html
Date 2023.04.10

33 Spatial distribution of dressed-photon–phonon confined by an impurity atom-pair in a crystal

Authors M.Ohtsu, E.Segawa, K.Yuki, and S.Saito
DOI 10.14939/2301O.001.v1
URL https://rodrep.or.jp/en/off-shell/original_2301O.001.v1.html
Date 2023.01.18

2022

32 Dressed-photon–phonon creation probability on the tip of a fiber probe calculated by a quantum walk model

Authors M.Ohtsu, E.Segawa, K.Yuki, and S.Saito
DOI 10.14939/2212O.001.v1
URL https://rodrep.or.jp/en/off-shell/original_2212O.001.v1.html
Date 2022.12.02

31 Numerical calculation of a dressed photon energy transfer based on a quantum walk model

Authors M.Ohtsu, E.Segawa, and K.Yuki
DOI 10.14939/2206O.001.v1
URL https://rodrep.or.jp/en/off-shell/original_2206O.001.v1.html
Date 2022.06.22

30 Off-shell science theories on interaction for dressed photons

Authors M.Ohtsu
DOI 10.14939/2201R.001.v1
URL https://rodrep.or.jp/en/off-shell/review_2201R.001.v1.html
Date 2022.01.31

2021

29 Progresses in theoretical studies of off-shell science for dressed photons

Authors M.Ohtsu

DOI 10.14939/2110R.002.v1
URL https://rodrep.or.jp/en/off-shell/review_2110R.002.v1.html
Date 2021.10.22

28 Generation Mechanism of Dressed Photon and Unique Features of Converted Propagating Light
Authors M.Ohtsu
DOI 10.14939/2110R.001.v1
URL https://rodrep.or.jp/en/off-shell/review_2110R.001.v1.html
Date 2021.10.01

27 A Quantum Walk Model for Describing the Energy Transfer of a Dressed Photon
Authors M.Ohtsu
DOI 10.14939/2109R.001.v1
URL https://rodrep.or.jp/en/off-shell/review_2109R.001.v1.html
Date 2021.09.03

26 The dressed photon as a member of the off-shell photon family
Authors M.Ohtsu
DOI 10.14939/2103R.001.v1
URL https://rodrep.or.jp/en/off-shell/review_2103R.001.v1.html
Date 2021.03.02

2020

25 Past, present, and future studies on the longitudinal electric field components of light
Authors M.Ohtsu
DOI 10.14939/2008R.001.v1
URL https://rodrep.or.jp/en/off-shell/review_2008R.001.v1.html
Date 2020.08.21

24 Errata: Route to Off-Shell Science
Authors M.Ohtsu

DOI 10.14939/2006R.001.v2
URL https://rodrep.or.jp/en/off-shell/review_2006R.001.v2.html
Date 2020.08.17

23 Route to Off-Shell Science
Authors M.Ohtsu
DOI 10.14939/2006R.001.v1
URL https://rodrep.or.jp/en/off-shell/review_2006R.001.v1.html
Date 2020.06.25

22 Nutation in energy transfer of dressed photons between nano-particles
Authors M.Ohtsu and T.Kawazoe
DOI 10.14939/2005O.001.v1
URL https://rodrep.or.jp/en/off-shell/original_2005O.001.v1.html
Date 2020.05.15

21 Progress in off-shell science in analyzing light–matter interactions for creating dressed photons
Authors M.Ohtsu
DOI 10.14939/2004R.001.v1
URL https://rodrep.or.jp/en/off-shell/review_2004R.001.v1.html
Date 2020.04.25

20 The present and future of numerical simulation techniques for off-shell science
Authors M.Ohtsu
DOI 10.14939/2003R.001.v1
URL https://rodrep.or.jp/en/off-shell/review_2003R.001.v1.html
Date 2020.02.27

2019

19 Note on the physical meaning of the cosmological term
Authors H.Sakuma and H.Ochiai
DOI 10.14939/1909O.001.v2

URL https://rodrep.or.jp/en/off-shell/original_1909O.001.v2.html
Date 2019.12.20

18 History, current developments, and future directions of near-field optical science
Authors M.Ohtsu
DOI 10.14939/1912R.001.v1
URL https://rodrep.or.jp/en/off-shell/review_1912R.001.v1.html
Date 2019.12.20

17 Dressed photon phenomena that demand off-shell scientific theories
Authors M.Ohtsu
DOI 10.14939/1911R.001.v1
URL https://rodrep.or.jp/en/off-shell/review_1911R.001.v1.html
Date 2019.11.12

16 Note on the physical meaning of the cosmological term
Authors H.Sakuma and H.Ochiai
DOI 10.14939/1909O.001.v1
URL https://rodrep.or.jp/en/off-shell/original_1909O.001.v1.html
Date 2019.09.10

15 Infrared lasers using silicon crystals
Authors M.Ohtsu and T.Kawazoe
DOI 10.14939/1908R.001.v1
URL https://rodrep.or.jp/en/off-shell/review_1908R.001.v1.html
Date 2019.08.01

14 Indications from dressed photons to macroscopic systems based on hierarchy and autonomy
Authors M.Ohtsu
DOI 10.14939/1906R.001.v1
URL https://rodrep.or.jp/en/off-shell/review_1906R.001.v1.html
Date 2019.07.06

13 Novel functions and prominent performance of nanometric optical devices made possible by dressed photons

Authors M.Ohtsu
DOI 10.14939/1904R.001.v1
URL https://rodrep.or.jp/en/off-shell/review_1904R.001.v1.html
Date 2019.04.02

2018

12 Embarking on theoretical studies for off-shell science guided by dressed photons

Authors M.Ohtsu
DOI 10.14939/1811R.001.v1
URL https://rodrep.or.jp/en/off-shell/review_1811R.001.v1.html
Date 2018.12.26

11 Theory of Single Susceptibility for Near-_eld Optics Equally Associated with Scalar and Vector Potentials

Authors I.Banno
DOI 10.14939/1809O.002.v1
URL https://rodrep.or.jp/en/off-shell/original_1809O.002.v1.html
Date 2018.12.26

10 Gigantic Ferromagnetic Magneto-Optical Effect in a SiC Light-emitting Diode Fabricated by Dressed-Photon–Phonon-Assisted Annealing

Authors M.Ohtsu and T.Kawazoe
DOI 10.14939/1809R.001.v1
URL https://rodrep.or.jp/en/off-shell/review_1809R.001.v1.html
Date 2018.12.26

9 Micro-Macro Duality for Inductions/Reductions

Authors I.Ojima
DOI 10.14939/1809O.001.v1
URL https://rodrep.or.jp/en/off-shell/original_1809O.001.v1.html
Date 2018.12.26

8 Logical Fallacy of using the Electric Field in Non-resonant Near-field Optics

Authors I.Banno and M.Ohtsu
DOI 10.14939/1808O.001.v1
URL https://rodrep.or.jp/en/off-shell/original_1808O.001.v1.html
Date 2018.12.26

7 Principles and Practices of Si Light Emitting Diodes using Dressed Photons

Authors M.Ohtsu and T.Kawazoe
DOI 10.14939/1805R.001.v1
URL https://rodrep.or.jp/en/off-shell/review_1805R.001.v1.html
Date 2018.12.26

6 Photon localization revisited

Authors I.Ojima, M.Ohtsu and H.Saigo
DOI 10.14939/1804O.002.v1
URL https://rodrep.or.jp/en/off-shell/original_1804O.002.v1.html
Date 2018.12.26

5 Experimental estimation of the maximum size of a dressed photon

Authors M.Ohtsu and T.Kawazoe
DOI 10.14939/1802R.001.v1
URL https://rodrep.or.jp/en/off-shell/review_1802R.001.v1.html
Date 2018.12.26

2017

4 Creation and Measurement of Dressed Photons: A Link to Novel Theories

Authors M.Ohtsu and H.Sakuma
DOI 10.14939/1712R.001.v1
URL https://rodrep.or.jp/en/off-shell/review_1712R.001.v1.html
Date 2018.12.26

3 Spatial and Temporal Evolutions of Dressed Photon Energy Transfer

Authors M.Ohtsu, T.Kawazoe, H.Saigo
DOI 10.14939/1710R.001.v1
URL https://rodrep.or.jp/en/off-shell/review_1710R.001.v1.html
Date 2018.12.26

2 High-Power Infrared Silicon Light-emitting Diodes Fabricated and Opereted using Dressed Photones

Authors M.Ohtsu and T.Kawazoe
DOI 10.14939/1804O.001.v1
URL https://rodrep.or.jp/en/off-shell/original_1804O.001.v1.html
Date 2018.12.24

1 New Routes to Studying the Dressed Photon

Authors M.Ohtsu
DOI 10.14939/OffShell.1709R.001.v1
URL https://rodrep.or.jp/en/off-shell/review_1709R.001.v1.html
Date 2018.12.23

[I] ORIGINAL PAPERS

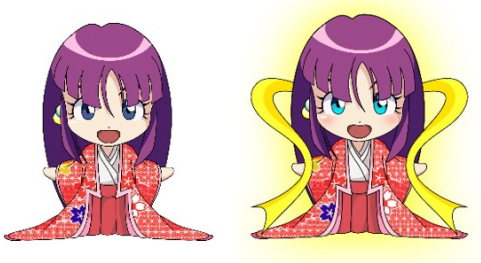

Optics Letters

Wavelength- and polarization-dependent enhancement of the magneto-optical effect with Al-doped 4H-SiC

Haoze Du,[1,*] Takuya Kadowaki,[2] Naoya Tate,[1] Yuji Oki,[1] Motoichi Ohtsu,[3] and Kenshi Hayashi[1]

[1]Graduate School and Faculty of Information Science and Electrical Engineering, Kyushu University, 744 Motooka, Nishi-ku, Fukuoka, 819-0395, Japan
[2]Nichia Corporation, 3-13-19 Moriya-cho, Kanagawa-ku, Yokohama, Kanagawa, 221-0022, Japan
[3]Research Origin for Dressed Photon, 3-13-19 Moriya-cho, Kanagawa-ku, Yokohama, Kanagawa, 221-0022, Japan
*duhaoze@laserlab.ed.kyushu-u.ac.jp

Received 8 May 2025; revised 3 September 2025; accepted 8 September 2025; posted 9 September 2025; published 1 October 2025

Al-doped 4H-SiC, a wide bandgap semiconductor, exhibits polarization rotation under a magnetic field similar to the magneto-optical effect after dressed-photon–phonon (DPP)-assisted annealing, which simultaneously irradiates the sample with a laser while applying a voltage. The magneto-optical effect exhibits wavelength- and polarization-dependence, which is attributed to the displacement of dopant clusters induced by DPP-assisted annealing. A significant enhancement of the magneto-optical response is observed when the incident light matches the DPP-assisted annealing conditions in wavelength and polarization. These findings suggest a promising route toward miniaturized optical devices in applications such as photonic computing or high-sensitivity sensing.

https://doi.org/10.1364/OL.567390

The magneto-optical effect, which occurs when light passes through certain materials and changes the relative phase of different polarization components, can be used in optical communication [1–3] to separate light [4,5] or multiplex optical signals [6,7], in optical metrology [8,9] to measure magnetic fields [10–12], stress [13–15], or chemical concentrations [16–18], and in optical computing [19–21]. However, most high-transparency materials [22,23] exhibiting the magneto-optical effect have a Verdet constant that typically falls within the range of 10^2 to 10^3 rad/T · m [24,25].

Doping impurities into semiconductors enables the formation of p–n junctions. Studies have shown that the formation of p–n junctions can also modify the material's optical response under a magnetic field [26–30], leading to phenomena resembling magneto-optical effects. In particular, it has been reported that injecting Al atoms into 4H-SiC crystals can cause them to exhibit the magneto-optical characteristics [26,27]. As a wide-bandgap semiconductor, 4H-SiC maintains high transmittance across the visible spectrum. Moreover, even while preserving this high transmittance, the transmitted light can be modulated by dopants, facilitating the development of spatial light modulators with low transmission loss.

Furthermore, the magneto-optical effect can be enhanced by simultaneously applying a bias voltage to Al-doped 4H-SiC and irradiating it with a laser [29,31]. Because this method relies on a quasi-particle called a dressed-photon–phonon (DPP), which is formed near the dopant clusters, this method is called DPP-assisted annealing. Based on DPP-assisted annealing, a novel SiC polarization rotator [30] was developed that exhibited a Verdet constant of 9.51×10^4 rad/T · m at a wavelength of 450 nm, which is a twofold increase compared with that before DPP-assisted annealing.

This magneto-optical effect, which is enhanced after DPP-assisted annealing, depends on the displacement of dopants [30,32]. The wavelength of the laser used for DPP-assisted annealing modifies the spatial distance between the dopant clusters, and the polarization direction governs the orientation of the dopant clusters. While previous studies verified DPP-assisted annealing enhancement at a single wavelength, in this study, it was experimentally demonstrated that the magnitude of the magneto-optical enhancement depends on the wavelength and polarization of the DPP-assisted annealing light.

The enhancement of the magneto-optical effect is considered to be related to dressed-photon (DP), which is a quasi-particle that describes the coupling between photon and electron, and its underlying principle and function have been investigated [33–35]. DPs can couple with coherent phonons, which are generated through energy exchange with the crystal lattice, leading to the generation of DPPs. It allows for the stimulated emission of photons that would otherwise be difficult to achieve through conventional electronic transitions. In other words, devices processed via DPP-assisted annealing exhibit not only significantly enhanced magneto-optical effects but also electroluminescent properties [31,32,36].

Efficient generation of DPPs can be achieved by modifying the spatial distribution of dopants through DPP-assisted annealing. During DPP-assisted annealing, a bias voltage is applied

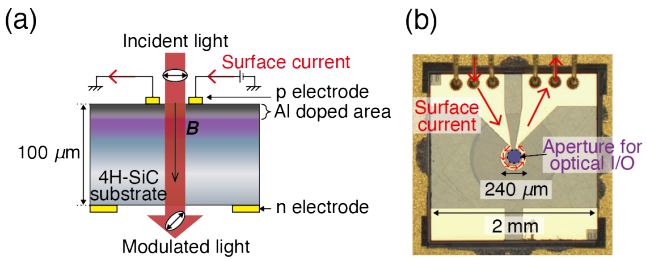

Fig. 1. (a) The current flowing through the surface ring electrode (p electrode) induces a magnetic field in the direction of light transmission, resulting in polarization rotation of the incident light and (b) surface image of the 4H-SiC device.

to the crystal, and Joule heating is generated at the p–n junction formed by dopant injection due to the resulting current flow. The dopants in the crystal will undergo thermally induced diffusion. Simultaneously, the crystal is irradiated with a laser. The photons that enter the crystal form DPs near the dopants and DPPs near the dopant clusters. With the assistance of a phonon sideband, the electrons can recombine with the holes, resulting in photon emission. The emission of photons consumes part of the Joule energy that would otherwise contribute to thermal diffusion of dopants, thereby localizing the dopants at positions where the generation of DPPs is favorable. After DPP-assisted annealing, the dopant clusters should have a consistent spatial distance [32,36]. This distribution of dopant clusters induces the polarization rotation of incident light and electroluminescence.

4H-SiC crystals were used as substrates. Al atoms were injected into n-type 4H-SiC crystals in the form of an ion beam with an accelerating energy of 300 keV and a dose of 1.8×10^{14} atoms/cm^2 (corresponding to an injection concentration of 1.0×10^{19} atoms/cm^3) to form a p–n junction. Then rapid thermal annealing was implemented at 1,700 °C for 10 minutes to recover crystallinity and to drive Al atoms diffusion to depths on the order of 1 μm from the crystal surface. Electrodes for DPP-assisted annealing were formed on the top and bottom surfaces of the crystal. The top electrode (p electrode) is a ring-shaped structure, as shown in Fig. 1(b), fabricated in Cr/Au (30/700 nm). The ring width is 20 μm, and its inner diameter is 200 μm, while the bottom electrode is a Cr/Au (30/700 nm) square shape that covers the entire backside of the crystal except for a circular central opening (diameter 1 mm) coaxial with the ring. In DPP-assisted annealing, a 635 nm laser was used (irradiation intensity: 20 W/mm^2), and the laser was adjusted through a half-wave plate (Thorlabs: WPH10M-633) and a Glan–Thompson polarizer (Thorlabs: GTH10M-A) to produce linearly polarized light parallel to the crystallographic axis of 4H-SiC. A positive bias voltage (20 V, current density: 0.022 A/mm^2) was applied to the crystal in parallel with the direction of light propagation. Under simultaneous laser irradiation and applied bias voltage, the device was subjected to DPP-assisted annealing for 30 minutes. A surface image of a fabricated device is shown in Fig. 1(b). When the surface current flows through the ring electrode, a magnetic field is generated in the center of the electrode, causing the polarized incident light to rotate.

In the experiment to investigate the magneto-optical effect of the device, as shown in Fig. 2, the laser beam was focused by a 4× objective onto a pinhole (diameter 8 μm). The laser transmitted through the pinhole was then collimated by a lens to form a parallel wave incident on the device. The crossed Nicols method was used. Two vertically oriented Glan–Thompson polarizers (Thorlabs: GTH10M-A, extinction ratio: 1×10^{-5}) were configured to form a crossed Nicols system, and the device was placed between them. The change in optical intensity was detected using a photomultiplier tube (PMT, Hamamatsu: H10720-01) to confirm the degree of polarization of the light passing through the device. The component of light that undergoes polarization rotation and is detected by the PMT after passing through GTP2 should satisfy the following formula:

$$V_{\mathrm{MO}} = V_{\mathrm{PMT0}} \sin^2 \theta_{\mathrm{rot}}. \tag{1}$$

Here, V_{MO} is the change in optical intensity caused by the magneto-optical effect, V_{PMT0} is the change in optical intensity when the polarization is 90°, and θ_{rot} is the angle of polarization rotation.

During verification, the light passing through the device was also affected by thermo-optical effects [37] because of the change in the light-induced birefringence of the crystal caused by the current flowing through the surface electrodes. The change in optical intensity caused by thermo-optical effects is superimposed on the change caused by the magneto-optical effect. The optical signal arriving at the PMT can be expressed as follows:

$$V_{\mathrm{PMT}} = V_{\mathrm{MO}} + V_{\mathrm{TO}}. \tag{2}$$

Here, V_{PMT} is the change in optical intensity. V_{TO} is the change in optical intensity caused by the thermo-optic effect.

To extract the components of optical intensity due to the magneto-optical effect, the following experiment was designed to counteract the thermo-optical effect. Because the thermo-optic effect is not affected by the orientation of the surface current flow, the direction of the current flow was changed. The polarization direction of light passing through the device changed to the opposite direction:

$$V_{\mathrm{PMT}\pm} = V_{\mathrm{PMT0}} \sin^2 \theta_{\pm\mathrm{rot}} + V_{\mathrm{TO}}. \tag{3}$$

Here, ± denotes the direction of the current. If the angle $\Delta\theta$ of GTP2 was changed:

$$V_{\mathrm{PMT}\pm} = V_{\mathrm{PMT0}} \sin^2 (\pm\theta_{\mathrm{rot}} + \Delta\theta) + V_{\mathrm{TO}}. \tag{4}$$

The difference ΔV_{PMT} is due to the change in the polarization rotation angle is defined by:

$$\Delta V_{\mathrm{PMT}} = V_{\mathrm{PMT+}} - V_{\mathrm{PMT-}} = V_{\mathrm{PMT0}} \sin 2\theta_{\mathrm{rot}} \sin 2\Delta\theta. \tag{5}$$

As depicted in Fig. 3, the polarization rotation angle (Experimental) is derived by using the following formula:

$$\theta_{\mathrm{rot}} = \frac{1}{2} \sin^{-1} \left(\frac{\Delta V_{\mathrm{PMT}}}{V_{\mathrm{PMT0}} \sin(2\Delta\theta)} \right). \tag{6}$$

To characterize the magneto-optical properties, Verdet constants were calculated based on the experimental values. Because the magneto-optical effect of the 4H-SiC device originates from the doping of Al and the generation of DPPs. Its effective interaction occurs at the p–n junction, and the interaction length is not consistent with that of conventional magneto-optical effects. Therefore, the interaction distance was unitized when calculating the Verdet constants. Unitized interaction length means that the polarization rotation is normalized with respect to the

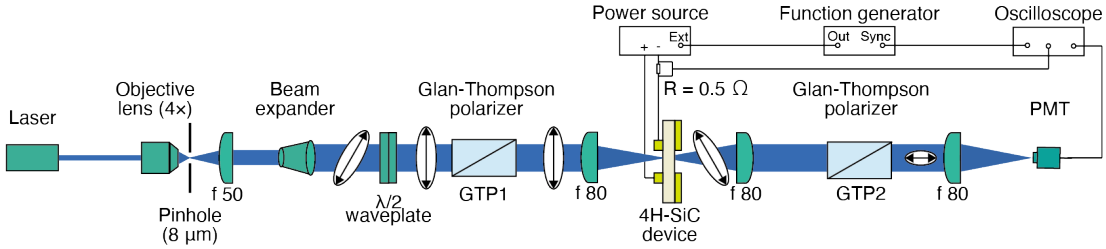

Fig. 2. Experimental setup for verifying the magneto-optical effects of the 4H-SiC device.

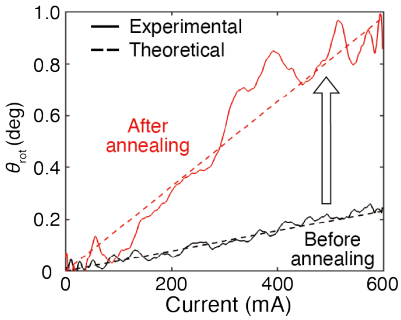

Fig. 3. Rotated angle θ_{rot} of incident light due to the surface current injection for $\lambda_{in} = 635$ nm.

magnetic-field line integral $\int B \cdot d\ell$ rather than to a geometric thickness. The generated rotation angle was converted to a magnitude $S = \theta_{rot}/B$ (rad/T) per unit magnetic field. The Verdet constants v (rad/A) were derived as follows [30]:

$$v = S\left(\frac{dB}{di}\right), \tag{7}$$

where dB/di is the magnetic flux density generated when a current of 1 A is injected into the electrode. Under quasi-static conditions, along a closed loop, $\int B \cdot d\ell = \mu_0 I$. This implies that a current of 1 A corresponds to a magnetic-field line integral of μ_0 in rad/T · m. To convert the unit (rad/A) to (rad/T · m) for the unit interaction length, the common conversion formula $1\,(\mathrm{A/m}) = 1.26 \times 10^{-6}$ (T) was used [30].

The magneto-optical effects of the device on incident light of λ_{in}= 457, 532, and 635 nm wavelength and polarization directions θ_{in}= 0°, 45°, and 90° were analyzed. First, as depicted in Fig. 3, when a surface current of 600 mA was applied to the ring electrode, a polarization rotation of less than 0.4° occurred before DPP-assisted annealing, at a wavelength of 635 nm. After DPP-assisted annealing, the angle increased to approximately 1.0°. According to the calculated Verdet constants, $(0.54 \pm 0.04) \times 10^4$ rad/T · m and $(2.27 \pm 0.03) \times 10^4$ rad/T · m before and after DPP-assisted annealing, respectively, this corresponds to approximately a 320.4% increase. On the other hand, in the case of $\lambda_{in} = 457$ nm and 532 nm, as depicted in Fig. 4(a), the Verdet constant changes slightly with DPP-assisted annealing: at 457 nm, Verdet constants are $(5.62 \pm 0.06) \times 10^4$ rad/T · m and $(5.22 \pm 0.05) \times 10^4$ rad/T · m before and after annealing, respectively; at 532 nm, Verdet constants are $(2.08 \pm 0.02) \times 10^4$ rad/T · m and $(1.88 \pm 0.03) \times 10^4$ rad/T · m, respectively (error bars denote 95% confidence intervals), unlike the pronounced variation observed at λ_{in}= 635 nm. This result revealed that the magneto-optical effect in Al-doped 4H-SiC is wavelength dependent; that is, the magneto-optical

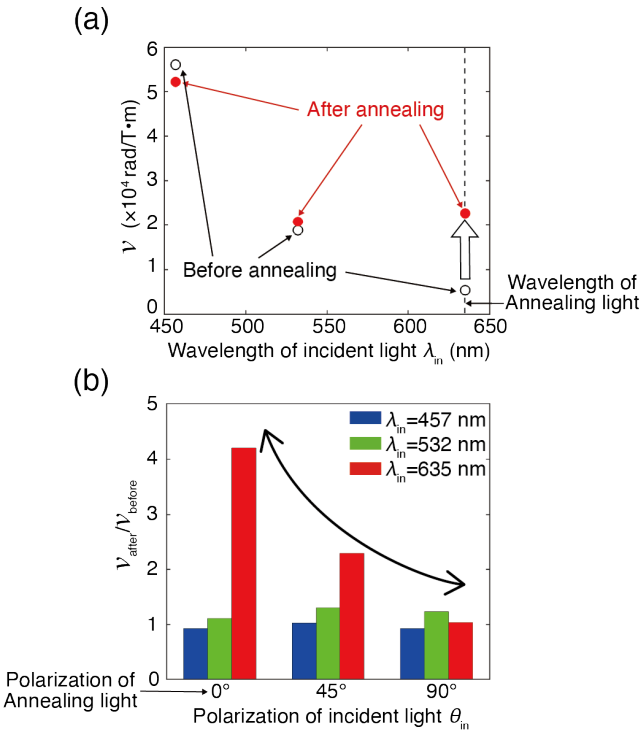

Fig. 4. (a) Verdet constant varying with wavelength before and after DPP-assisted annealing (white dots represent the values before annealing, and red dots represent those after annealing) and (b) relative change in the Verdet constant before and after DPP-assisted annealing (red, green, and blue bars represent the data obtained under incident light wavelength λ_{in} of 457 nm, 532 nm, and 635 nm).

enhancement is maximized near the wavelength irradiated during DPP-assisted annealing, compared with other wavelengths.

In the verification of the magneto-optical effect, the polarization direction θ_{in} of the incident light was modulated. The results are compared in Fig. 4(b); the ratio of the Verdet constant after annealing (v_{after}) to that before annealing (v_{before}) was calculated for different wavelengths and polarization directions of incident light. For incident light at λ_{in} = 635 nm, when the polarization of the incident light θ_{in}(= 0°) matches that used during the DPP-assisted annealing, the sample exhibits the most significant enhancement in Verdet constants. Conversely, little change is observed when incident light with an orthogonal polarization direction θ_{in}(= 90°). In other words, the Verdet constants of the 4H-SiC device before and after DPP-assisted annealing reveal that the change in the magneto-optical effect is the largest when the wavelength λ_{in} and the polarization θ_{in} of incident light are identical as the conditions of DPP-assisted annealing light. In other words, the enhancement of the magneto-optical effect

after DPP-assisted annealing exhibits a dependence on both the wavelength and the polarization of the incident light.

Building on previous work showing that DPP-assisted annealing of Al-doped 4H-SiC enhances polarization rotation, the present study experimentally demonstrates that an enhanced magneto-optical effect is observed when the incident light's wavelength and polarization are identical to those used during the DPP-assisted annealing. These illumination conditions coincide with those under which DPPs are efficiently generated. The wavelength- and polarization-dependence of the enhanced magneto-optical effect observed in the 4H-SiC device after DPP-assisted annealing is attributed to the displacement of Al dopants. After DPP-assisted annealing, the displacement of Al atoms led to the formation of new Al–Al dimers [38–41] possessing a magnetic moment under the influence of the magnetic field generated by the annealing current. However, the underlying mechanisms of this magneto–optical effect, such as the interaction between the incident light and Al–Al dimers in the presence of a magnetic field, are still under investigation. Ongoing tests aim to identify the wavelength and polarization ranges that induce a response in order to further clarify the interaction mechanism between the incident light and Al dopant pairs under a magnetic field. In addition, efforts are underway to fabricate 4H-SiC devices using circularly polarized light as the DPP-assisted annealing light, with the goal of further investigating the relationship between the polarization dependence of the magneto-optical effect and the polarization of the irradiation light during DPP-assisted annealing and ultimately enhancing the magneto–optical response of 4H-SiC devices.

The magneto-optical effect of the 4H-SiC device fabricated by DPP-assisted annealing was experimentally verified to be wavelength- and polarization-dependent. The wavelength- and polarization-dependence, which have not been observed in conventional magneto-optical effects, indicate that this magneto-optical effect, produced by applying a magnetic field to a semiconductor material, is more sensitive to incident light conditions. This finding will contribute to the development of spatial light modulators with wavelength- or polarization-selective functionality. The novel magneto-optical effect in this study can increase the magnitude, which is the Verdet constants, by an order of magnitude at a specific wavelength due to its unique wavelength dependence. Moreover, unlike conventional magneto-optical materials, which require a long interaction length to achieve significant polarization rotation and generally cannot simultaneously realize a high Verdet constant and high optical transmittance. This novel magneto-optical effect occurs in the region infiltrated by dopants, with a distance ranging from several hundred nanometers to a few micrometers. The significantly shorter interaction length allows the effect to manifest even in materials with high transmittance. This is advantageous for reducing the volume of optical systems and the loss of light intensity during light propagation, rendering optical systems more compact and higher-performance.

Moreover, in this study, the enhanced magneto-optical effect has not yet been optimized, as the doping concentrations and the DPP-assisted annealing conditions were not optimized. In the next phase of work, the relationship between the fabrication parameters and the annealing effects will be investigated individually. This will aid in developing higher-performance devices and elucidating the mechanism behind the novel magneto-optical effect exhibited by these 4H-SiC devices.

Funding. Japan Society for the Promotion of Science (JP22H04952, JP25K22229); JST SPRING (JPMJSP2136).

Disclosures. The authors declare no conflicts of interest.

Data availability. Data underlying the results presented in this paper are not publicly available at this time but may be obtained from the authors upon reasonable request.

REFERENCES

1. L. Eldada, Rev. Sci. Instrum. **75**, 575 (2004).
2. Y. Han and G. Li, Opt. Express **13**, 7527 (2005).
3. G. Li, Adv. Opt. Photonics **1**, 279 (2009).
4. I. Moreno, J. A. Davis, T. M. Hernandez, *et al.*, Opt. Express **20**, 364 (2012).
5. D. Dai, J. Bauters, and J. E. Bowers, Light Sci. Appl. **1**, e1 (2012).
6. N. Cvijetic, D. Qian, J. Yu, *et al.*, J. Light Technol. **28**, 1218 (2010).
7. Y. Feng, L. Li, J. Lin, *et al.*, Opt. Express **24**, 25491 (2016).
8. J. L. Pezzaniti and R. A. Chipman, Proc. SPIE **1317**, 280 (1990).
9. R. Hocken, N. Chakraborty, and C. Brown, CIRP Ann. **54**, 169 (2005).
10. R. J. Wijngaarden, K. Heeck, M. Welling, *et al.*, Rev. Sci. Instrum. **72**, 2661 (2001).
11. D. Budker, Nature **422**, 574 (2003).
12. D. Budker and M. Romalis, Nat. Phys. **3**, 227 (2007).
13. M. Huang, Int. J. Solids Struct. **40**, 1615 (2003).
14. A. Kniazkov, Opt. Spectrosc. **122**, 338 (2017).
15. A. Kniazkov, J. Appl. Phys. **122**, 125106 (2017).
16. R. C. Studinski and I. A. Vitkin, J. Biomed. Opt. **5**, 330 (2000).
17. V. Sankaran, J. T. Walsh, Jr, and D. J. Maitland, J. Biomed. Opt. **7**, 300 (2002).
18. D. M. Jameson and J. A. Ross, Chem. Rev. **110**, 2685 (2010).
19. D. E. Browne and T. Rudolph, Phys. Rev. Lett **95**, 010501 (2005).
20. R. Prevedel, P. Walther, F. Tiefenbacher, *et al.*, Nature **445**, 65 (2007).
21. B. Javidi, A. Carnicer, M. Yamaguchi, *et al.*, J. Opt. **18**, 083001 (2016).
22. M. Johnson, P. P. Bloemen, F. den, *et al.*, Rep. Prog. Phys. **59**, 1409 (1996).
23. S. H. Wemple, J. Electron. Mater. **3**, 243 (1974).
24. T. Haider, Int. J. Electromagn. Appl. **7**, 17 (2017).
25. K. J. Carothers, R. A. Norwood, and J. Pyun, Chem. Mater. **34**, 2531 (2022).
26. B. Song, H. Bao, H. Li, *et al.*, J. Am. Chem. Soc. **131**, 1376 (2009).
27. L. Yu, H. Jin, D. Liu, *et al.*, Chem. Phys. Lett. **496**, 276 (2010).
28. N. Tate, T. Kawazoe, W. Nomura, *et al.*, Sci. Rep. **5**, 12762 (2015).
29. T. Kawazoe, N. Tate, and M. Ohtsu, in *22nd International Display Workshops (IDW)* (2015), p. 1438.
30. T. Kadowaki, T. Kawazoe, and M. Ohtsu, Sci. Rep. **10**, 12967 (2020).
31. T. Kawazoe and M. Ohtsu, Appl. Phys. A **115**, 127 (2014).
32. M. Ohtsu and T. Kawazoe, Adv. Mater. Lett. **10**, 860 (2019).
33. M. Ohtsu, Nanophotonics **1**, 83 (2012).
34. M. Ohtsu, *What is a Dressed Photon?* (Springer, 2014).
35. M. Ohtsu, *Off-Shell Applications in Nanophotonics: Dressed Photon Science and Technology* (Elsevier, 2021).
36. T. Kawazoe, K. Nishioka, and M. Ohtsu, Appl. Phys. A **121**, 1409 (2015).
37. H. Du, H. Takeda, T. Kadowaki, *et al.*, in *2023 Conference on Lasers and Electro-Optics Europe & European Quantum Electronics Conference* (2023), p. ce_6_5.
38. T. Upton, J. Phys. Chem. **90**, 754 (1986).
39. X. Wang and L. Wang, J. Chem. Phys. **107**, 7667 (1997).
40. M. Calleja, C. Rey, M. Alemany, *et al.*, Phys. Rev. **60**, 2020 (1999).
41. J. Lv, F. Zhang, J. Jia, *et al.*, J. Mol. Struct. THEOCHEM **955**, 14 (2010).

[II] PRESENTATIONS

IN INTERNATIONAL CONFERENCES

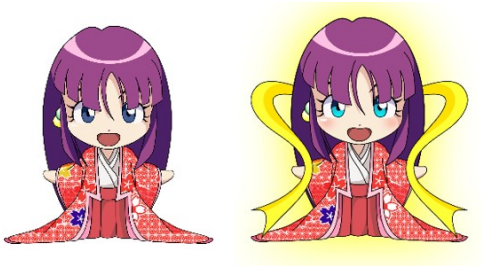

Plenary-05

Embarking on off-shell Science Guided by Dressed Photons

Motoichi OHTSU
Research Origin for Dressed Photon
3-13-19 Moriya-cho, Kanagawa-ku, Yokohama, Kanagawa 221-0022 Japan
** Email: ohtsu@rodrep.or.jp; mohtsu0@gmail.com*

Abstract: First, progress in experimental studies and application to generic technology are reviewed. Second, this talk answers the question "Dressed photon (DP), What?" It should be noted that conventional optical method (on-shell scientific method) does not give any answers because it does not deal with light-matter interaction in a nanometer-sized space. To give the answer, we have succeeded in formulating an off-shell scientific theory on physical space-time. It also derived the maximum size of the DP. Third, a quantum walk model for analyzing autonomous DP energy transfer are presented for analyzing the experimental results. Finally, future outlook will be given.

1 Introduction: Dressed photon (DP) is a quantum field that mediates the interaction between nanometer-sized particles (NPs). It localizes at the NP and its size is much smaller than the wavelength of a propagating light (a free photon: an onshell field). That is, the DP is not an entity directly observed by conventional methods in optics. It should not be confused with a special type of linear evanescent field because the DP is generated by nonlinear light-matter interactions, for which quantum off-shell momentum field plays an important role. DP has unique features that are complimentary to those of the free photon, and variety of novel phenomena originated from DP. By noting that the DP is a quantum field whose energy–momentum relation deviates from the mass-shell, novel theoretical studies of so-called "off-shell science" have been launched. This talk reviews the recent progress in experimental and theoretical studies on mechanisms of creating the DP.

2 Experimental studies and application to generic technologies: Experimental studies have resulted in the development of generic technologies [1-3]. They are nano-optical devices, nano-fabrication technology, optical energy conversion, and silicon (Si) light-emitting devices. These technologies are complementary to those of the conventional ones. For example, the DP enables the Si lightemitting devices even though Si is an indirect-transition-type semiconductor [4]. Furthermore, it is shown that these devices exhibit a unique feature, named photon breeding. Conventional on-shell scientific methods have intrinsic problems in describing these features.

3 Light-matter interactions for creating dressed photons: The off-shell scientific method overcomes the problems above. Our theory on "physical space-time" covers not only timelike but also spacelike components of it by utilizing Greenberg-Robinson theorem in the axiomatic quantum field theory. This section reviews recent progress in theoretical studies in off-shell science that has been recently established for correctly describing light–matter interactions [5, 6]. These studies produced the Clebschdual (CD) field theory to deal with the spacelike momentum field that is indispensable in such interactions. Our theory describes that the spacelike momentum field is converted to a timelike field at a singular point to create a timelike Majorana field of a particle–antiparticle pair. This pair is annihilated promptly because of its nonpropagating nature. However, a non-propagating electromagnetic field remains in the interacting system, which is the very field of the DP. Based on the correlation between theoretical models of the CD field and dark energy, the maximum size of the DP is expressed by using basic physical constants (Planck length and cosmological constant). It means that the off-shell quantum field connects the DP and cosmology. This size is called the DP constant that is put on the list of basic physical constants. The derived value (40 nm) agrees with the experimental value. Furthermore, is pointed out that, in the case where the timelike Majorana particle and anti-particle have anti-parallel spins, the pair annihilation creates a DP with a spin 0. The light converted from this DP is a unique light field with spin 0, which behaves as a particle. It has been experimentally confirmed that a cluster of photons emitted from the Si lightemitting device behave as such a particle.

4 A quantum walk model for analyzing autonomous energy transfer of dressed photons: This section reviews the unique phenomena of dressed-photon—phonon (DPP) energy transfer and numerical calculations based on a quantum walk (QW) model that was developed to analyze this transfer. Although the essential question is how to identify the origin of the autonomous DP energy transfer, conventional random walk (RW) model does not answer this question. One reason is that the RW model has never dealt with the light-matter interaction process. This section reviews the numerical simulation for analyzing the spatial-temporal evolution of the DPP energy transfer by taking the interaction process into account. The QW model is used for this simulation because it can deal with "non-commutativity" and "localization". Here, numerically calculated experimental results are, DPP creation probability on the tip of a fiber probe, spatial distribution of DPP confined by an impurity atom-pair in a crystal with energy dissipation, and photon breeding with respect to photon spin. The calculated results agreed with the experimental results. Furthermore, in order to analyze the autonomous transfer of DPP, calculations were carried out for optimum dissipation of the DPP transfer, DPP transfer among a small number of NPs, and contributions of bright and dark walks for DPP transfer.

5 Concluding remark: Since variety of novel phenomena, originated from DP, are similar to many physical, chemical, and biological phenomena, these similarities are the manifestation of underlying scientific universality represented by nonlinear off-shell field interactions. Now, it is the moment of embarking on off-shell science guided by the DP.

References

[1] M. Ohtsu, *Dressed Photons* (Springer, Heidelberg, 2014).
[2] M. Ohtsu, *Off-shell Application in Nanophotonics* (Elsevier, Amsterdam, 2021).
[3] H. Sakuma, I. Ojima, M. Ohtsu and T. Kawazoe, "Drastic advancement in nanophotonics achieved by a new dressed photon study, " *J. of Euro. Opt. Soc.-Rapid Publication* (2021)**17**:28. https://jeos.springeropen.com/articles/10.1186/s41476-021-00171-w
[4] M. Ohtsu, *Silicon Light-Emitting Diodes and Lasers* (Springer, Heidelberg, 2016).
[5] M. Ohtsu and H. Sakuma, "Dressed Photon as an Off-Shell Quantum Field," in *Progress in Optics*, vol.64 (ed. by T.D. Vissor) (Elsevier, Amsterdam, 2019) pp. 45-97.
[6] M. Ohtsu and H. Sakuma, *Dressed Photons to Revolutionize Modern Physics* (Springer, Heidelberg, 2025).

BIOGRAPHIES OF PLENARY LECTURERS

PLENARY LECTURER: ***Motoichi OHTSU***

Prof. Motoichi Ohtsu, Emeritus Professor of the University of Tokyo and a globally recognized pioneer in nanophotonics and near-field optics, has revolutionized nanoscale light-matter interactions through his groundbreaking research. As the founder of optical near-field theory, he overcame the diffraction limit of light, enabling sub-10-nm resolution imaging via his invention of apertureless near-field microscopy and establishing the paradigm-shifting concept of "dressed photons" for quantum-inspired nanofabrication. His work laid the foundation for advanced applications ranging from single-molecule sensing to ultra-compact photonic devices. An elected Fellow of OSA, he has been honored with the Japan Society of Applied Physics Award (1998) and has authored over 400 publications, including the seminal Springer series Progress in Nanophotonics. Former Director of Japan's Photonics Research Institute, he has collaborated with leading industries (e.g., JEOL, Hitachi) to translate near-field optics into semiconductor metrology tools. Currently, he spearheads cutting-edge research in quantum nanophotonics, exploring topological light control and scalable single-photon sources for next-generation quantum technologies. Prof. Ohtsu's visionary contributions continue to define the frontier of nano-optics, inspiring a generation of researchers worldwide.

[IV] PREPRINT DEPOSITORIES

[IV-1] OFF-SHELL ARCHIVE

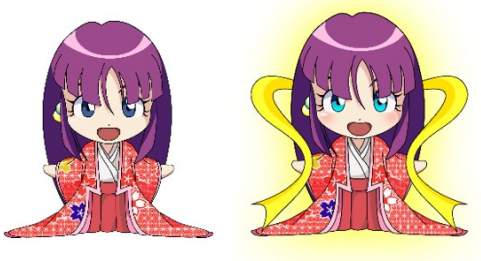

Non-adiabatic relaxation process that lies behind the adiabatic relaxation of dressed-photon–phonon transfer

M. Ohtsu[1], E. Segawa[2], K. Yuki[3,4], and S. Saito[4]

[1]Research Origin for Dressed Photon,3-13-19 Moriya-cho, Kanagawa-ku, Yokohama, Kanagawa 221-0022, Japan

[2]Yokohama National University, 79-8 Tokiwadai, Hodogaya-ku, Yokohama, Kanagawa 240-8501, Japan

[3]Middenii, 3-3-13 Nishi-shinjuku, Sinjuku-ku, Tokyo 160-0023, Japan

[4]Kogakuin University, 2665-1, Nakano-machi, Hachioji, Tokyo 192-0015, Japan

Abstract

This paper reports the results of numerical calculations based on a quantum walk (QW) model in order to analyze the temporal behavior of the dressed-photon–phonon (DPP) transfer. Since a random walk (RW) process lies behind the QW process, the time evolution operator of the interpolation model is used by introducing a probability p. The results reveal that: The crossover time t_x decreases with increasing p and χ / J (the ratio between the DP hopping energy J and the DP-phonon coupling energy χ). In contrast, th slope S_{RW} of the curve for the RW process increases. The slope S_{QW} of the curve for the QW process increases with increasing χ / J, which indicates that a part of the adiabatic relaxion energy is apt to be spontaneously converted to the non-adiabatic relaxation energy. In the case of $\chi / J \ll 1$, the nutation cycle is long and the slopes are small, which is advantageous for operating novel nanometer-sized devices.

1 Introduction

A dressed photon (DP) is created by a photon-exciton (or electron) interaction in a nanometer-sized particle (NP). Furthermore, the DP creates a dressed-photon–phonon (DPP) when it couples with a phonon. A previous article reviewed experimental results on the temporal behavior of DPP transfers among NPs [1]. Notable features of this behavior were: When two semiconductor NPs (NP_1 and NP_2) are illuminated by an optical pulse, a DPP is created and transferred bi-directionally between the two NPs (Fig. 1(a) in [1]).

As a result, these NPs emitted photoluminescence components (PL_1 and PL_2). The temporal behaviors of the light intensities PL_1 and PL_2 were as follows:

[1] In the early short time-span, the emitted light intensities pulsated due to the DPP nutation between the two NPs and decreased with a short time constant τ_{QW}. This decrease was due to the adiabatic energy relaxation, which was fitted by the function $y_{QR} = \exp(-t / \tau_{QW})$ of a quantum walk (QW) model.

[2] Subsequently, intensities decreased with a long time constant τ_{RW}. This was due to non-adiabatic energy relaxation, which was fitted by the function $y_{RW} = \exp(-\sqrt{t/\tau_{RW}})$ of a random walk (RW) model [2]. Finally, the nutation in **[1]** was buried in the non-adiabatic energy relaxation. Measured values of these time constants were τ_{QW} = 150 – 600 ps and τ_{RW} =0.7 – 15 ns. The nutation cycle was τ_r =50 – 155 ps [3].

This paper reports the results of numerical calculations carried out in order to analyze the experimentally found features **[1]** and **[2]** described above.

2 Methods and results of numerical calculation

Recent theoretical studies have found that a RW process lies behind the QW process, and the time evolution operator $\mathcal{L}$ for the interpolation model is represented by the sum of those of the QW and RW models ($\mathcal{L}^{\mathrm{QW}}$ and $\mathcal{L}^{\mathrm{RW}}$, respectively):

$$\mathcal{L} = (1-p)\mathcal{L}^{\mathrm{QW}} + p\mathcal{L}^{\mathrm{RW}}, \qquad (1)$$

where p $(0 \le p \le 1.0)$ is a probability [4,5].

This section presents the numerically calculated results of the temporal behaviors of the emitted light intensity in the early short time-span and in the subsequent long time-span based on eq. (1). For calculation, $\mathcal{L}^{\mathrm{QW}}$ is chosen with probability $1-p$, while $\mathcal{L}^{\mathrm{RW}}$ is chosen with probability p at each time step, independently. As a result, one can evaluate the temporal behavior of the emitted light intensity. The ratio χ/J between the DP hopping energy J and DP-phonon coupling energy χ was used as the physical parameter. It should be noted that the phonon is a quantum of the crystal lattice vibration that can induce non-adiabatic energy relaxation.

Figure 1 shows the calculated dependence of the emitted light intensities on the probability p in the case of χ/J =1.0. The slopes S_{QW} and S_{RW} correspond to the rates of intensity decreases that are due to the adiabatic and non-adiabatic relaxations (**[1]** and **[2]** in Section 1), respectively. Figure 1(a) represents the result at p =0, that is, the light intensities due to the adiabatic relaxation. Pulsative variations of the curves represent the nutation of the DPP transfer. Figure 1(b) is the result at p =0.15. Here, the nutation due to the adiabatic relaxation is seen in the early time-span shorter than t_x. In the time-span longer than t_x, the light intensity due to the non-adiabatic relaxation surpasses that due to the adiabatic relaxation. This means that the nutation is

buried in the non-adiabatic energy relaxation, as was pointed out in **[2]** in Section 1. Thus, t_x is named the crossover time. Figure 1(c) shows the results at p=1.0, which are governed by the non-adiabatic relaxation. It is easily confirmed that t_x is shorter than that in Fig. 1(b). The nutation can be faintly seen in the early time-span shorter than t_x.

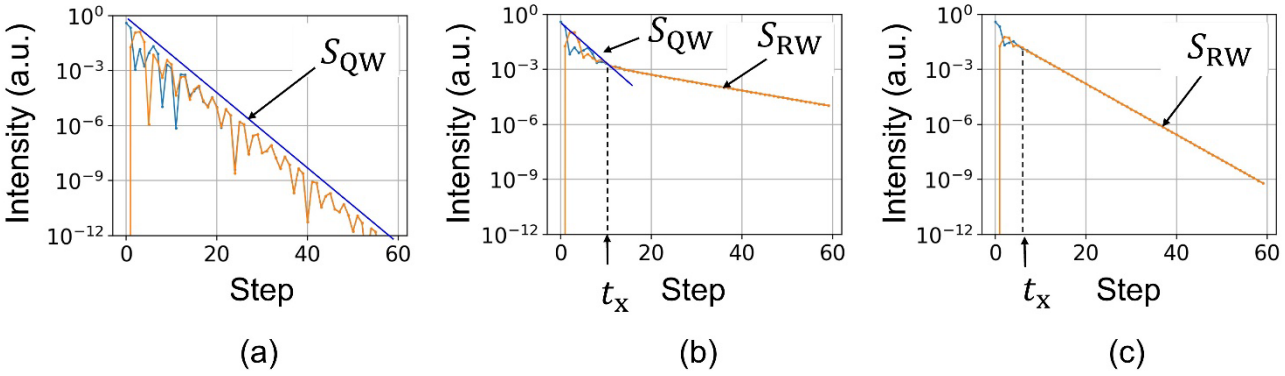

Fig. 1 Temporal variations of the emitted light intensities at χ / J =1.0.

Blue and red curves represent the intensities of PL_1 and PL_2, respectively. t_x is the crossover time.

(a) The results at p=0. Pulsation represents the nutation. S_{QW} is the slope due to the adiabatic relaxation. (b) The results at p=0.15. S_{RW} is the slope due to the non-adiabatic relaxation. (c) The results at p=1.0.

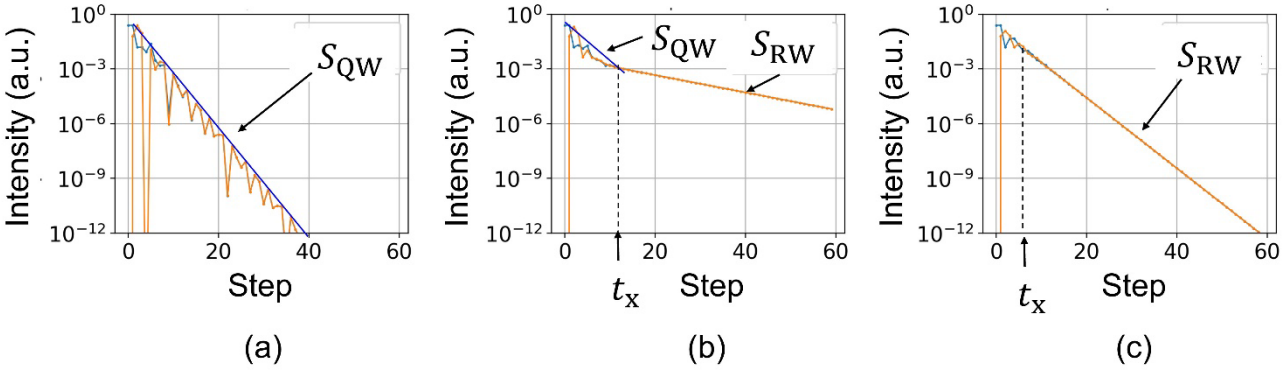

Fig. 2 Temporal variations of the emitted light intensities at χ / J =1.41.

(a) p=0. (b) p=0.15. (c) p=1.0.

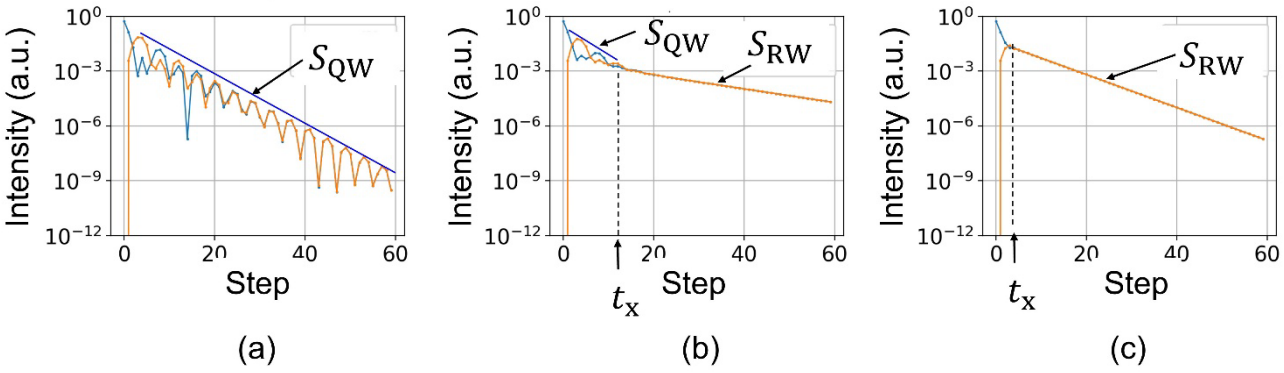

Fig. 3 Temporal variations of the emitted light intensities at χ / J =0.816.

(a) p =0. (b) p =0.15. (c) p =1.0.

Figures 2 and 3 represent the results at χ / J =1.41 and 0.816, respectively. Figure 4 presents the features of the curves in Figs. 1, 2, and 3. They are:

(1) (Fig. 4(a)) The crossover time t_x decreases with increasing p and χ / J. For practical applications, it should be pointed out that a longer crossover time t_x is advantageous for improving the performance in novel nanometer-sized devices such as a nano-optical condenser and an optical buffer memory [1].

(2) (Fig. 4(b)) The slope S_{RW} increases with increasing p and χ / J.

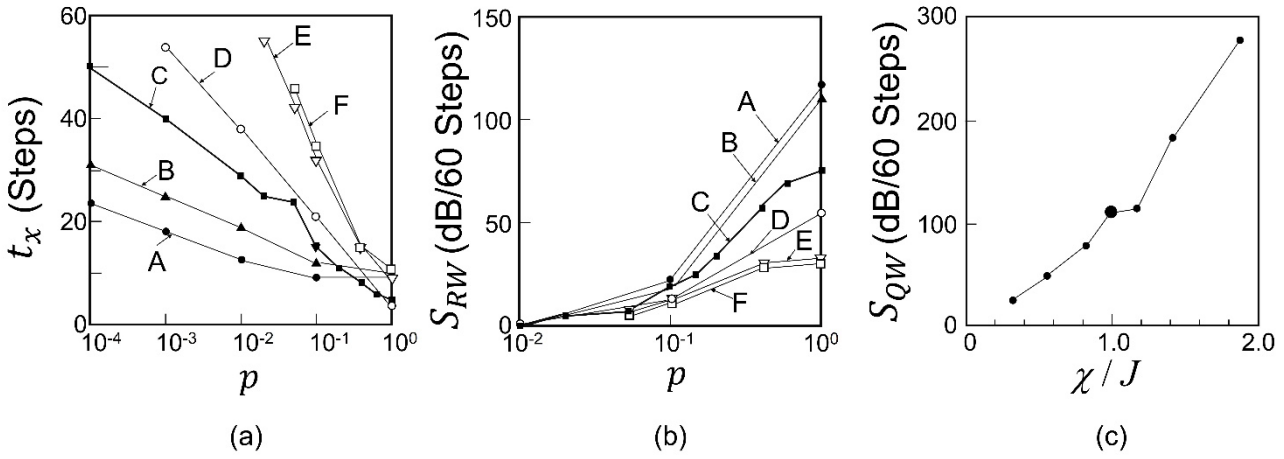

Fig. 4 Crossover time t_x, the slopes S_{RW} and S_{QW} of the curves.

χ / J =1.84 (A), 1.41 (B), 1.00 (C), 0.816 (D), 0.585 (E), and 0.329 (F).

(3) (Fig. 4(c)) The slope S_{QW} increases with increasing χ / J. This increase indicates that a part of the adiabatic relaxion energy is apt to be spontaneously converted to the non-adiabatic relaxation energy. The conversion rate is represented by ε in eqs. (4) and (5) of ref. [1].

Previous calculations using the QW model have confirmed that the DPP localized at the B atom-pairs in a Si crystal when $\chi / J \gg 1$ [6]. This localization has been used to invent a novel method of DPP-assisted annealing, resulting in the successful fabrication of revolutionary Si-LED and Si-laser devices [7]. To examine these revolutionary works, Fig. 5(a) represents the calculated results at $\chi / J = 10$. It is easily found that the crossover time t_x is shorter than that in Fig. 4(a), which means that the adiabatic relaxation is rapidly buried in the non-adiabatic relaxation. This is because the phonon, a possible source of the non-adiabatic energy relaxation, can efficiently couple with the DP when $\chi / J \gg 1$. Furthermore, it is found that the slope S_{QW} is larger than that in Fig. 4(c), which means that a part of the adiabatic relaxion energy is apt to be spontaneously converted to the non-adiabatic relaxation energy, as was presented in **(3)** above. In this situation, the DPP efficiently localizes at the position of the B atom-pair in the Si crystal for optimizing the spatial profiles of the B atom-pair by DPP-assisted annealing. As a result, highly efficient Si-LED and Si-laser devices were successfully fabricated [6].

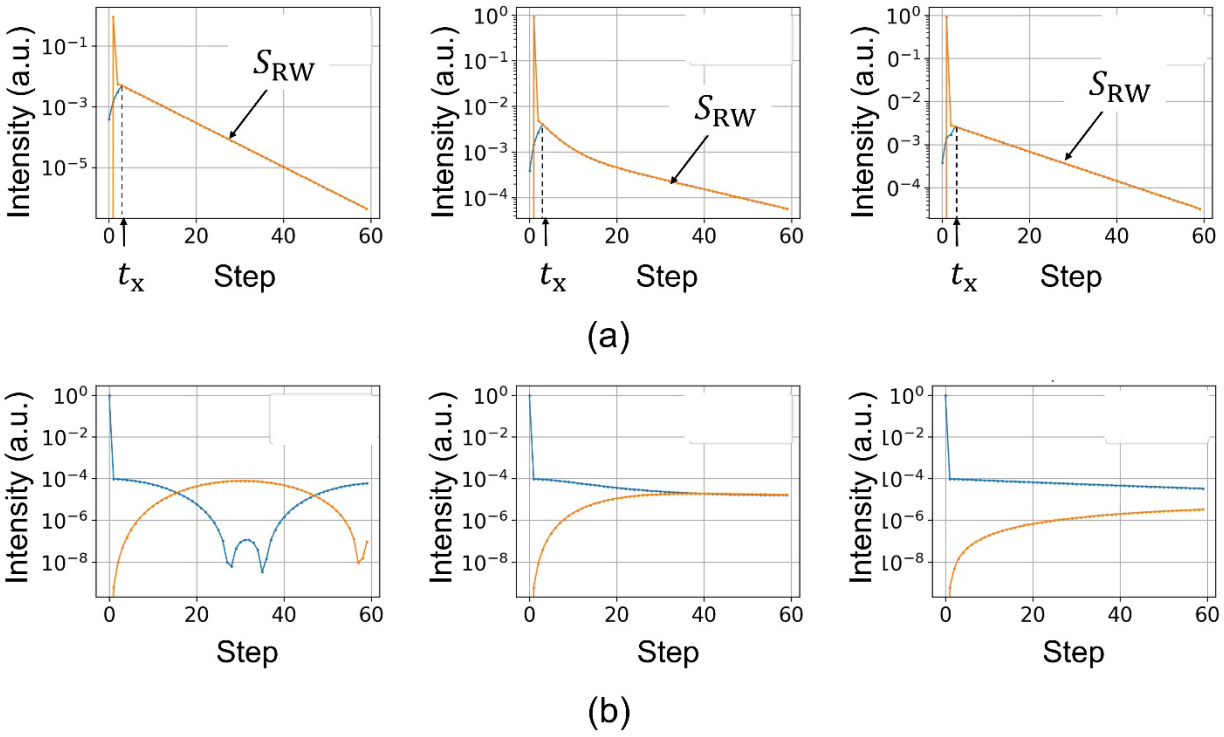

Fig. 5 Calculated results. (a) χ / J=10. (b) χ / J=0.1.
Left, center, and right figures are at p=0, 0.15, and 1.0, respectively.

Figure 5(b) represents the calculated results at $\chi / J = 0.1$. The profiles of the curves in this figure are conspicuously different from those in Fig. 5(a) and Figs. 1-3. The left figure shows that the nutation cycle is much longer than those in Figs. 1(a), 2(a), and 3(a). Furthermore, the slopes S_{RW} and S_{QW} are small. This is because the phonon, a possible source of the non-adiabatic relaxation, does not efficiently couple with the DP when $\chi / J \ll 1$. Thus, in this figure, the leading role in the energy transfer is played by the DP and not the DPP. The long nutation cycle and small slopes indicate that the condition $\chi / J \ll 1$ is advantageous for operating the novel nanometer-sized devices above.

5 Summary

In order to analyze the experimentally found features of the temporal behavior of the DPP transfer, this paper used the time evolution operator of the interpolation model because a RW process lay behind the QW process. The calculated results indicated the following unique features: The crossover time t_x decreased with increasing p and χ / J. In contrast, the slope S_{RW} increased. The slope S_{QW} increased with increasing χ / J, which indicated that a part of the adiabatic relaxation energy is apt to be spontaneously converted to the non-adiabatic relaxation energy. In the case of $\chi / J \ll 1$, the nutation cycle was long and the slopes were small, which are advantageous for operating novel nanometer-sized devices.

Acknowledgements

The authors thank Dr. S. Sangu (Ricoh Corp.) for his valuable comments.

References

[1] M. Ohtsu, “Quantum walk and random walk behaviors of dressed-photon–phonon transfers,” *Off-shell Archive* (October, 2025) Offshell: 2510O.001.v1.

DOI 10.14939/2510R.001.v1 https://rodrep.or.jp/en/off-shell/review_2510R.001.v1.html

[2] H. Saigo, Quantum Probability for Dressed Photons, *Prog. in Nanophotonics* 5 (ed. T. Yatsui) (Springer,2018) pp 79-106.

[3] M. Ohtsu, *Off-Shell Science Guided by Dressed Photons* (Design-Egg, 2025) pp.29-49.

[4] E. Segawa, “Seamless connection between quantum walk and random walk,” in *Off-Shell Science Forum* (August 2025), ((General Incorporated Association) Research Origin for Dressed Photon, Yokohama, Japan), in Japanese. https://rodrep.or.jp/img/forum/67)Segawa_20250818.pdf

[5] S. Yoshino, H. Shiratori, T. Yamagami, R. Horisaki, and E. Segawa, “Normal variance mixture with arcsine law of an interpolating walk between persistent random walk and quantum walk,” Entropy 2025, 27(7), 670; https://doi.org/10.3390/e27070670.

[6] M. Ohtsu, E. Segawa, K. Yuki, and S. Saito, “Spatial distribution of dressed-photon–phonon confined by an impurity atom-pair in a crystal,” *Off-shell Archive* (January, 2023) Offshell: 2301O.001.v1.

DOI 10.14939/2301O.001.v1 https://rodrep.or.jp/en/off-shell/original_2301O.001.v1.html

[7] M. Ohtsu, *Silicon Light-Emitting Diodes and Lasers* (Springer, Heidelberg, 2016) pp.1-192.

Speed of dressed-photon–phonon transfer among a small number of particles

M. Ohtsu[1], E. Segawa[2], K. Yuki[3], S. Saito[4] and S. Sangu[5]

[1]Research Origin for Dressed Photon,3-13-19 Moriya-cho, Kanagawa-ku, Yokohama, Kanagawa 221-0022, Japan

[2]Yokohama National University, 79-8 Tokiwadai, Hodogaya-ku, Yokohama, Kanagawa 240-8501, Japan

[3]Middenii, 3-3-13 Nishi-shinjuku, Sinjuku-ku, Tokyo 160-0023, Japan

[4]Kogakuin University, 2665-1, Nakano-machi, Hachioji, Tokyo 192-0015, Japan

[5]Ricoh Co., Ltd., 2-7-1 Izumi, Ebina, Kanagawa 243-0460, Japan

Abstract

This paper analyzes dynamic behaviors of dressed-photon—phonon (DPP) energy transfer by using a blown-up quantum walk model. Numerical calculations are carried out in the case when a large nanometer-sized particle NP_O is surrounded by five small particles NP_Is. Spectral profiles of the DPP transfer indicate that the speeds of the inter-NP transfer, intra-NP transfer, and local transfer are different with each other. This difference is the possible origin of the pulsative behavior found in the transitional period. In the case when the number of the transfer routes is large, the DPP rapidly transfers to reach the NP_O. Conversely, in the case where the number of transfer routes is small, the DPP transfers slowly. It is presumed that such unique nature of the DPP transfer is governed by the off-shell scientific principle of maximizing the average entropy generation.

1 Introduction

Recent theoretical studies have succeeded in drawing a precise physical picture of the creation process of a dressed photon (DP) [1-3]. Furthermore, by using a quantum walk (QW) model, detailed analyses of energy transfers of a dressed-photon−phonon (DPP) among nanometer-sized particles (NPs) have made striking progress. Here, the DPP is a quantum field that is created as a result of interactions between DPs and phonons.

As a successful example of these analyses, the QW model has been used to evaluate the experimental results on optical-wavelength conversion realized by the DPP energy transfer from small NPs to a large NP [4]. Numerical calculations have been carried out in the case where a large NP used as an output signal terminal (OST: NP_O) was surrounded by small NPs used as input signal terminals (ISTs: NP_Is). Figure 1 schematically illustrates this arrangement, in which an NP_O is fixed on a hub [5]. Five NP_Is are fixed on the rim in a rotationally symmetric manner. They are also connected to the NP_O, as represented by spokes. This rim and spoke arrangement represents the DPP energy transfer routes.

Numerical calculations evaluated the stationary values of the input signal transfer rates (ISTR) from the ISTs to the OST. The value of the output signal transfer rate (OSTR) from the OST to the outer space was also evaluated.

Further calculations have been carried out for the case where the rotational symmetry above was broken, that is, when some spokes were lost. The results indicated that the DPP energy transfer routes were a three-fold degenerate bright walk in the case where the number of connected spokes, n_{con}, was odd. Thus, even if some spokes were lost, the stationary values of the OSTR were kept equal to that of n_{con}=5.

In the case where n_{con} was even, the energy transfer routes were composed of bright and dark walks. Since some input signals flowed into the dark walks, the stationary value of the OSTR was smaller than that of the case when n_{con} was odd. The degeneracy in the bright walk and the contribution of the dark walk were found not only in the pentagonal arrangement (Fig. 1) but also in other polygonal arrangements, which demonstrated that their features were independent of the number of NP_Is on the rim.

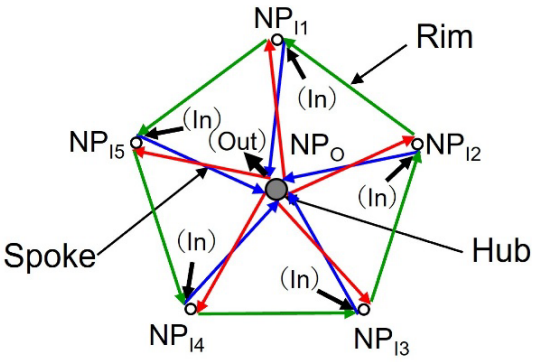

Fig. 1 Arrangement of nanometer-sized particles (NPs).
(In) and (Out) represent an input signal and an output signal, respectively.

It should be noted that the stationary values were governed by the dynamic behavior of the DPP energy transfer in the transitional period prior to reaching the stationary state. A representative feature of such behavior was the pulsative variations of ISTR and OSTR, as shown in Fig.2(a) in ref. [5]. The present paper reports the numerically calculated results of this dynamic behavior.

2 Analyses using a blown-up quantum walk model

The arrangement in Fig. 1 is replaced by Fig. 2 in order to demonstrate a blown-up QW model that was used for analyzing the dynamic behavior [6]. Red arrows represent the inter-NP transfer routes of the DP between adjacent NP_Is and between the NP_Is and NP_O. Small blue circles in the NP_Is and NP_o represent the inner sites that are connected with the red arrows. Blue arrows represent the intra-NP transfer routes of the DP between these inner sites. Green arrows are the self-loops that represent

the local transfer routes of a localized phonon at each inner site. The numbers of the red, blue, and green arrows are 20, 26, and 26, respectively. Thus, the total number of arrows is 72.

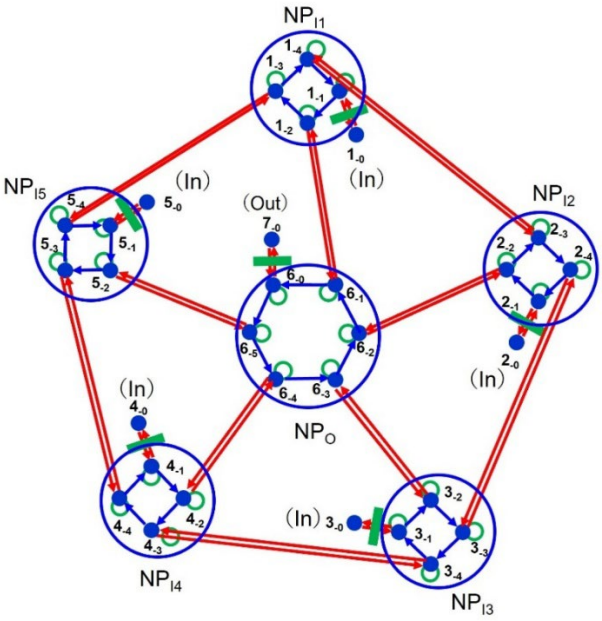

Fig. 2 A blown-up QW model.

A three-row vector is used to represent the probability amplitude of creating the DPP [7]:

$$\vec{\psi}_{t,(x,y)} = \begin{bmatrix} y_{\mathrm{DP+}} \\ y_{\mathrm{DP-}} \\ y_{\mathrm{Phonon}} \end{bmatrix}_{t,(x,y)}, \tag{1}$$

where [ ] represents the vector at time t and at the position (x, y). y_{DP+} and y_{DP-} are the probability amplitudes of the DPs that hop in mutually- opposite directions, and y_{Phonon} is that of the phonon. Its tempo-spatial behavior is derived by solving evolution equations for $\vec{\psi}_{t,(x,y)}$, in which the sum of the coefficient matrices (P_+, P_-, and P_0) is [7]

$$U = \begin{bmatrix} \varepsilon_+ & J & \chi \\ J & \varepsilon_- & \chi \\ \chi & \chi & \varepsilon_0 \end{bmatrix}. \tag{2}$$

Here, off-diagonal elements J and χ are the DP hopping energy and DP-phonon coupling energy, respectively. Diagonal elements $\varepsilon_\pm$ and ε_0 are eigen-energies of DPs and phonon. The numbers of the eigen-vectors and eigen-values of this matrix are both 72, which corresponds to the total number of arrows above. Figure 3 shows the absolute values $|\lambda_n|$ of the eigen-values plotted in descending

order n (=1–72). Their maximum and minimum values are 1.0 and 0.92, respectively.

In order to analyze the features of the DPP transfer rate C_n, the value C_n on each arrow in Fig. 2 is spectrally resolved based on these eigen-values in Fig. 3. Figures 4(a), (b), and (c) show examples of these spectra on red, blue, and green arrows, respectively.

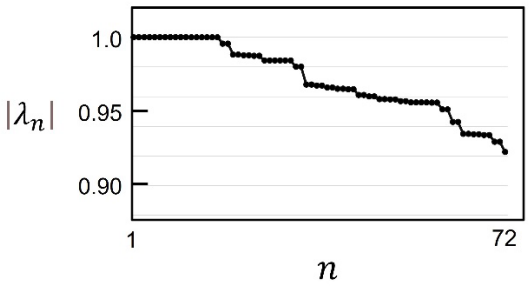

Fig. 3 The absolute values $|\lambda_n|$ of the eigen-values arranged in descending order n (=1–72).

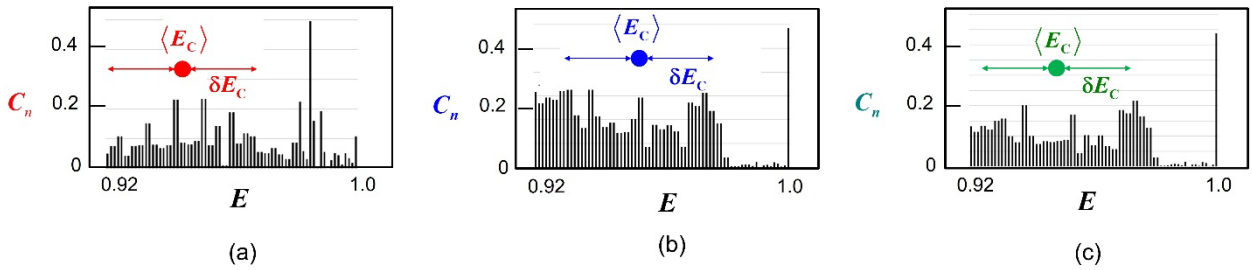

Fig. 4 Examples of spectral profiles.

(a), (b), and (c) are the spectra for the routes of inter-NP transfer ($6_{-1} - 1_{-2}$), intra-NP transfer ($1_{-1} - 1_{-2}$), and local transfer ($1_{-1} - 1_{-1}$), which are represented by the red, blue, and green arrows, respectively.
$\langle E_C \rangle$: The energy at the spectral center. δE_C: The spectral width.

In order to understand the features of these complicated and wide spectral profiles, the energy $\langle E_C \rangle$ at the spectral center is calculated by taking an average of C_n, with $|\lambda_n|$ used as a weighting factor:

$$\langle E_C \rangle = \sum_{n=1}^{72} |\lambda_n| C_n \Big/ \sum_{n=1}^{72} C_n \quad . \tag{3}$$

The spectral width, a measure for representing the magnitude of energy fluctuations, is evaluated by the value of the standard deviation δE_C:

$$\delta E_C = \sqrt{\langle E_C^2 \rangle - \langle E_C \rangle^2} \quad . \tag{4}$$

3 The energy at the spectral center and the magnitude of fluctuations

The left, center, and right parts of Fig. 5 show the energies $\langle E_C \rangle_R$, $\langle E_C \rangle_B$, and $\langle E_C \rangle_G$ at the spectral centers for red (n=1–20), blue (n=21–46), and green (n=47–72) arrows, respectively. This figure indicate that their average values ($\langle \bar{E}_C \rangle_R$, $\langle \bar{E}_C \rangle_B$, and $\langle \bar{E}_C \rangle_G$) satisfy the inequality

$$\langle \bar{E}_C \rangle_G > \langle \bar{E}_C \rangle_R > \langle \bar{E}_C \rangle_B . \tag{5}$$

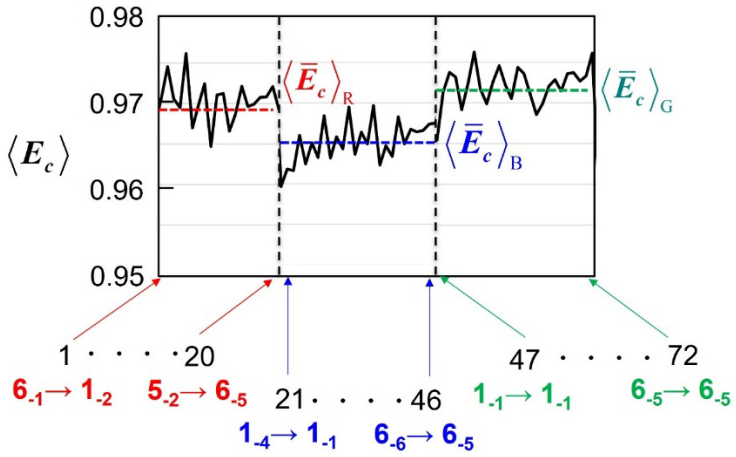

Fig. 5 The energy at the spectral center.
$\langle \bar{E}_C \rangle_R$, $\langle \bar{E}_C \rangle_B$, and $\langle \bar{E}_C \rangle_G$ are the average values for red (n=1–20), blue (n=21–27), and green (n=28–72) arrows. They are represented by horizontal broken lines.

It should be noted that the temporal behavior of the probability amplitude of eq. (1) is the unitary transform of its initial value $\vec{\psi}_{0,(0,0)}$ and is expressed as

$$\vec{\psi}_{t,(x,y)} = \exp(i(E/\hbar)t)\vec{\psi}_{0,(0,0)}, \tag{6}$$

where E is the energy. Since the exponential function in this expression indicates that the speed of the temporal variation of $\vec{\psi}_{t,(x,y)}$ is proportional to E, the inequality of eq. (5) is transformed to

$$s_G > s_R > s_B, \tag{7}$$

where s_R, s_B, and s_G represent the transfer speeds of the DPPs that pass through the red, blue, and green arrows, respectively. That is, the transfer speeds on these arrows are different from each other. This difference is a possible origin of the pulsative behavior that was pointed out at the end of Section 1 (Fig. 2(a) in ref. [5]).

The discussions above are for the arrangement of Figs. 1 and 2, in which five spokes are

connected (n_{con} =5). However, since ref. [5] dealt also with arrangements in which some spokes were lost, the discussions below deal with these arrangements, as shown in Fig. 6. (The arrangement {1} in this figure corresponds to that of Figs. 1 and 2.) Table 1 summarizes the numbers of arrows for arrangements {1} to {9}.

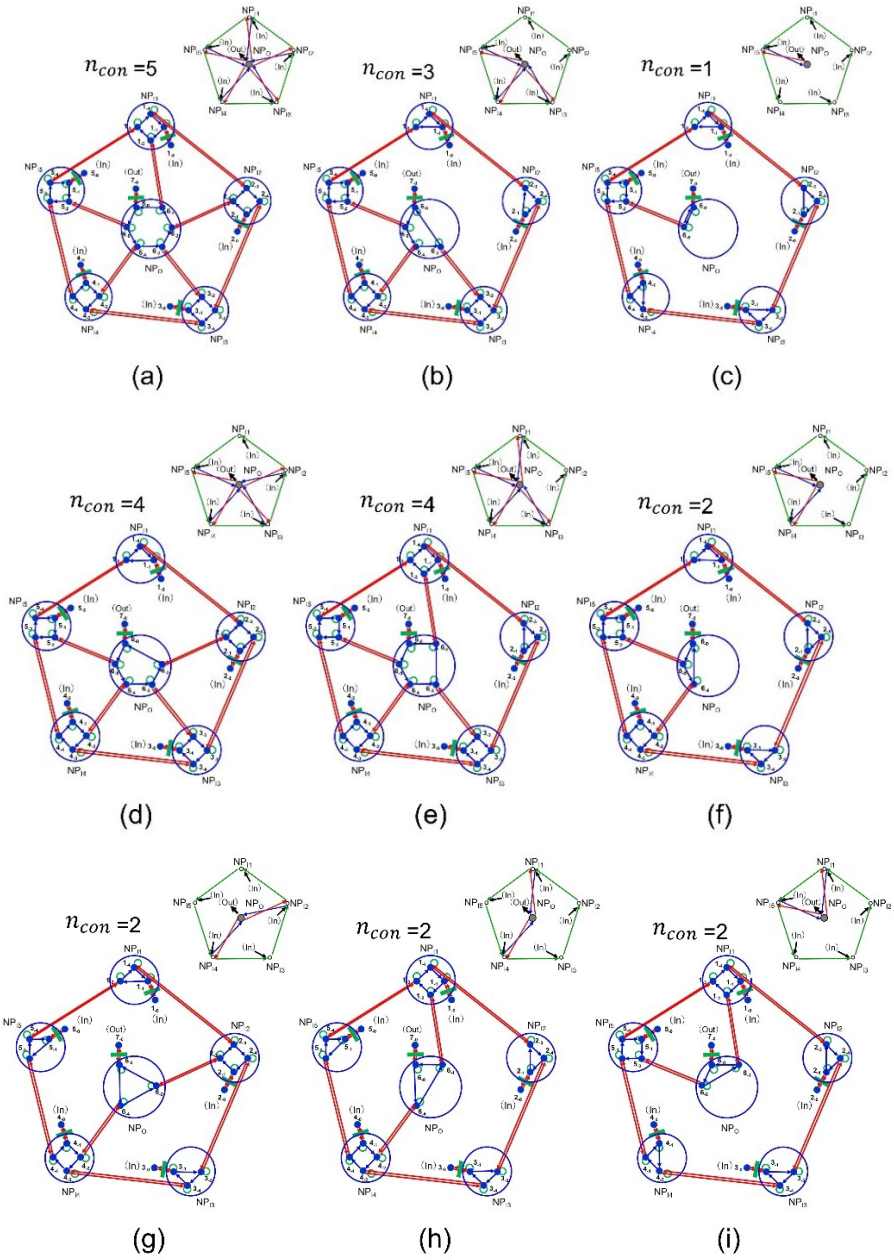

Fig. 6 Blown-up QW models for nine arrangements.

(a)-(c) Arrangements {1}–{3}, for which the number of connected spokes, n_{con}, is odd (=5,3,1).

(d)-(f) Arrangements {4}–{6}, for which the number of connected spokes, n_{con}, is even (=4,4,2).

(g)-(i) Arrangements {7}–{9}, for which the number of connected spokes, n_{con}, is even (=2,2,2).

Table 1 The numbers of arrows for arrangements {1}–{9}.

The number n_{con} of the connected spokes is odd for {1}–{3} and even for {4}–{9}.

Arrangement	n_{con}	Number of red arrows	Number of blue arrows	Number of green arrows	Total number of arrows N
{1}	5	20	26	26	72
{2}	3	16	22	22	60
{3}	1	12	18	18	48
{4}	4	18	24	24	66
{5}	4	18	24	24	66
{6}	2	14	20	20	54
{7}	2	14	20	20	54
{8}	2	14	20	20	54
{9}	2	14	20	20	54

Figure 7(a) shows the averaged values $\langle \bar{E}_{\mathrm{C}} \rangle_{\mathrm{R}}$, $\langle \bar{E}_{\mathrm{C}} \rangle_{\mathrm{B}}$, and $\langle \bar{E}_{\mathrm{C}} \rangle_{\mathrm{G}}$. It shows that the inequality of eq. (5) for arrangement {1} holds also for arrangements {2}–{9}. Furthermore, it shows that the averaged values ($\langle \bar{E}_{\mathrm{C}} \rangle_{\mathrm{R}}$, $\langle \bar{E}_{\mathrm{C}} \rangle_{\mathrm{B}}$, and $\langle \bar{E}_{\mathrm{C}} \rangle_{\mathrm{G}}$) are the smallest for arrangement {3}, in which the n_{con} is the smallest (=1). In contrast, Fig. 7(b) shows that the calculated value of the average $\delta \bar{E}_{\mathrm{C}}$ of the standard deviation of eq. (4) is the largest for arrangement {3} (n_{con}=1).

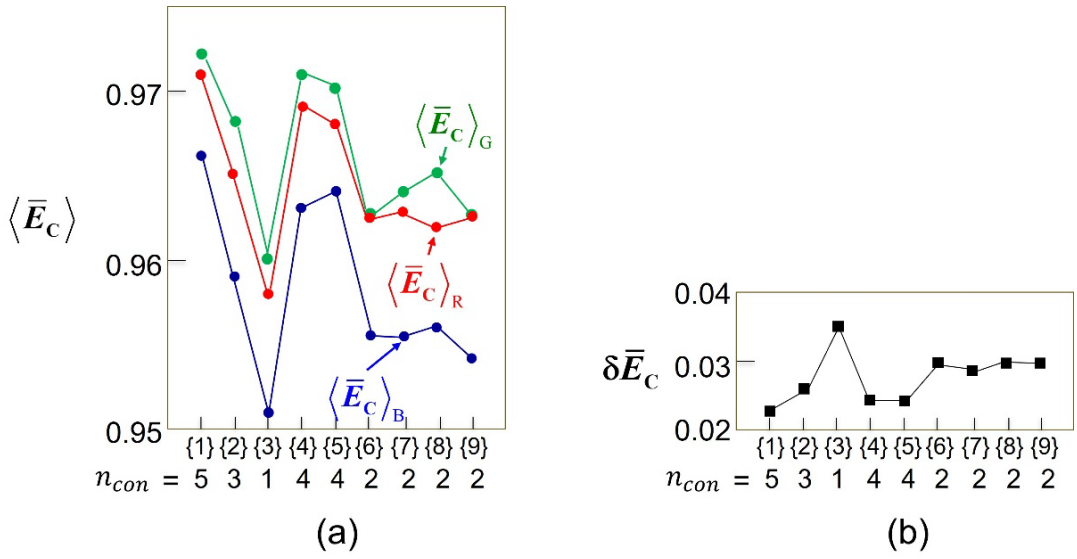

Figures 7 Calculated values for arrangements {1}–{9}.

(a) The value $\langle \bar{E}_{\mathrm{C}} \rangle_{\mathrm{R}}$, $\langle \bar{E}_{\mathrm{C}} \rangle_{\mathrm{B}}$, and $\langle \bar{E}_{\mathrm{C}} \rangle_{\mathrm{G}}$.

(b) The average $\delta \bar{E}_{\mathrm{C}}$ of the standard deviation for the green, red, and blue arrows. Since the values for these three arrows were nearly equal, they are represented by black squares.

4 Relation between the total number of arrows and the transfer speed

Figure 8(a) shows the calculated values of the average $\langle \bar{E}_{\mathrm{C}} \rangle_{\mathrm{Total}}$ that were derived by combining the values of $\langle \bar{E}_{\mathrm{C}} \rangle_{\mathrm{R}}$, $\langle \bar{E}_{\mathrm{C}} \rangle_{\mathrm{B}}$, and $\langle \bar{E}_{\mathrm{C}} \rangle_{\mathrm{G}}$. This figure indicates that the value $\langle \bar{E}_{\mathrm{C}} \rangle_{\mathrm{Total}}$ is the smallest for arrangement {3}, as was the case of Fig. 7(a). It is fairly small for arrangements {6}–{9}.

In order to understand this, Fig. 8(b) shows the values $\langle \bar{E}_{\mathrm{C}} \rangle_{\mathrm{Total}}$ that were plotted as a function of the total number of arrows, N, for arrangements {1}–{9}. By referring to eq. (6), the linear relation between N and $\langle \bar{E}_{\mathrm{C}} \rangle_{\mathrm{Total}}$ in this figure indicates that the transfer speed increases with increasing N. Thus, in the case where the number of connected spokes is large (n_{con}=5; arrangement {1} in Fig.6; N=72), the DPP rapidly transfers to reach the OST even though it has to pass through the large number of arrows. In contrast, in the case of a small n_{con} (n_{con}=1; arrangement {3} in Fig.6; N=48), the DPP slowly transfers to reach the OST even though the number of arrows is small. It can be presumed that such a unique nature of the DPP transfer is governed not by the on-shell scientific principle of least action but by the off-shell scientific principle of maximizing the average entropy generation, as has been pointed out in refs. [8,9].

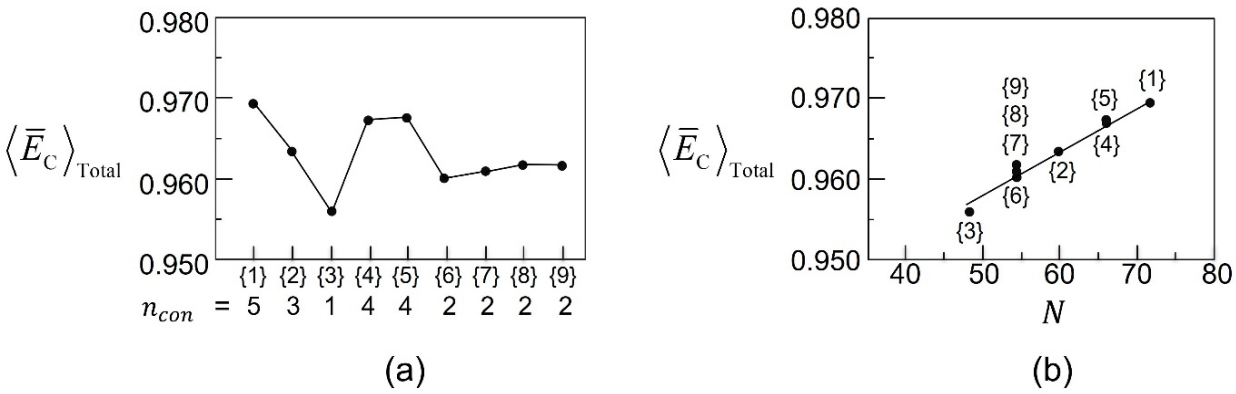

Fig. 8 Calculated values of the average $\langle \bar{E}_{\mathrm{C}} \rangle_{\mathrm{Total}}$.

(a) Horizontal axis: Arrangements {1}–{9} and the number of connected spokes, n_{con}.

(b) Horizontal axis: The total number of arrows, N, for arrangements {1}–{9}.

5 Summary

This paper analyzed the dynamic behavior of DPP energy transfer by using a blown-up quantum walk model. Numerical calculations were carried out in the case where a large $\mathrm{NP_O}$ (an output signal terminal: OST) was surrounded by five small particles $\mathrm{NP_I}$s (input signal terminals: ISTs).

Spectral profiles of the DPP transfer indicated that the speeds of the inter-NP transfer, intra-NP transfer, and local transfer were different from each other. This difference was the possible origin of the pulsative behavior that was found in the transitional period.

In the case where the number of transfer routes was large, the DPP rapidly transferred to reach the OST. In contrast, in the case where this number was small, the DPP transferred slowly. It was presumed that such a unique nature of the DPP transfer is governed by the off-shell scientific principle of maximizing the average entropy generation.

References

[1] H. Sakuma, I. Ojima, M. Ohtsu, and T. Kawazoe, Drastic advancement in nanophotonics achieved by a new dressed photon study," *J. European Opt. Soc.-Rapid Publication* (*JEOS-RP*) (2021) **17**: 28.

[2] H. Sakuma, I. Ojima, and M. Ohtsu, "Perspective on an Emerging Frontier of Nanoscience Opened up by Dressed Photon Studies," *Nanoarchitectonics*, Vol. 5, Issue 1 (2024) pp.1-23.

[3] M. Ohtsu and H. Sakuma, Dressed Photons to Revolutionize Modern Physics (Springer, Heidelberg, 2025).

[4] M. Ohtsu, E. Segawa, K. Yuki, and S. Saito, "Quantum walk analyses of the off-shell scientific features of dressed-photon–phonon transfers among a small number of nanometer-sized particles," *Off-shell Archive* (July, 2024) Offshell: 2407O.001.v1. **DOI** 10.14939/2407O.001.v1

[5]M. Ohtsu, E. Segawa, K. Yuki, and S. Saito, "Bright and dark walks for dressed-photon–phonon transfer," *Off-shell Archive* (January, 2025) Offshell: 2501O.001.v1. **DOI** 10.14939/2501O.001.v1

[6] Y. Higuchi and E. Segawa, "Quantum walks on graphs embedded in orientable surfaces," Annales de l'Institut Henri Poincaré D (2025), Online first, DOI 10.4171/AIHPD/206 arXiv: 2402.00360.

[7] M. Ohtsu, "A Quantum Walk Model for Describing the Energy Transfer of a Dressed Photon," *Off-shell Archive* (September, 2021) Offshell: 2109R.001.v1. **DOI** 10.14939/2109R.001.v1

[8] I. Ojima, "Entropy generation and van Hove limit," Theoretical Particle Physics, vol. 78, no. 2 (1988) pp. B14-B41 (in Japanese). **DOI** https://doi.org/10.24532/soken.78.2_B14

[9] M. Ohtsu, E. Segawa, K. Yuki, and S. Saito, "Optimum dissipation for governing the autonomous transfer of dressed photons, "*Off-shell Archive* (May, 2024) Offshell: 2405O.001.v1. **DOI** 10.14939/2405O.001.v1

Bright and dark walks for dressed-photon–phonon transfer

M. Ohtsu[1], E. Segawa[2], K. Yuki[3], and S. Saito[4]

[1]Research Origin for Dressed Photon,3-13-19 Moriya-cho, Kanagawa-ku, Yokohama, Kanagawa 221-0022, Japan

[2]Yokohama National University, 79-8 Tokiwadai, Hodogaya-ku, Yokohama, Kanagawa 240-8501, Japan

[3]Middenii, 3-3-13 Nishi-shinjuku, Sinjuku-ku, Tokyo 160-0023, Japan

[4]Kogakuin University, 2665-1, Nakano-machi, Hachioji, Tokyo 192-0015, Japan

Abstract

This paper analyzes the dressed-photon–phonon energy transfer from several nanometer-sized particles for an input signal terminal (NP_I) to that for output signal terminals (NP_O), which are arranged in rotationally symmetric and asymmetric manners. A quantum walk model is used for numerical calculations by assuming a pentagonal wheel arrangement. In the case where the number n_{con} of connected spokes of the wheel is odd, the signal transfer route is a triply degenerate bright walk. In the case where n_{con} is even, this route is decomposed into bright and dark walks. Since some input signals are injected into the dark walk and are confined in this walk, the output signal transfer rate is smaller than that in the case of the odd n_{con}. The degeneracy in the bright walk and confinement in the dark walk are found also in other polygonal arrangements. It was demonstrated that their features are independent of the number of NP_I on the rim of the wheel of these arrangements.

1. Introduction

Theoretical studies on the creation process of dressed photons (DPs) have made striking progress in recent years and have succeeded in drawing an intuitive physical picture based on the concept of Majorana fermions [1,2]. In parallel with these studies, intensive experimental studies have precisely evaluated the intrinsic features of the energy transfer between nanometer-sized particles (NPs) mediated by dressed-photon–phonons (DPPs) for a variety of applications [3,4]. A typical example of such applications is optical-wavelength conversion, which is realized by the DPP energy transfer from a small NP to a large NP [5]. It was confirmed that the optical/electrical energy conversion efficiency of a solar cell battery was increased by utilizing the optical-wavelength conversion realized by dispersing NPs into a resin film and installing the film on the surface of the battery.

The intrinsic characteristics of the DPP energy transfer between these NPs have been analyzed based on a quantum walk (QW) model [6]. The reasons why the QW model was successfully used in these analyses were due to two features that were common to the dynamic properties of the QW model and the DPP energy transfer process: *non-commutativity* and *localization* [7]. Numerical calculations based on the results of these analyses have been carried out in the case where a large NP for the output

signal terminal (NP_O) was surrounded by small NPs for the input signal terminals (NP_Is) in a rotationally symmetric manner [6]. Figure 1(a) schematically illustrates this arrangement, in which NP_O is fixed on a hub at the center of a wheel. NP_Is are fixed on the rim and are connected to each other. They are also connected to NP_O, as represented by spokes. These rim and spokes represent the DPP energy transfer routes. It was confirmed by numerical calculations that the efficiency of the energy transfer from NP_Is to NP_O was the highest when the number of NP_Is was in the range between 4 and 6, which revealed unique autonomous features of the DPP energy transfer.

In order to advance the analyses and discussions on the DPP energy transfer, the present paper reports the results of numerical calculations for the case where the rotational symmetry above is broken.

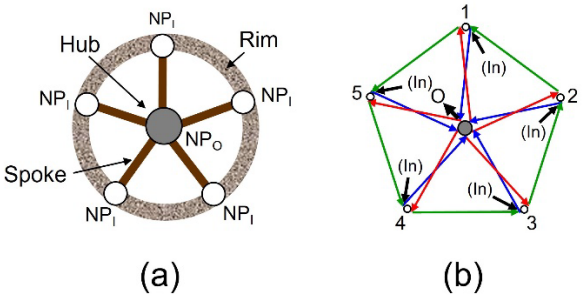

Fig. 1 Rotationally symmetric arrangement of nanometer-sized particles (NPs).

(a) Schematic explanation of a wheel. NP_Is and NP_O are fixed on the rim and on a hub at the center of a wheel, respectively. (b) A pentagonal arrangement of five NP_Is and one NP_O. Five NP_Is on the rim serve as the input signal terminals (ISTs). The NP_O at the hub serves as the output signal terminal (OST). Red and blue arrows represent the directions of signal transfer from and to the hub, respectively. Green arrows represent the transfer direction from one NP_I to the adjacent one on the rim. Short black arrows at the ISTs and OST represent the directions of the input signal injection and output signal transfer, respectively. The symbol **(In)** indicates that the input signal is injected to the ISTs inside the facial closed walk.

2. A quantum walk model

As an example of the broken rotational symmetry, this paper adopts the case in which several spokes between NP_I and NP_O are disconnected. This disconnection is experimentally plausible when the optical properties of the relevant NP_I are deteriorated or the separation between the NP_I and NP_O is extraordinarily large.

Preliminary numerical calculations have been carried out based on the quantum master equations for the creation probabilities of excitons in the NPs [8]. However, since these calculations did not deal with DPP creation probabilities, they were inconsistent with the off-shell science of the theoretical framework of the DPP creation process. Even so, several suggestive results were obtained. One of such results is that, even when several spokes were disconnected, the output signal intensity was as high as, or even higher than that without any disconnections. This reveals that the DPP energy reaches the NP_O by ingeniously detouring via routes to avoid disconnected spokes. This feature

suggests the autonomous features mentioned in Section 1.

In order to compare with the preliminary results above, in the present work we carried out numerical calculations based on the QW model in ref. [6] by assuming that N NP_Is are arranged around NP_O. As was the case of ref. [8], a pentagonal arrangement is dealt with (N=5). The results for tetragonal (N=4) and hexagonal (N=6) arrangements are also presented.

3. Results of numerical calculations

The results of numerical calculations for the pentagonal arrangement elucidated that the value of the output signal transfer rate (OSFR) depended on whether the number n_{con} of connected spokes was odd or even. Sections 3.1 and 3.2 present the results for these two cases. Section 3.3 claims that these features are independent of the total number N of corners of the polygon.

3.1. An odd number n_{con} of connected spokes

a. The case of n_{con}=5

Figure 1(b) shows that five NP_Is are fixed on the rim. They work as the input signal terminals (ISTs). NP_O is fixed at the hub and works as the output signal terminal (OST). Short black arrows connected to these terminals represent the directions of the input signal injection and output signal transfer, respectively. The symbol **(In)** indicates that the input signal is injected to the IST inside the facial closed walk. This figure also shows that the number N_{in} of these input signals is 5, which means that all of the input signals transfer from the IST to the OST and generate the output signal. Thus, the transfer routes in Fig. 1(b) are called a bright walk.

Figure 2(a) shows the results of numerical calculations. The horizontal axis represents the time passed after starting the input signal injection. The curve O is the OSTR that is emitted to the outer space by energy dissipation at the OST. The curves 1–5 are the input signal transfer rates (ISTRs) from the ISTs 1–5 to the OST. This figure shows that the values of the curves 1–5 are different from each other even though the five NP_Is in Fig. 1(b) are arranged in a rotationally symmetric manner. This indicates that the signal transfer features do not reflect the rotational symmetry, which was due to the output signal extraction. That is, the symmetry was broken by adding the short black arrow at the hub.

By comparing the stationary values of curves 1–5 a sufficiently long time after the input signal injection, it is found that the value for curve 1 is the largest, and those of curves 3, 5, 2, and 4 are smaller in this order. The first row of Table 1 summarizes these stationary values. This order depends on the distance of the signal transfer routes to the OST. Since the distance from IST 1 to the OST is the shortest (Fig. 2(b)), the injected signal reaches the OST most efficiently, making the stationary value of the curve 1 the largest. In contrast, since that from IST 4 to the OST is the longest,

the stationary value of curve 4 is the smallest.

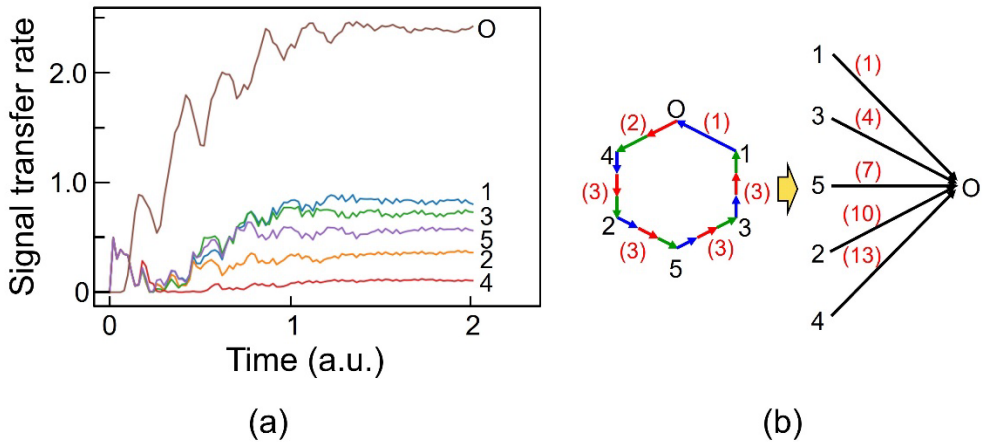

Fig. 2 Results of numerical calculations for the arrangement in Fig. 1(b).

(a) Temporal variations of the input and output signal transfer rates (ISTR and OSTR). Curve O is for the OSTR. Curves 1–5 are for the ISTRs from the ISTs 1–5.

(b) (Left) Number of steps required to transfer from one terminal to the other. They are the numbers of red, blue and green arrows in Fig. 1(b)). (Right) The number in ( ) represents the number of steps that represents the distance from each IST to the OST.

b. The case of n_{con} =3

Figure 3 shows the arrangement for n_{con} =3 in which spokes 1 and 2 are disconnected. It also shows that N_{in} =5, as was the case in Fig. 1(b). That is, all the input signals transfer to the OST and generate the output signal. Thus, the transfer routes in Fig. 3 are also the bright walk. Figure 4(a) shows the results of numerical calculations. The second row of Table 1 summarizes the stationary values for the curves O and 1–5. Since the distance from IST 3 to the OST is the shortest (Fig. 4(b)), the injected signal reaches the OST most efficiently, making the stationary value of the curve 3 the largest. In contrast, since that from IST 4 to the OST is the longest, the stationary value of curve 4 is the smallest. This distance-dependent feature is consistent with that of Fig. 2(b).

The results of numerical calculations for the cases of disconnecting the spokes 1 and 3 and also the spokes 2 and 4 are equal to those in Fig. 4. Their stationary values are given in the third and fourth rows of Table 1, respectively.

By comparing the stationary values of the OSFR on the second-to-fourth rows of Table 1 with that of the first row (n_{con} =5), it is easily found they are equal to each other. Furthermore, the values of the ISFRs are equal in spite of the fact that they change their positions in each row. It is confirmed from these equalities that the walks of n_{con} =5 and 3 are degenerate.

Table 1 Stationary values of the ISFR and OFSR. The number n_{con} of connected spokes is odd (=5,3, and 1).

	n_{con}	The terminal number of disconnected spokes	ISFR					OSFR
			From terminal 1	From terminal 2	From terminal 3	From terminal 4	From terminal 5	
1	5	N.A.	0.834	0.357	0.731	0.108	0.575	2.396
2	3	1,2	0.575	0.357	0.834	0.108	0.731	2.396
3	3	1,3	0.357	0.834	0.731	0.108	0.575	2.396
4	3	2,4	0.834	0.731	0.357	0.108	0.575	2.396
5	1	1,2,3,4	0.731	0.575	0.357	0.108	0.834	2.396

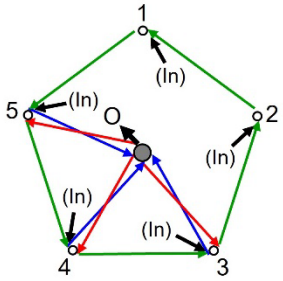

Fig. 3 Arrangement with two disconnected spokes 1 and 2.

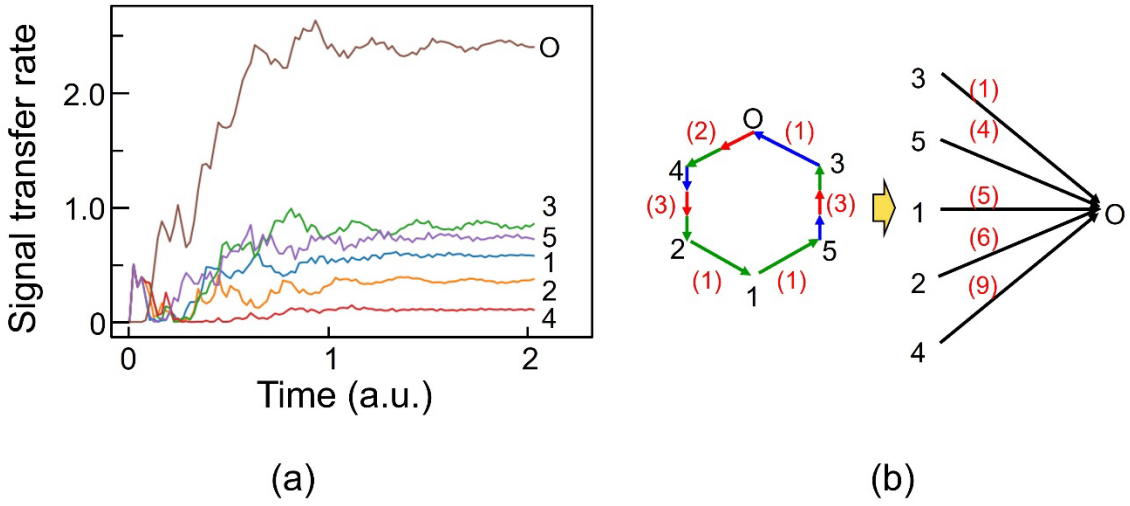

Fig. 4 Results of numerical calculations for the arrangement in Fig. 3.

For captions of (a) and (b), refer to those in Fig. 2.

c. The case of n_{con} =1

Figure 5 shows the arrangement of n_{con} =1 in which only spoke 5 survives. Even so, this figure

represents also N_{in} =5 and thus, the bright walk. Figure 6(a) shows the results of numerical calculations. The fifth row of Table 1 summarizes the stationary values for the curves O and 1–5. This figure and table show that the stationary value of curve 5 is the largest. This distance-dependent feature is consistent with that of Fig. 2(b) because the distance from IST 5 to the OST is the shortest (Fig. 6(b)). For other arrangements of n_{con} =1, numerical calculations gave results that are equal to those of Fig. 6(a). From this equality, it is confirmed that the bright walk of Fig. 5 is degenerate with the bright walks of **a.** (n_{con} =5) and **b.** (n_{con} =3).

To summarize the results of **a.** – **c.** above, all the input signals transfer to the NP_O through the bright walk and generate the output signal. Thus, even if some spokes are disconnected, the stationary values of the OSFR remain unchanged, which means that these bright walks are triply degenerate.

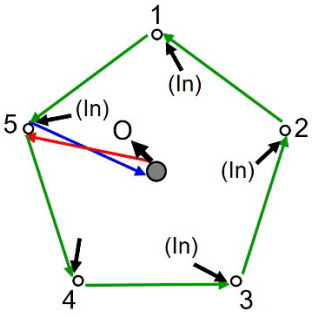

Fig. 5 Arrangement with four disconnected spokes 1–4.

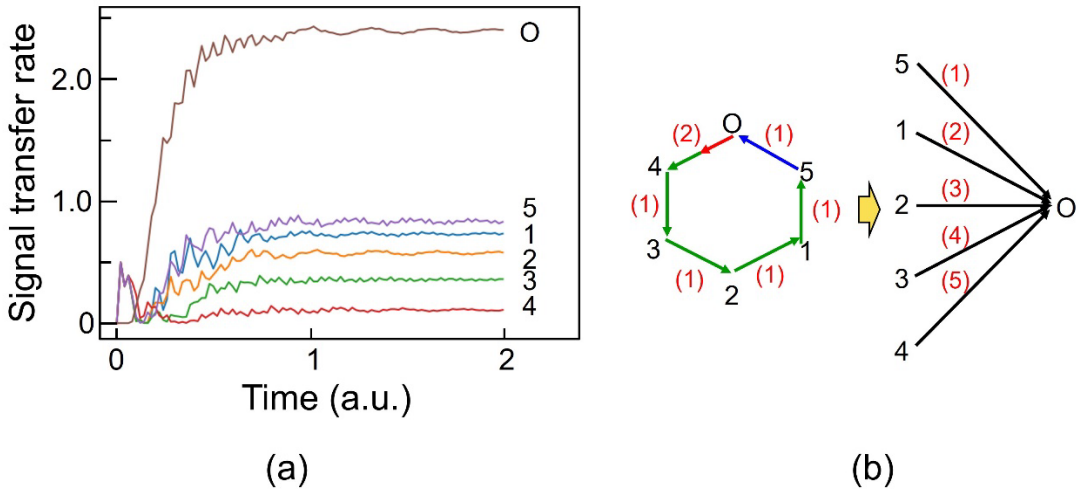

Fig. 6 Results of numerical calculations for the arrangement in Fig. 5.

For captions of (a) and (b), refer to those in Fig. 2.

3.2. An even number n_{con} of connected spokes

a. The case of n_{con} =4

The arrangements have two configurations **(1)** and **(2)** below.

(1) Figure 7(a) schematically illustrates the arrangement of disconnecting the spoke for IST 1, which can be decomposed into two modes (Fig. 7(b))*. Since the red and blue arrows for the transfer routes in Mode 1 contact the short black arrow for the output signal at the hub, the input signal is successfully converted to the output signal at the OST. In Mode 2, on the other hand, since these arrows do not contact the short black arrow at the hub, the input signal fails to be converted to the output signal. Instead, it is confined in the wheel. That is, Mode 2 represents the dark walk, while Mode 1 is the bright walk**.

Because Mode 2 does not generate the output signal, it is sufficient to carry out numerical calculations only for Mode 1. Here, it should be noted that the value of N_{in} is 2 for Mode 1 (Fig. 7(b)).

(*) These modes are orthogonal to each other. This is because the directions of the red arrows along the spokes are opposite between these modes. Those of the blue arrows are also opposite. Furthermore, the positions of the green arrows on the rim do not overlap between these modes.

(**) The bright and dark walks correspond to the bright and dark states of the electronic energy states in a molecule, respectively. These states have already been studied with respect to the DPP [9]. Furthermore, a method for building a buffer memory has been proposed by extracting the DPP energy confined in the dark state [10-13].

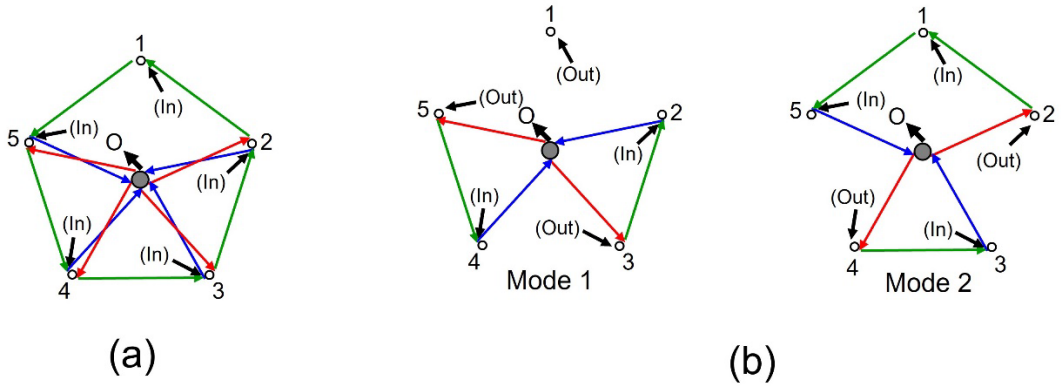

Fig. 7 Arrangement with one disconnected spoke 1.

(a) Schematic explanation of the arrangement. (b) Modes 1 and 2 correspond to the bright and dark walks, respectively. The symbol **(Out)** indicates that the input signal is injected to the ISTs outside the bright walk (Mode 1) and the dark walk (Mode 2).

Figure 8(a) and the first row of Table 2 show the calculated results. They represent the three features below.

1) The stationary value of the OSFR on curve O is smaller than the values of Fig. 2(a) and the first row of Table 1. This is because only the two input signals generate the output signal after transforming through the Mode 1 (bright walk) (N_{in} =2). Since the other three input signals transfer through the Mode 2 (dark walk) (N_{in} =3), they do not generate the output signal.

2) Curves 2 and 4 represent the ISFRs that transfer from ISTs 2 and 4 to the OST, respectively. Since

these input signals are injected into the bright walk of Fig. 7(b) (N_{in} =2), they generate the output signal. Since the distance from IST 2 to the OST is shorter than ~~equal to~~ that from IST 4 (Fig. 8(b)), the ISFR from the former is larger. This distance-dependent feature is ~~in~~consistent with those of Fig. 2(b).

3) Curves 1, 3, and 5 represent the ISFRs that transfer from ISTs 1, 3, and 5 to the OST, respectively. Since these input signals are injected into the dark walk of Fig. 7(b) (N_{in} =3), they are confined in this walk without generating the output signal.

The three features above are inherent to the rotational asymmetric arrangement. In the case of disconnecting the spoke for the IST with other odd number 3 or 5 (IST 3 or 5), the features are equivalent to those of Fig. 8.

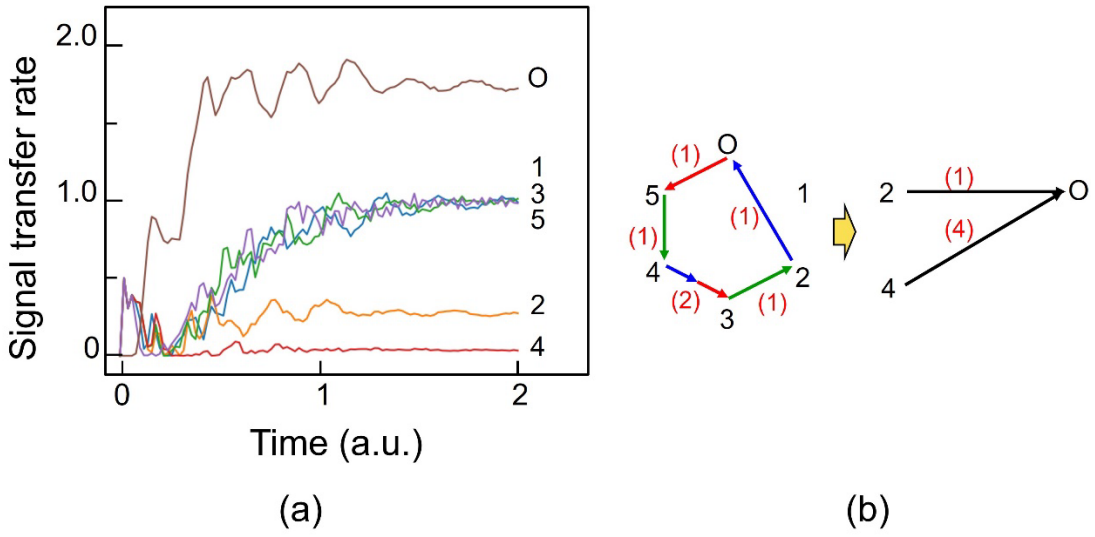

Fig. 8 Results of numerical calculations for the arrangement in Fig. 7.

For captions of (a) and (b), refer to those in Fig. 2.

Table 2 Stationary values of the ISFRs and the OSFRs. The numbers n_{con} of connected spokes are even (=4 and 2).

	n_{con}	The terminal number of the disconnected spokes	ISFR					OSFR
			From terminal 1	From terminal 2	From terminal 3	From terminal 4	From terminal 5	
1	4	1	1.000	0.260	1.000	0.034	1.000	1.706
2	4	2	0.541	0.312	1.000	0.070	1.000	2.077
3	2	1,2,3	1.000	1.000	1.000	0.000	1.000	1.000
4	2	1,3,5	1.000	0.260	0.034	1.000	1.000	1.706
5	2	2,4,5	0.260	0.034	1.000	1.000	1.000	1.706

(2) Figure 9 schematically explains the arrangement in the case of disconnecting the spoke for IST 2. Figure 10 and the second row of Table 2 show the calculated results. They represent features similar to those of Fig. 8. However, the OSFR is larger than that of **(1)** because the value of N_{in} is 3 for Mode 1 (bright walk). Figure 10(a) shows that the ISFRs in the dark walk (curves 3 and 5) are larger than those in the bright walk (curves 1, 2, and 4). However, they are confined in the dark walk without generating the output signal.

In the case of disconnecting the spoke for IST with the other even number 4 (IST 4), the features are equivalent to those of Fig. 10.

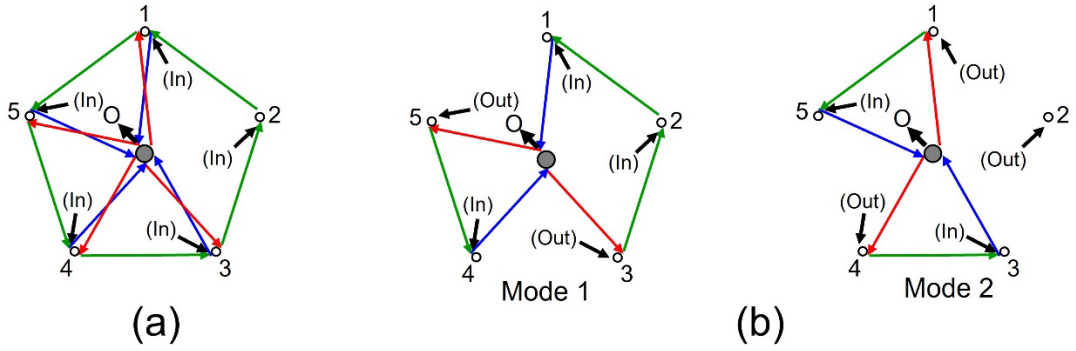

Fig. 9 Arrangement with one disconnected spoke 2.

(a) Schematic explanation of the arrangement. (b) Modes 1 and 2 are the bright and the dark walk, respectively.

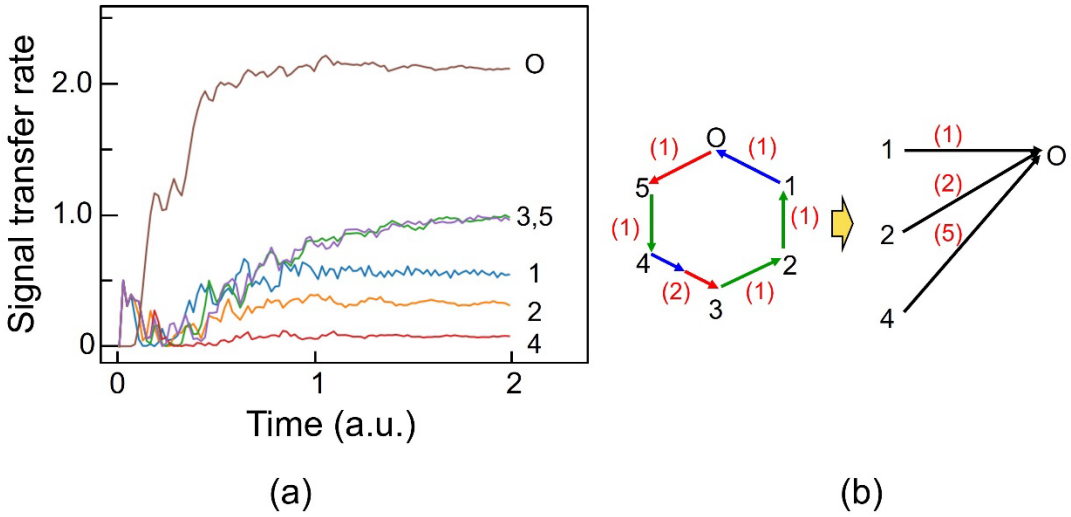

Fig. 10 Results of numerical calculations for the arrangement of Fig. 9.

For captions of (a) and (b), refer to those in Fig. 2.

b. The case of n_{con} =2

The arrangements have the two configurations below.

(1) In the case of the arrangement in which three consecutive spokes 1, 2, and 3 are disconnected (Fig. 11(a)), the value of N_{in} is 1 for Mode 1 (bright walk) (Fig. 11(b)). Figure 12(a) and the third row of

Table 2 show the calculated results for Mode1. Curves 1, 2, 3, and 5 represent the ISFRs to the OST. Since they are in the dark walk, they do not generate the output signal and are confined in the dark walk. Only the input signal 4 is injected into the bright walk. However, the third row of Table 2 indicates that the stationary value of the ISFR to the OST is zero. In the case of the arrangement in which three consecutive spokes 2, 3, and 4 are disconnected (Fig. 11(c)), the value of N_{in} is 4 for Mode 1 (bright walk), as is shown by Fig. 11(d). There are more arrangements in which three consecutive spokes are disconnected, for which the value of N_{in} is also 1 or 4. Their features are equivalent to those of Fig. 11.

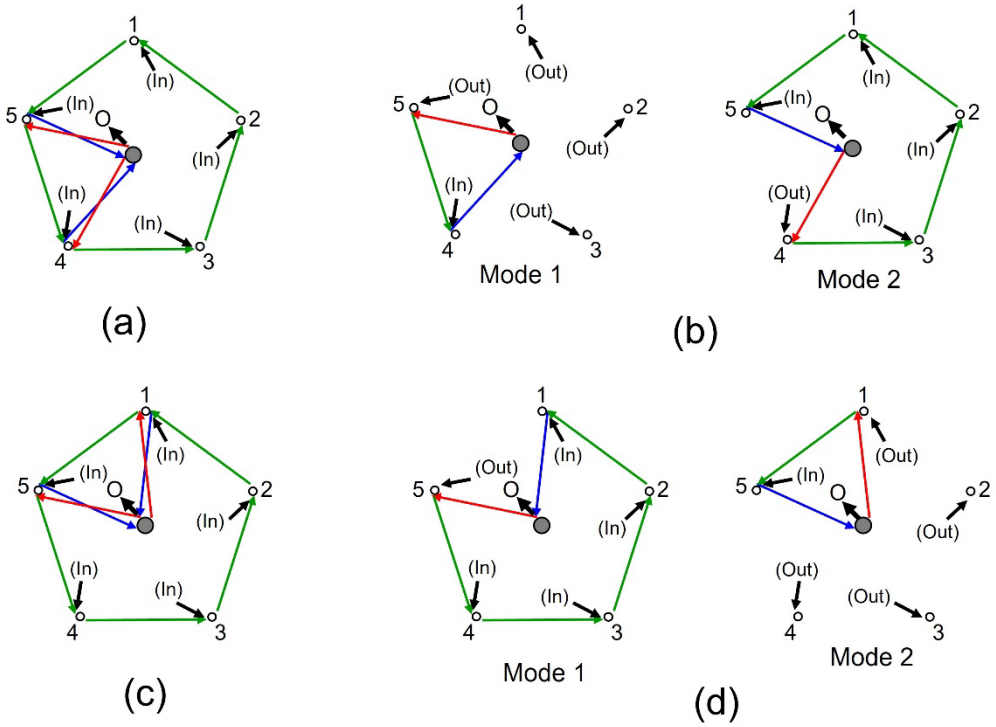

Fig. 11 Arrangement with three disconnected consecutive spokes.

(a) Schematic explanation of the arrangement with the disconnected spokes 1, 2, and 3.

(b) Tw modes for the arrangement (a). Modes 1 and 2 are the bright and dark walks, respectively.

(c) Schematic explanation of the arrangement with the disconnected spokes 2, 3, and 4.

(d) Two modes for the arrangement (a). Modes 1 and 2 are the bright and dark walks, respectively.

(2) Figure 13(a) shows the arrangement in which three spokes 1, 3, and 5 are disconnected. They are not consecutive but there are two connected spokes 2 and 4 between them. Figure 14(a) and the fourth row of Table 2 show the calculated results for Mode 1 (bright walk) (Fig. 13(b)). Since the value of N_{in} is 2 in this Mode 1, the OSFR is larger than that of **(1)** above (N_{in} =1). Other features are equivalent to those of **(1)**. Curves 1, 4 and 5 of Fig. 14(a) represent the ISFRs to the OST. Since ISTs 1, 4, and 5 are in the dark walk, they do not generate the output signal and are confined in the dark walk. ISTs 2 and 3 are in the bright walk. Here, the values of ISTRs 2 and 3 (curves 2 and 3) are smaller than the values of ISTRs 1, 4, and 5 (curves 1, 4, and 5).

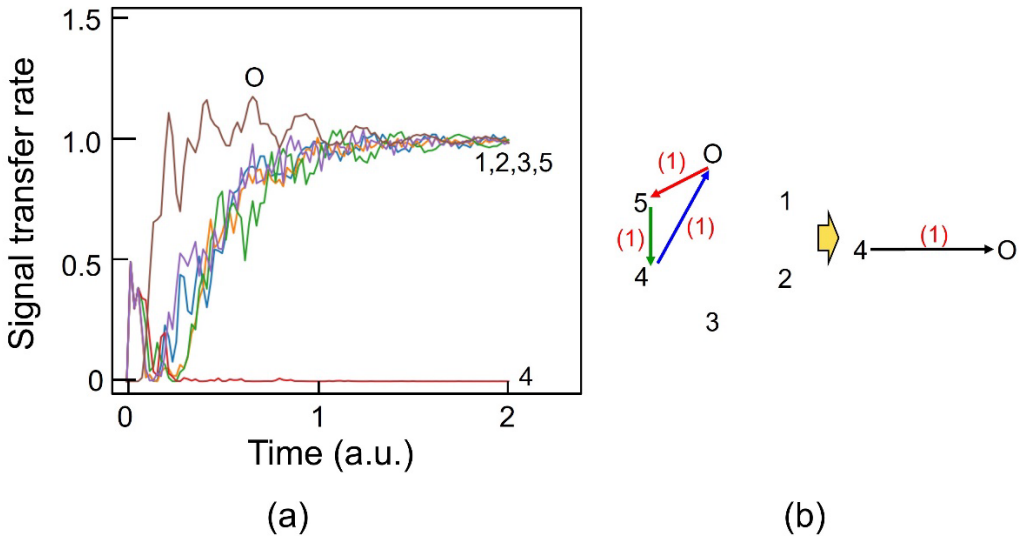

Fig. 12 Results of numerical calculations for the arrangement of Fig. 11(a).

For captions of (a) and (b), refer to those in Fig. 2.

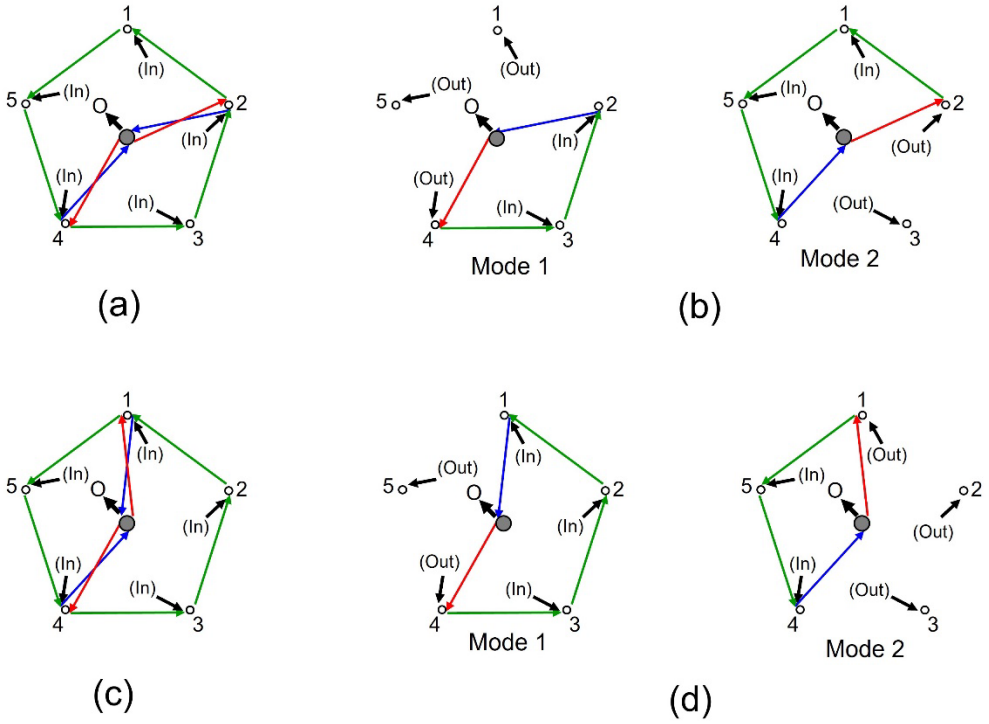

Fig. 13 Arrangement with three disconnected spokes between which two connected spokes exist.

(a) Schematic explanation of the arrangement with the disconnected spokes 1, 3, and 5.

(b) Tw modes for the arrangement (a). Modes 1 and 2 are the bright and dark walks, respectively.

(c) Schematic explanation of the arrangement with the disconnected spokes 2, 3, and 5.

(d) Two modes for the arrangement (a). Modes 1 and 2 are the bright and dark walks, respectively.

Figures 13(c) and (d) show the arrangement in which three spokes 2, 3, and 5 are

disconnected and between which connected spokes 1 and 4 exist. The value of N_{in} is 3 for Mode 1 (bright walk). There are more arrangements in which three spokes are disconnected, as is the case in Figs. 13(a)-(d) (refer to the fifth row of Table 2, as an example). Their values of N_{in} are also 2 or 3, and their features are equivalent to those of Fig. 13.

The third to fifth rows in Table 2 show that the values of the OSFR depend on whether three disconnected spokes are consecutive or not. Table 3 summarizes the relation between the number of connected spokes n_{con} and the value of N_{in} for Mode 1 (bright walk).

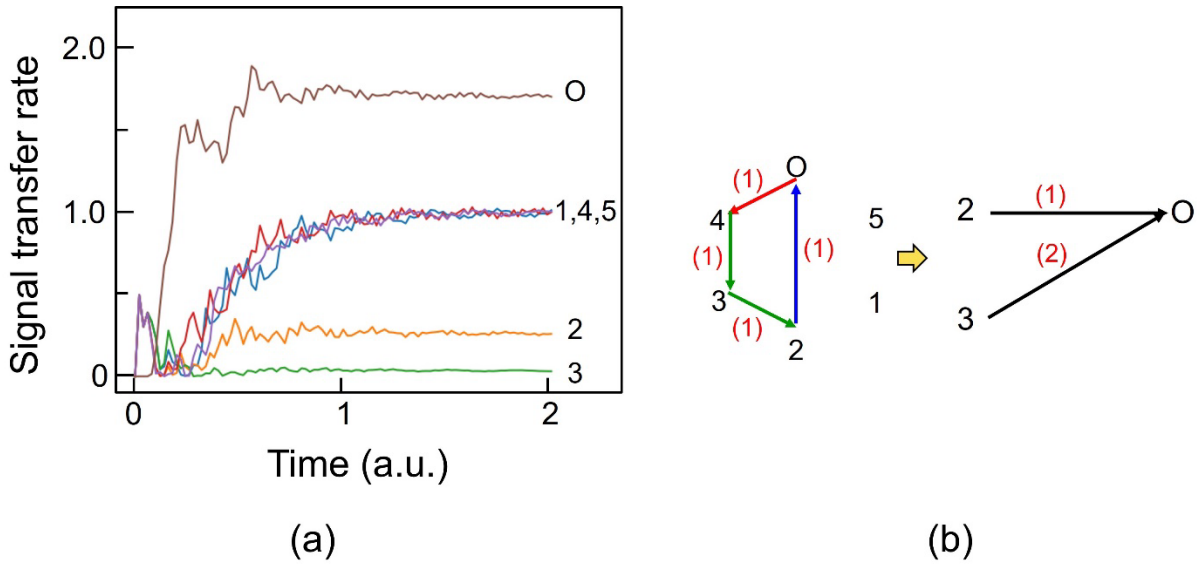

Fig. 14 Results of numerical calculations for the arrangement of Fig. 13(a).
For captions of (a) and (b), refer to those in Fig. 2.

Table 3 Relation between an even number n_{con} (=4 or 2) of connected spokes and the number N_{in} of the input signals injected into the bright walk.

	n_{con}	The terminal number of disconnected spokes	N_{in}
1	4	1	2
2	4	3	2
3	4	5	2
4	4	2	3
5	4	4	3
6	2	1,2,3	1
7	2	2,3,4	4
8	2	3,4,5	4

	n_{con}	The terminal number of disconnected spokes	N_{in}
9	2	4,5,1	1
10	2	5,1,2	1
11	2	1,3,5	2
12	2	2,3,5	3
13	2	1,2,4	2
14	2	2,4,5	2
15	2	1,3,4	3
16	2	2,3,5	3

To summarize **(1)** and **(2)** above, the signal transfer routes are composed of bright and dark

walks when the value of n_{con} is even. If the input signal is injected into the dark walk, it is confined in this walk without generating the output signal. Since only the input signal injected into the bright walk generates the output signal, the stationary value of the OSTR is lower than those in Section 3.1 in which the value of n_{con} is odd.

3.3. Relation between the number of connected spokes and stationary value of the output signal flow rate

Figure 15(a) summarizes the relation between the number n_{con} of connected spokes and the number N_{in} of the input signals injected to the bright walk. The symbol n_{dis} (=5-n_{con}) on the horizontal axis represents the number of disconnected spokes. Figure 15(b) is the relation between N_{in} and the OSFR β_{κ} that was derived from the QW theory [14]. This theory claims that the value of β_{κ} increases with increasing N_{in}, as is shown by Fig. 16. Figure 15(b) was derived by using the values of N_{in} in Fig. 15(a) and the relation in Fig. 16. The values of β_{κ} in Fig. 15(b) agree with the values of the OSFR in Tables 1 and 2.

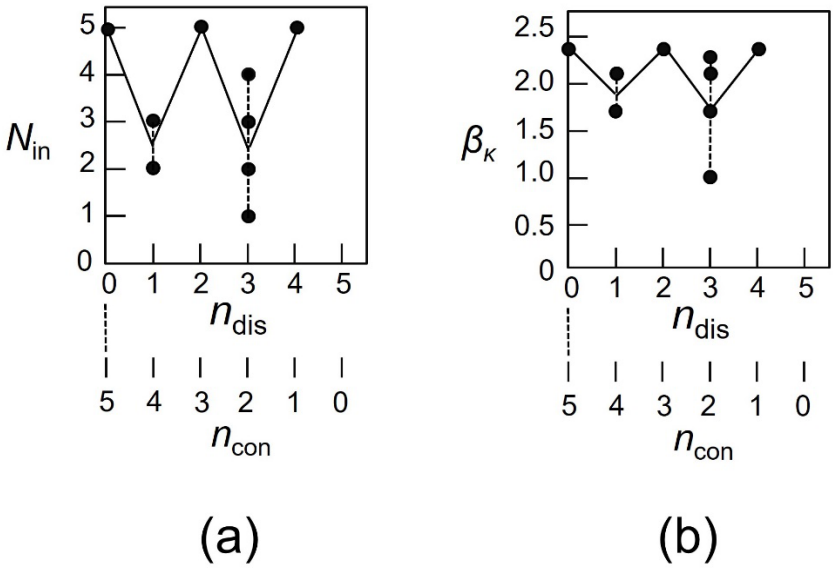

Fig. 15 Dependences of the numerically calculated values on n_{con}.
The symbol n_{dis} (=5-n_{con}) on the horizontal axis represents the number of disconnected spokes.
(a) The number N_{in} of input signals injected inside the bright walk.
(b)The output signal flow rate β_{κ} that was derived from the QW theory [14].

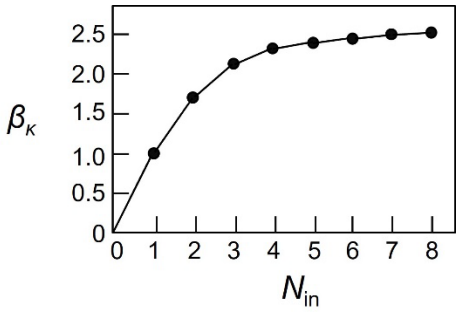

Fig. 16 Relation between N_{in} and β_K [14].

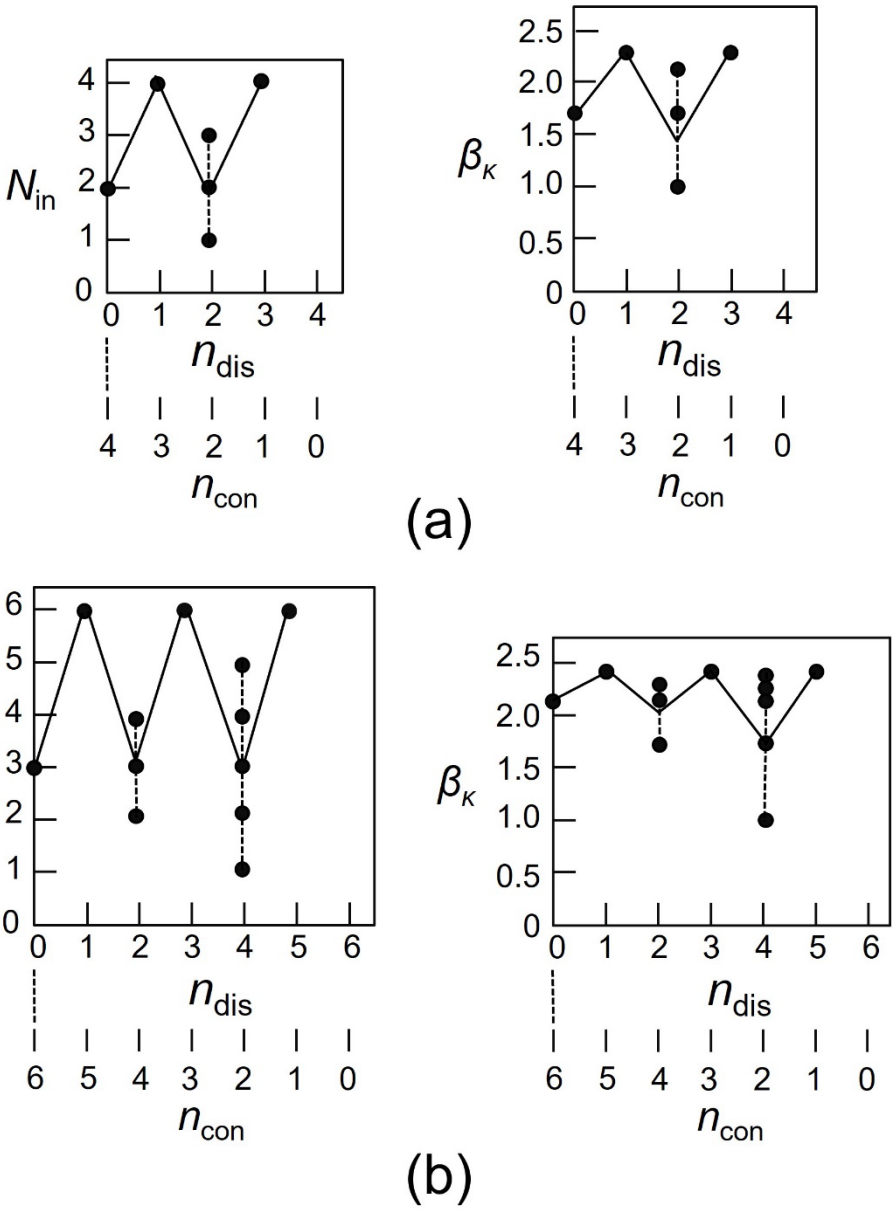

Fig. 17 Dependences of the results of numerically calculated values on n_{con}.
(a) and (b) are for tetrahedral and hexagonal arrangements, respectively.

Figures 15(a) and (b) show that the values of N_{in} and β_{κ} vary periodically, and are due to the following dependences **(1)** and **(2)** on n_{con} :

(1) In the case where the number n_{con} of connected spokes is odd, the signal transfer routes correspond to the bright walk, and thus, N_{in} =5 for the cases of n_{con} =1, 3, and 5. This means that the bright walks are triply degenerate.

(2) In the case where the number n_{con} of connected spokes is even (=2 or 4), the number N_{in} of the bright walk is smaller than 5, which is due to the existence of the dark walk. Thus, the OSFR is smaller than that of **(1)** because the input signals in the dark walk do not generate the output signal.

Figures 17(a) and (b) show the results of numerical calculations for tetrahedral and hexagonal arrangements, respectively. Their periodic variation features are consistent with those of Fig. 15, by which it was proved that these features are independent of the number of NP_I on the rim of the wheel. However, it should be noted that the periodically varying features of Fig. 17 are in anti-phase with respect to those of Fig. 15.

4. Summary

This paper reported that the DPP energy transfer routes are triply degenerate bright walks in the case where the number n_{con} of connected spokes is odd. Thus, even if some spokes are disconnected, the stationary values of the OSFR are kept equal to that of the arrangement without any disconnection. Such an n_{con} -independent feature is consistent with the results of preliminary numerical calculations [8].

In the case where the number n_{con} of connected spokes is even, the energy transfer routes are decomposed into bright and dark walks. Since some input signals are injected into the dark walk, the value of the OSFR is smaller than that of the case of the odd number of the connected spokes above.

The degeneracy in the bright walk and the existence of the dark walk above were found not only in the pentagonal arrangement but also in other polygonal arrangements, which showed that their features are independent of the number of NP_I on the rim of the wheel of these arrangements.

It will be interesting to find a method of extracting the confined signal from the dark walk to the outer system in order to use it in a variety of applications.

References

[1] H. Sakuma, I. Ojima, M. Ohtsu, and T. Kawazoe, Drastic advancement in nanophotonics achieved by a new dressed photon study, “JEOS-RP (2021) **17**: 28.

[2] H. Sakuma, I. Ojima, and M. Ohtsu, “Perspective on an Emerging Frontier of Nanoscience Opened up by Dressed Photon Studies,” *Nanoarchitectonics*, Vol. 5, Issue 1 (2024) pp.1-23.

[3] M. Ohtsu, *Dressed Photons*, Springer

[4] M. Ohtsu, Silicon LED and Lasers, Springer

[5] M. Naruse, T. Kawazoe, R. Ohta, W. Nomura, M. Ohtsu, "Optimal mixture of randomly dispersed quantum dots for

optical excitation transfer via optical near-field interactions," Phys. Rev. B **80**, 125325 (2009)

[6] M. Ohtsu, E. Segawa, K. Yuki, and S. Saito, "Quantum walk analyses of the off-shell scientific features of dressed-photon–phonon transfers among a small number of nanometer-sized particles," *Off-shell Archive* (July, 2024) Offshell: 2407O.001.v1. **DOI** 10.14939/2407O.001.v1

[7] M. Ohtsu and H. Sakuma, *Dressed Photon to Revolutionize Modern Physics*, Springer, Heidelberg (to be published in 2025) Section 4.1.

[8] M. Naruse, K. Leibnitz, F. Peper, N. Tate, W. Nomura, T. Kawazoe, M. Murata, M. Ohtsu, "Autonomy in excitation transfer via optical near-field interactions and its implications for information networking," Nano Commun. Networks **2**, (2011) pp. 189-195.

[9] M. Ohtsu, *Dressed Photons*, Springer, Heidelberg (2014) pp.38-39

[10] M. Ohtsu, *Dressed Photons*, Springer, Heidelberg (2014) pp.115-117.

[11] S. Sangu, K. Kobayashi, M. Ohtsu, IEICE Trans. Electron., **E88-C**, 1824 (2005)

[12] M.Ohtsu, "Novel functions and prominent performance of nanometric optical devices made possible by dressed photons," ," *Off-shell Archive* (April, 2019) Offshell: 1904O.001.v1. **DOI** 10.14939/1904O.001.v1

[13] M. Ohtsu, *Off-shell Applications in Nanophotonics*, Elsevier, Amsterdam (2021) pp.58-59.

[14] E. Segawa, S. Saito, K. Yuki, and M. Ohtsu, "Quantum walk simulation of energy transport problem for dressed photon on wheel graph," Abstracts of the 84th Jpn. Soc. Appl. Phys. Autumn Meeting, September 19-23, 2023 (Kumamoto Castle Hall and Online meeting), paper number 22p-A310-6.

Quantum walk and random walk behaviors of dressed-photon–phonon transfers

M. Ohtsu

Research Origin for Dressed Photon,3-13-19 Moriya-cho, Kanagawa-ku, Yokohama, Kanagawa 221-0022, Japan

Abstract

This paper reviews measured results on the temporal variation behavior of the dressed photon (DP) transfers between nanometer-size particles (NPs). The NPs are illuminated with a short optical pulse, and the resulting behavior of the emitted photoluminescence (PL) intensity is evaluated. Even after the optical pulse is turned off, the PL intensity exhibits nutation within a short time span. The envelope intensity of the nutation decreases due to adiabatic and non-adiabatic processes. They are described by using a quantum walk (QW) model and a random walk (RW) model, respectively. It is revealed that the values of several relevant quantities in these models must be adjusted in an appropriate manner to clearly observe the DP transfer features. The rate of conversion from the adiabatically dissipated energy to the non-adiabatically dissipated energy must also be adjusted. An antenna system composed of photosynthetic bacteria is presented, suggesting that a future direction of DP research is to draw a universal physical picture of DP transfers that are commonly found in nature.

1 Introduction

A dressed photon (DP) is a quantum field that is created by a photon–exciton (or electron) interaction in a nanometer-sized particle (NP). Recent theoretical studies on off-shell science have succeeded in drawing a precise physical picture of the DP creation process [1,2]. Furthermore, intensive experimental studies have confirmed that a dressed-photon–phonon (DPP) is created by DP–phonon coupling. These studies have also revealed a unique DPP transfer behavior between adjacent NPs, which was used to develop a variety of innovative technologies [3,4].

This paper indicates that short and long time-span temporal variations of the DPP transfer exhibit unique behaviors that can be described by quantum walk (QW) and random walk (RW) models.

2 Revisiting experimental results

This section reviews the experimentally confirmed temporal variation behaviors of the DPP transfer. Here, the DPP is replaced by a DP because the phonons in the DPP do not give any noticeable contributions to characterize the temporal variation behavior. Several features of these behaviors have been analyzed by using QW models [5–7][1)].

1) The reason why this analysis is possible is that the principles of the QW model and the nature of the DP have at least two features in common [7]:

(A) Nonreciprocity: A mathematical formulation of the QW uses nonreciprocal algebra involving vectors and matrices. On the other hand, the DP is a field that mediates the interaction between NPs. Since the interaction is a typical nonreciprocal physical process, the QW and DP have a common feature, represented by nonreciprocity.

(B) Site: The QW deals with the phenomenon of the energy transfer from one site to its neighbor. On the other hand, since the DP is spatially localized, its quantum mechanical position operator can be defined. Thus, in the case where the site of the QW is the NP on which the DP is created, the position of the DP is equivalent to that of the site of the QW.

2.1 Basic properties of temporal variation [8]

Figure 1(a) shows a pair of cubic CuCl NPs grown in a NaCl crystal. A small NP (NP_S) and a large NP (NP_L) correspond to nodes 1 and 2 in the QW model in Fig. 1(b). The DP transfers between these NPs and plays the role of a link in this model. The incident light (an optical pulse; pulse width of 10 ps and wavelength of 381 nm) in Fig. 1(a) corresponds to the input signal in Fig. 1(b). The created excitons in NP_S and NP_L emit photoluminescences (PL_1 and PL_2) that correspond to the output signals 1 (wavelength of 382 nm) and 2 (wavelength of 385 nm).

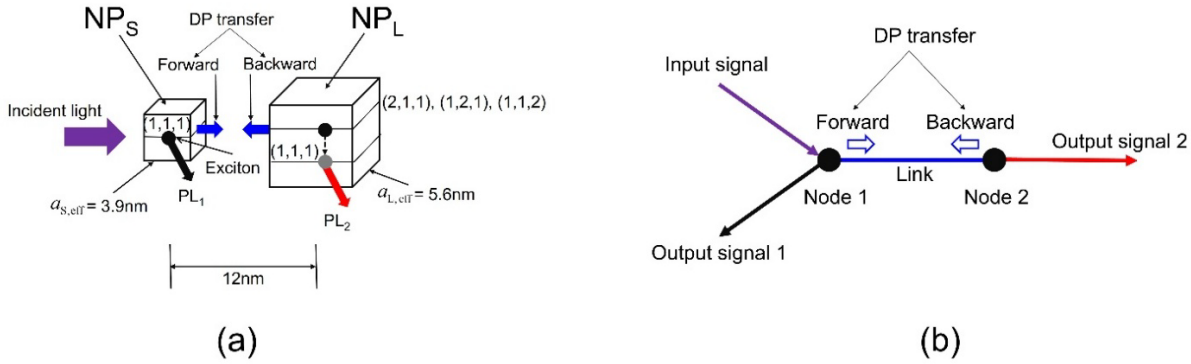

Fig. 1 A pair of NPs composed of small and large NPs (NP_S and NP_L).
(a) Experimental system. The exciton in NP_L has triply degenerate energy levels. (b) QW model.

The output signals are created by five successive steps. They are:

(Step 1) The incident light creates an exciton in the energy level (1,1,1) of NP_S.

(Step 2) This exciton emits PL_1 (the output signal 1) and also creates a DP.

(Step 3) The created DP transfers to the NP_L to excite an exciton in the triply degenerate energy levels (2,1,1), (1,2,1), and (1,1,2) of NP_L.

(Step 4) This exciton creates a DP, and the created DP transfers back to the NP_S.

(Step 5) This exciton is also de-excited to the lower energy level (1,1,1) of NP_L and subsequently emits PL_2 (the output signal 2).

As long as the incident light is applied, these five steps repeat, and the DP repeatedly transfers between NP_S and NP_L in a bi-directional manner (**Step 4**); this is called nutation. In the case where the incident light is an optical pulse, this bi-directional transfer is maintained within a short time-span even after the incident optical pulse is turned off. Thus, the intensities of PL_1 and PL_2 continue to pulsate due to the DP nutation.

However, these intensities gradually decrease due to non-radiative energy dissipation to the heat bath (the NaCl crystal), so that PL_1 and PL_2 fade away. This dissipation is composed of adiabatic and non-adiabatic processes. The former is the process in which the exciton in NP_s or NP_L excites other excitons (or electrons) in another NP or in the heat bath. The latter is the process in which the exciton energy is converted to thermal energy and is dissipated in the heat bath. The magnitude of the latter process depends on the device temperature, and the time constant of the PL intensity variation is longer than that due to the former process. Although these adiabatic and non-adiabatic processes contribute to the intensities of the outputs 1 and 2, the ratio of the magnitudes of these contributions has not been precisely evaluated by measurements. Theoretical studies are required to evaluate it.

The wavelength (385 nm) of the output signal 2 (PL_2) is longer than that of the output signal 1 (PL_1, 383 nm) because a part of the energy is dissipated from the triply degenerate energy level during the de-excitation to the lower energy level (1,1,1). Even though the magnitude of this dissipated energy is as low as 1/100 times the photon energy of the output signal 1, it is sufficiently large to spectrally resolve the output signals 1 and 2 for separate measurements.

Figure 1(b) can be redrawn as Fig. 2(a) by noting the triple degeneracy of the exciton energy levels in NP_L and the energy dissipation from these levels during the de-excitation to (1,1,1). For basic discussions of the QW process, Fig. 2(a) can be approximated by the simpler system in Fig. 2(b) because of the sufficiently low magnitude of the energy dissipation above.

Since the sizes, a_S and a_L, of NP_S and NP_L are different from each other, the magnitudes of the created DP energies and their spatial extents are different, as represented by a Yukawa-type function $V(r)$ ($\propto \exp(-r/a)/r$, where a is the size of the NP). Thus, because the time required for the DP transfer is inversely proportional to $V(r)$, the transfer times along the forward path (NP_S to NP_L) and backward path (from NP_L to NP_S) are different from each other.

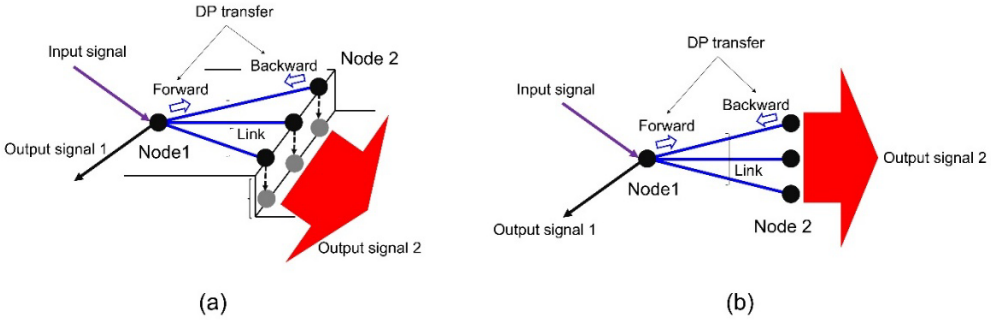

Fig. 2 The revised QW system.

For basic discussion, (a) is approximated by (b).

The black and red curves in Fig. 3(a) represent the measured temporal variations of PL_1 and PL_2 (the output signals 1 and 2), respectively. In the short time-span 0–500 ps immediately after applying the pulsed input signal, the intensity decrease is attributed to the adiabatic process and is fitted by $\exp(-t/\tau_{f1})$ (blue line) of the QW model, where τ_{f1} is the decay time constant. The subsequent decrease in the long time-span from 500 ps to 4 ns is slower and is fitted by $\exp(-\sqrt{t/\tau_{f2}})$ (red line) of the RW model, which is attributed to the non-adiabatic process [9]. The decay time constant τ_{f2} is longer than τ_{f1}.

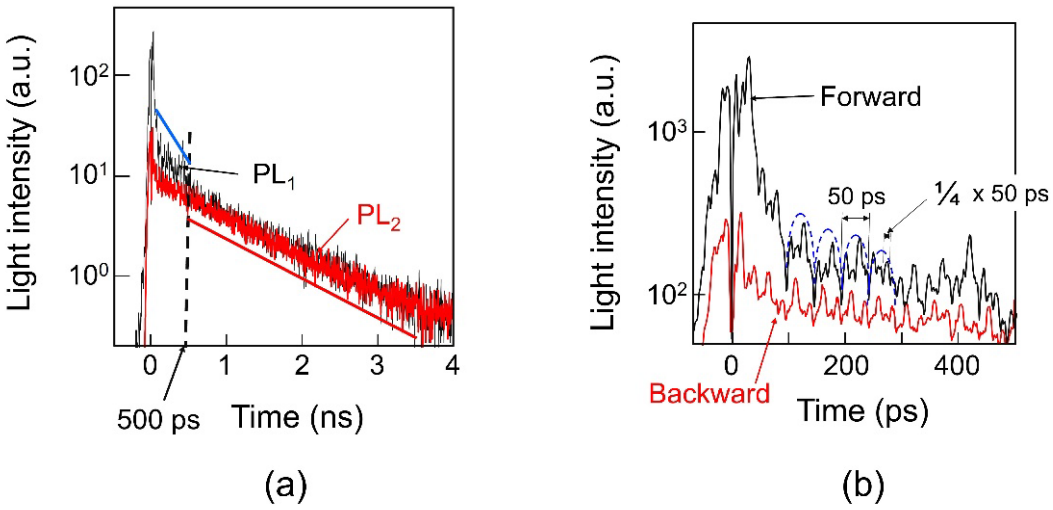

Fig. 3 The measured temporal variations of the PL_1 and PL_2 intensities.

(a) For the short time-span of 0-4 ns. The blue and red lines represent $\exp(-t/\tau_{f1})$ and $\exp(-\sqrt{t/\tau_{f2}})$, respectively.

(b) For the long time-span of 0-500 ps. The black and red curves indicate the temporal variations of the DP transfer along the forward and backward paths, respectively.

2.2 Characteristics caused by triple degeneracy [8]

Since the present paper focuses on the phenomena relevant to the QW process, Fig. 3(b) is presented by expanding the horizontal axis of Fig. 3(a) to analyze the temporal variations in the time-span 0–500 ps. The black and red curves indicate the magnified temporal variations of the DP energy transfer along the forward and backward paths, respectively. Their pulsatory variations represent nutation with a period of 50 ps. This value is compatible with the cycle time of 40 ps that was estimated from the relation between the NP_S–NP_L distance (10 nm) and the transferred DP energy (1×10^{-4} eV) [10].

Figure 3(b) indicates inherent characteristics of DP transfer caused by the triple degeneracy of the exciton energy levels in NP_L. They are:

(Characteristic 1) The phases of the pulsatory variations of the two curves are different from each other. In order to derive the magnitude of this difference, the nutation components of the 50 ps-period are extracted from these curves and are shown in Fig. 4. The sinusoidal black curve has a phase lag of $\pi/3$ behind that of the red curve. This is because the triple degeneracy caused a lag of one-third of π [2]. That is, within one-third of the DP transfer time along the backward path, the energy level (1,1,1) in NP_S is promptly occupied by the exciton that is initially created in the triply degenerate energy levels in NP_L [3].

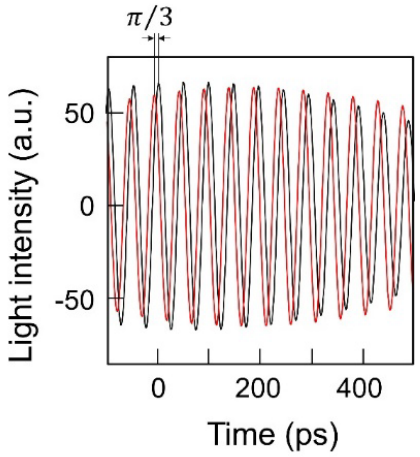

Fig. 4 Fourier components of the measured temporal variations of PL_1 and PL_2.
The nutation components with a 50 ps period were extracted from the black and red curves in Fig. 3(b).

(Characteristic 2) Blue broken curves in Fig. 3(b) represent that the pulsatory variations of the PL intensities are modulated. This is attributed to the fact that the transfer times along the forward path and along the backward path are different from each other.

(Characteristic 3) Additional pulsatory variations exist, the period of which is one-fourth that of the nutation. Such a short period is attributed to the fact that, among the four energy levels (level (1,1,1) in NP_S and the triply degenerate energy levels in NP_L), only the energy level (1,1,1) in NP_S is initially occupied by an exciton at the commencement of the nutation.

Figure 5 shows the Fourier spectral profiles of the two curves in Fig. 3(b). The spectral peak (A) at 20 GHz corresponds to the nutation period of 50 ps. Because the profiles of the measured pulsatory variations deviate from sinusoidal curves, the spectral peak (B) of the second-order higher harmonic can be seen. The spectral peak of the third-order higher harmonic is missing due to the difference between the forward and backward transfer times. The spectral peak (C) is attributed to the superposition of the fourth-order higher harmonic and the additional pulsatory variations whose period is one-fourth of the nutation cycle.

Sections 2.3 and 2.4 will review temporal variations observed in other experimental systems that were used to develop practical devices. The effect of the triple degeneracy can be neglected in these sections because of its minor contribution to these systems.

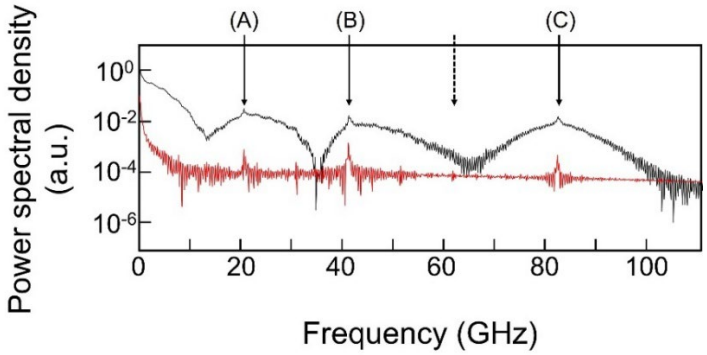

Fig. 5 The Fourier spectral profiles of the two curves in Fig. 3(b).

Spectral peaks A and B correspond to the nutation of the 50 ps period and its second-order higher harmonic. The peak C is attributed to the superposition of the fourth-order higher harmonic and the additional pulsatory variations.

---

2) This kind of phase lag has never been observed when using a large number of NPs as the macroscopic material system for inducing conventional optical phenomena. This is because the NPs in this system have been approximated as a coupled quantum state having a singlet state of the exciton.

3) Since the DP transferred bi-directionally between NP_S and NP_L, the profiles of the two curves in Fig. 4 should be anti-correlated, and thus, their phase difference should be as large as π. However, the phase lag was found to be $\pi/3$. The reason for this discrepancy was considered to be as follows: Since a large number of CuCl NPs were buried in the NaCl crystal, the DP could transfer not only between NP_S and NP_L but also between multiple NP_Ls (or between multiple NP_Ss). Furthermore, since the number of NP_Ls was larger than the number of NP_Ss, the DP transfer between neighboring NP_Ls could contribute to the phase difference between the two curves. However, since the phase of the DP transfer between these NP_Ls is random, the anti-correlation characteristics did not clearly appear, and thus, the phase difference remained as small as $\pi/3$.

2.3 DP transfer in nanometer-sized devices [11]

Nano-optical condenser [12]: Figure 6(a) schematically explains the structure of a nano-optical condenser device. Three kinds of cubic CuCl NPs (NP_S, NP_M, and NP_L) grown in a NaCl crystal are used: A large NP (NP_L) is surrounded by a large number of small NPs (NP_S). Medium-sized NPs (NP_M) are placed in the spaces between the NP_Ss and the NP_L.

This device uses DP transfers from the NP_Ss to the NP_M and subsequently to the NP_L for collecting the incident optical energy at the NP_L. As a result, the output signal of a sub-wavelength-sized (20 nm-diameter) spot is emitted from the NP_L, as is demonstrated by Fig. 6(b). Figure 6(c) shows the measured spatial and temporal variations of the light intensity, from which one can find that the energy is collected at NP_L within a time as short as 1 ns. Since this variation behavior reminds one of a fountain of gushing water (Fig. 6(d)), this device is called an optical nano-fountain.

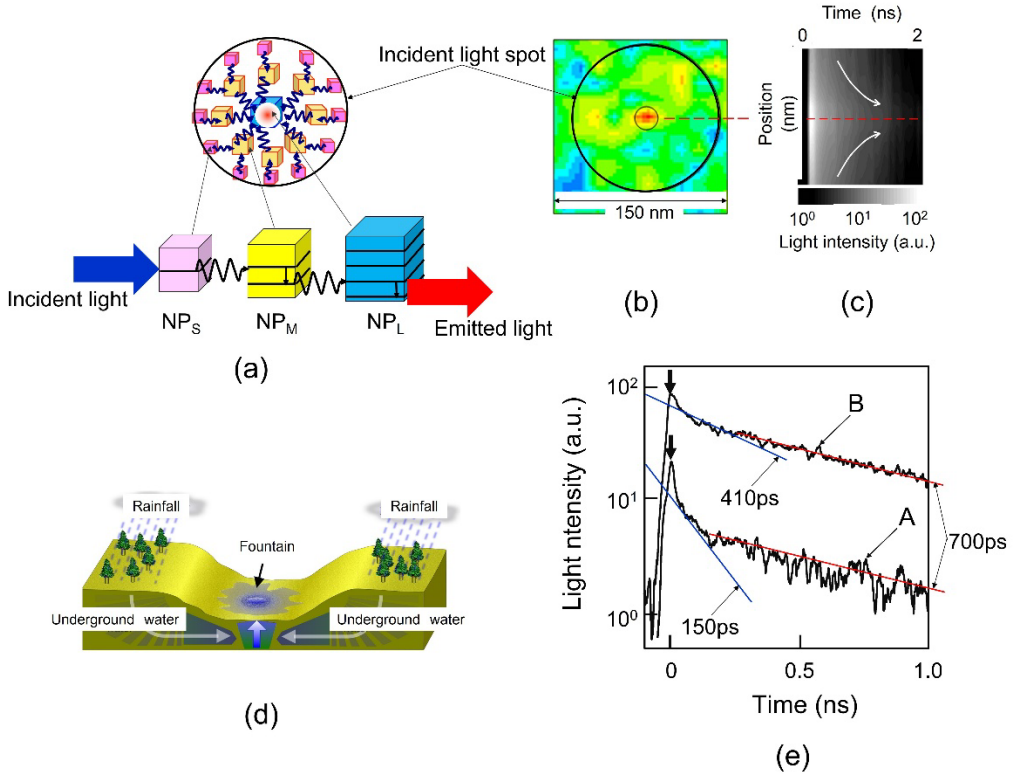

Fig. 6 Nano-optical condenser (Optical nano-fountain).

(a) The device structure. (b) and (c) are the measured spatial distribution and temporal variation of the emitted light intensity, respectively. (d) Schematic explanation of the fountain. (e) Measured temporal variation of the emitted light intensities. Curves A and B represent the intensities, emitted from NP_Ms and NP_L, respectively. The peaks at $t=0$, identified by the downward arrows, represent artifacts originating from the incident optical pulse. Blue and red lines represent $\exp(-t/\tau_{f1})$ and $\exp(-\sqrt{t/\tau_{f2}})$, respectively.

Figure 6(e) shows the measured relation between time (t) and the light intensity emitted from the device when it was illuminated by a short optical pulse of 325 nm-wavelength at t=0. Curve A is the intensity of the light emitted from the NP_Ms as a result of the DP transfer from the NP_Ss to the NP_Ms and subsequent energy dissipation of the excitons in the NP_Ms. Curve B is the intensity of the light that is finally emitted from the NP_L. It is confirmed that the light is efficiently collected at NP_L by noting that the value of curve B is more than ten times that of curve A. The peaks of these curves at t=0, identified by the downward arrows, represent artifacts originating from the incident optical pulse.

The profiles of curves A and B are similar to those of the curves in Fig. 3(a). They have two time constants that originate from the adiabatic and non-adiabatic processes. The former is the constant τ_{f1} in $\exp(-t/\tau_{f1})$ (blue line) whose values are 150 ps and 410 ps for curves A and B,

respectively. The latter is the constant τ_{f2} in $\exp(-\sqrt{t/\tau_{f2}})$ (red line) whose value is 700 ps for both curve A and curve B.

Optical buffer memory [13]: Figure 7(a) schematically explains the structure of an optical buffer memory device. For holding the input signal in this device, DP nutation between two NPs of the same size (two blue cubes) is used. The buffering time corresponds to the cycle time of the nutation. To read out the held signal, a NOT logic gate, whose operation is based on the DP transfer, is installed in proximity to the two NPs. Application of a readout optical pulse to the NOT logic gate creates an output signal.

Figure 7(b) is the temporal variation of the output signal intensity plotted as a function of the time delay defined as the time difference between the application of the input and readout pulses to the device. Curves A and B represent the measured values. Curve C is the theoretical curve fitted to them by using three values: τ_{f1} of 600 ps, τ_{f2} of 1300 ps, and a nutation cycle of 155 ps. Curve C exhibits a pulsating behavior that takes a first local maximum immediately after the readout pulse is applied. This corresponds to the first output signal. Subsequently, a series of output signals repeatedly appears with a period of 150 ps, which corresponds to the nutation cycle above.

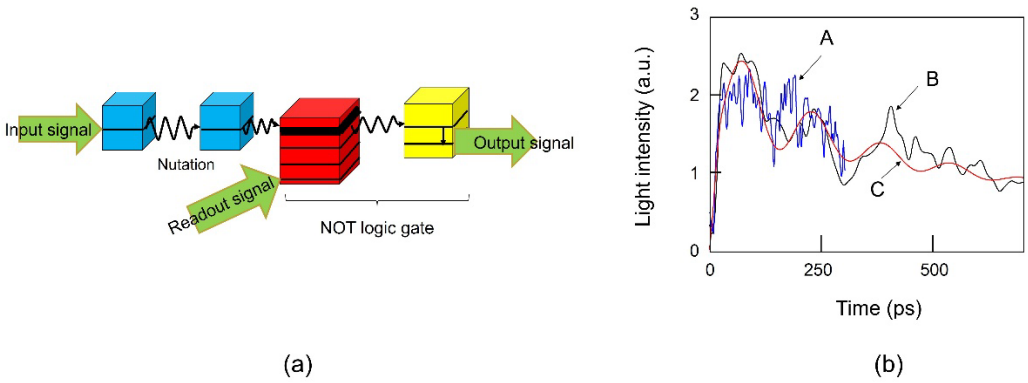

Fig. 7 Optical buffer memory device.

(a) The device structure. (b) Temporal variation of the output signal intensity as a function of the time delay. Curves A and B represent the measured results. Curve C is the theoretical curve fitted to the curves A and B.

2.4 DP transfer between different kinds of NPs [14,15]

Even when the two CuCl NPs (NP_S and NP_L in Fig. 1(a)) are replaced by different kinds of NPs, the DP exhibits temporal variation similar to Fig. 3. This suggests that the DP transfer is a universal phenomenon that can be observed in a variety of NP-systems in the natural world. For example, experiments have been carried out by using a pair of NPs composed of a semiconductor ZnO NP and a dye-molecular DCM NP. In this case, electrons in these NPs play the role of the excitons in CuCl NPs.

The left and right parts of Fig. 8 show the electron energy levels of ZnO NP and DCM NP, respectively. Photoluminescence is emitted from electrons in these levels. The measured results are indicated by curves A, B, and C in Fig. 9(a).

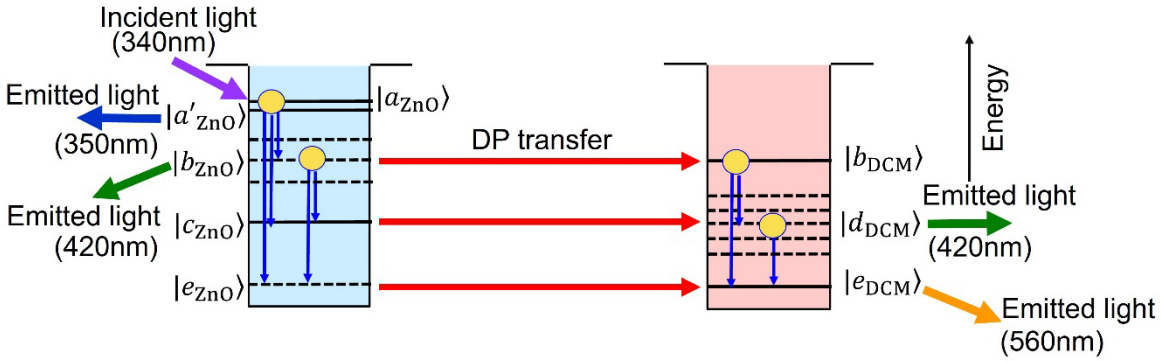

Fig. 8 Electron energy levels of ZnO NP (left) and DCM NP (right).
The wavelength of the emitted light is shown in the parenthesis.

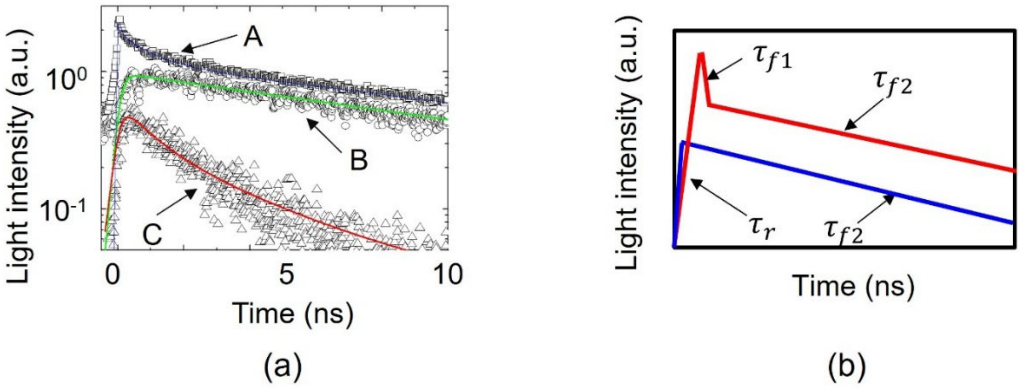

Fig. 9 Temporal evolutions of the emitted light intensities.
(a) Measured values. (b) Schematic explanation of the curves in (a).

The identities of these curves are:

Curve A: The light intensity (wavelength 350 nm) that is emitted from the electron in the energy level $|a'_{ZnO}\rangle$ of the ZnO NP. The wavelength of the incident light is 340 nm, which is resonant with the energy level $|a_{ZnO}\rangle$.

Curve B: The light intensity (wavelength 560 nm) that is emitted from the electron in the energy level $|e_{DCM}\rangle$ of the DCM NP. The wavelength of the incident light is 340 nm, which is resonant with the energy level $|a_{ZnO}\rangle$.

Curve C: The light intensity (wavelength 420 nm) that is emitted from the electron in the energy levels $|b_{\mathrm{ZnO}}\rangle$ and $|d_{DCM}\rangle$ of the ZnO NP and the DCM NP, respectively. The wavelength of the incident light is 420 nm, which is resonant with the energy level $|c_{ZnO}\rangle$ in the ZnO NP.

Figure 9(b) is a schematic explanation of the curves in Fig. 9(a). The red zigzag line corresponds to curve A in Fig. 9(a). The rise-up time constant is represented by τ_r, that is 100-150 ps in Fig. 9(a). The rapid decrease of curve A in a short time-span is attributed to the adiabatic process. It is represented by a short time constant τ_{f1} of the red zigzag line. Its value is nearly equal to τ_r of Fig. 9(a). The subsequent slow decrease is attributed to the non-adiabatic process, whose time constant τ_{f2} is as long as 15 ns in Fig. 9(a). The blue zigzag line corresponds to curves B and C in Fig. 9(a). Its rise-up time constant τ_r is equal to that of the red zigzag line. Since curves B and C do not show rapid decreases with the time constant τ_{f1}, they are represented only by the slowly decreasing blue zigzag line in Fig. 9(b) with the long time constant τ_{f2}.

3 Theoretical models for describing temporal variation behaviors of the output signals.

The features of the experimental results and theoretical models in Section 2 can be summarized as follows:

(1) The output signal intensity pulsates in a short time-span immediately after the pulsive input signal is applied. This pulsation is called nutation. The signal intensity rapidly decreases with a short time constant that is attributed to the adiabatic process and is fitted by $y_{QR} = a_{QW}\exp(-t/\tau_{QW})$ based on the QW model. Here, since this process is compatible with the QW model, the time constant τ_{f1} in Section 2 is rewritten as τ_{QW}.

(2) In a long time-span, the output signal intensity decreases slowly due to a non-adiabatic process that is fitted by $y_{RW} = a_{RW}\exp(-\sqrt{t/\tau_{RW}})$ based on the RW model. Here, since this process is compatible with the RW model, the time constant τ_{f2} in Section 2 is rewritten as τ_{RW}.

Measured values of nutation cycle and time constants are summarized in Table 1. This table indicates that the time constant τ_{QW} is shorter than τ_{RW}. That is, τ_{QW}/τ_{RW} = 6.7×10^{-3}- 0.58 and is expressed as

$$\tau_{QW}/\tau_{RW} < 1. \quad (1)$$

Table 1 Measured values of nutation cycle and time constants.

*) The nutation cycle of 400 ps was also measured for an optical switching device that was composed of CuCl NPs [15].

**) The time constants τ_{f1} and τ_{f2} in Section 2 are rewritten as τ_{QW} and τ_{RW}, respectively.

	Nutation cycle*)	τ_r	τ_{QW} **)	τ_{RW} **)
Section 2.2	50 ps			
Section 2.3				
Nano-optical condenser	155 ps		150 ps, 410 ps	700 ps
Optical buffer memory			600 ps	1,300 ps
Section 2.4		100-150 ps	100-150 ps	15 ns

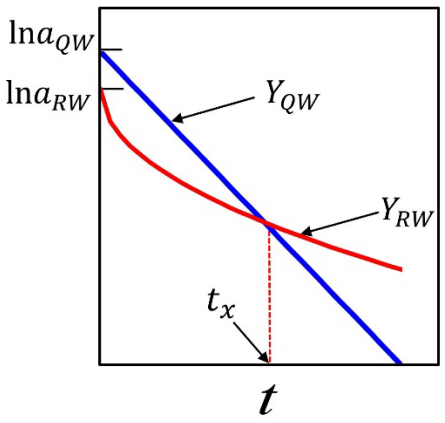

Fig. 10 Temporal variations of eqs. (2) (blue line) and (3) (red curve).

Temporal variations of the exponential functions in **(1)** and **(2)** are schematically explained by Fig. 10, in which the vertical axis is indicated on a logarithmic scale:

$$Y_{QW} = \ln y_{QW} = \ln a_{QW} - t/\tau_{QW}, \quad (2)$$

and

$$Y_{RW} = \ln y_{RW} = \ln a_{RW} - \sqrt{t/\tau_{RW}}. \quad (3)$$

Due to the small value of τ_{QW}/τ_{RW}, the slope of the blue line (Y_{QW}) in this figure is steeper than that of the red curve (Y_{RW}). The value of a_{RW} is assumed to be smaller than that of a_{QW} ($a_{RW}/a_{QW}<1$) by referring to the curves in Figs. 3(a), 6(e), 7(b), and also curve A in Fig. 9(a).

This figure indicates that the QW feature can be clearly observed in the early short time-span because the signal intensity of Y_{QW} (blue line) is larger than that of Y_{RW} (red curve). However, after that, this feature is obscured by the RW feature (red curve) due to the rapid decreases of Y_{QW}. The time at which the blue line and red curve cross is represented by t_x in this figure.

For making full use of the output signal originating from the DP transfer for device applications[4)], a sufficiently long crossing time t_x is required to ensure a time during which the QW features can be clearly observed. To meet this requirement, the values of a_{RW}/a_{QW} and τ_{QW}/τ_{RW} must be adjusted in an appropriate manner. It should be noted that the values of a_{RW} and τ_{RW} depend on the device temperature T (they are proportional to T and T^{-1}, respectively).

[4)] Since curves B and C in Fig. 9(a) correspond the case of $a_{RW}/a_{QW}>1$, the QW features are obscured by the RW features and are not advantageous for practical applications.

Furthermore, it should be pointed out that a part of the adiabatically dissipated energy may be converted to non-adiabatically dissipated energy. Even though this conversion mechanism has not yet been precisely evaluated by experiments, the exponential functions y_{QR} and y_{RW} should be revised to

$$y'_{QW}=(1-\varepsilon)a_{QW}\exp(-t/\tau_{QW}) \tag{4}$$

and

$$y'_{RW}=\left(a_{RW}+\varepsilon a_{QW}\right)\exp(-\sqrt{t/\tau_{RW}}), \tag{5}$$

respectively, by referring to this conversion. Here, ε (<<1) is the conversion rate. In order to maintain

the long time t_x, the value of ε must also be adjusted in an appropriate manner. It can be assumed that this value can be optimized for maximizing the output signal intensity by means of the adjustment above. Such an optimum value has been discussed in the case of the QW model [16]. The example is the optimum value κ_{opt} of the dispersion constant κ for maximizing the output signal, as is shown by Fig. 11.

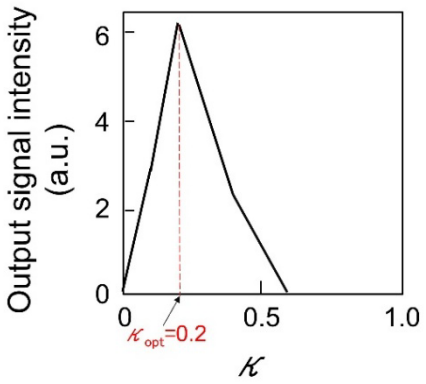

Fig. 11 Relation between the dissipation constant κ and the output signal intensity [16].

4 Future directions

DP transfer is presumed to be a universal phenomenon that can be observed in a variety of NPs in the natural world. To demonstrate an example of such universality, Fig. 12 schematically explains the structure of an antenna system that is composed of photosynthetic bacteria [17], by which solar energy is collected at the reaction center. Here, the essential problem is that the excitation energy transfer (ETT) process in this system has not yet been precisely analyzed using traditional Förster theory. This is because this theory is based on the primitive concept of electric-dipole transitions and the long-wavelength approximation. Detailed studies are in progress to solve this problem by improving the accuracy of the theory [18].

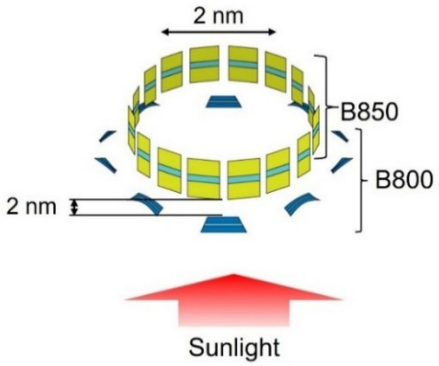

Fig. 12 The structure of an antenna system made of photosynthetic bacteria [17].

This problem may be solved if the theoretical model of DP creation [1,2] and the QW model for DP transfer [5-7] are used because the DP creation and transfer processes have several equivalences with the ETT process. Actually, the motivation for inventing the nano-optical condenser (optical nano-fountain) in Fig. 6 was to build a practical semiconductor device to realize a function equivalent to that of the system in Fig. 12 [12]. Experiments have already confirmed that this device succeeded in collecting the incident optical energy at NP_L at the center.

By referring to the example above, one of the promising directions of future DP research is to discover a route to the precise analysis of the DP transfer phenomena, not only in physical and chemical systems but also in biological systems and other systems. For reference, novel features such as hierarchy [19] and autonomy [20, 21] have been found in the DP transfer, and these features have several equivalences with biological signal transmission processes in neurons.

5 Summary

This paper reviewed the measured results of the temporal variation behavior of the DP transfer between NPs. By illuminating the NPs with a short optical pulse, the temporal variation of the emitted PL intensity was evaluated. Even after the optical pulse was turned off, the PL intensity exhibited nutation within a short time-span. The envelope intensity of the nutation decreased due to adiabatic and non-adiabatic processes. They were described by using a QW model and a RW model, respectively. It was pointed out that the values of several relevant quantities in these models must be adjusted in an appropriate manner to clearly observe the DP transfer features. The rate of conversion from the adiabatically dissipated energy to the non-adiabatically dissipated one must also be adjusted.

An antenna system composed of photosynthetic bacteria was presented for demonstrating the ETT process that is equivalent to those of the DP creation and transfer. It was suggested that future research of DPs will involve analyzing this process and building more precise theoretical models for drawing a universal physical picture of the DP transfers that are commonly found in nature.

References

[1] M. Ohtsu and H. Sakuma, *Dressed Photons to Revolutionize Modern Physics* (Springer, Heidelberg, 2025) 65-118.

[2] H. Sakuma, I. Ojima, and M. Ohtsu, "Perspective on an Emerging Frontier of Nanoscience Opened up by Dressed Photon Studies," *Nanoarchitectonics*, Vol. 5, Issue 1 (2024) 1-23.

[3] M. Ohtsu, *Dressed Photons* (Springer, Heidelberg, 2014) 89-214.

[4] M. Ohtsu, *Silicon Light-Emitting Diodes and Lasers* (Springer, Heidelberg, 2016) 1-138.

[5] M. Ohtsu, *Off-Shell Applications in Nanophotonics* (Elsevier, Amsterdam, 2021) 162-165.

[6] M. Ohtsu and H. Sakuma, *Dressed Photons to Revolutionize Modern Physics* (Springer, Heidelberg, 2025)41-64.

[7] M. Ohtsu, "Off-shell scientific nature of dressed photon energy transfer and dissipation," Off-shell Archive (April, 2024) Offshell: 2404R.001.v1. **DOI** 10.14939/2404R.001.v1, https://rodrep.or.jp/en/off-shell/review_2404R.001.v1.html

[8] M. Ohtsu and T. Kawazoe, "Nutation in energy transfer of dressed photons between nano-particles," Off-shell Archive (May, 2020) Offshell: 2005O.001.v1. **DOI** 10.14939/2005O.001.v1,

https://rodrep.or.jp/en/off-shell/original_2005O.001.v1.html
[9] H. Saigo, Quantum Probability for Dressed Photons: The Arcsine Law in Nanophotonics, *Prog. in Nanophotonics 5* (ed. T. Yatsui) (Springer, Heidelberg,2018) 79-106.
[10] T. Kawazoe, K. Kobayashi, J. Lim, Y. Narita, and M. Ohtsu, "Direct Observation of Optically Forbidden Energy Transfer between CuCl Quantum Cubes via Near-Field Optical Spectroscopy," *Phys. Rev. Lett*., **88** (2002) 067404.
[11] M. Ohtsu, "Novel functions and prominent performance of nanometric optical devices made possible by dressed photons," Off-shell Archive (April, 2019) Offshell: 1904R.001.v1. **DOI** 10.14939/1904R.001.v1, https://rodrep.or.jp/en/off-shell/review_1904R.001.v1.html
[12] T. Kawazoe, K. Kobayashi, and M. Ohtsu, "Optical nanofountain: A biomimetic device that concentrates optical energy in a nanometric region", *Appl. Phys. Lett.*, **86** (2005) 103102.
[13] M. Ohtsu, *Off-Shell Applications in Nanophotonics* (Elsevier, Amsterdam, 2021) 58-59.
[14] M. Ohtsu, *Off-Shell Applications in Nanophotonics* (Elsevier, Amsterdam, 2021) 95-101.
[15] M. Ohtsu, T. Kawazoe, and H. Saigo, "Spatial and temporal evolutions of dressed photon energy transfer," Off-shell Archive (October, 2017) Offshell: 1710R.001.v1. **DOI** 10.14939/1710R.001.v1, https://rodrep.or.jp/en/off-shell/review_1710R.001.v1.html
[16] M. Ohtsu, E. Segawa, K. Yuki, and S. Saito, "Optimum dissipation for governing the autonomous transfer of dressed photons," *Off-shell Archive* (May, 2025) Offshell: 2405O.001.v1.
DOI 10.14939/2405O.001.v1, https://rodrep.or.jp/en/off-shell/original_2405O.001.v1.html
[17] H.-M. Wu、N.R.S. Reddy, and G.J. Small, "Direct observation and hole burning of the lowest exciton level (B870) of the LH2 antenna complex of *Rhodopseudomonas acidophila*," *J. Phys. Chem.*, B**101** (1996) pp.651-656.
[18] H. Sumi, "Theory on rates of excitation-energy transfer between molecular aggregates through distributed transition dipoles with application to antenna system in bacterial photosynthesis ," *J. Phys. Chem.*, B**103** (1996) pp.252-260.
[19] M. Ohtsu and H. Sakuma, *Dressed Photons to Revolutionize Modern Physics* (Springer, Heidelberg, 2025) 29-31.
[20] M. Ohtsu, *Off-Shell Applications in Nanophotonics* (Elsevier, Amsterdam, 2021) 54-55.
[21] M. Ohtsu and H. Sakuma, *Dressed Photons to Revolutionize Modern Physics* (Springer, Heidelberg, 2025) 31-33.

[V] PUBLISHED BOOKS

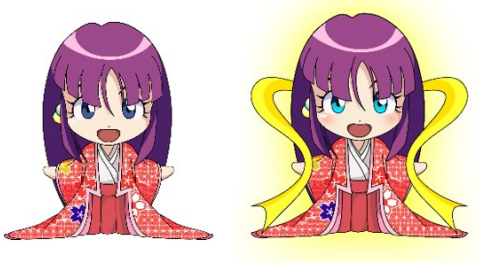

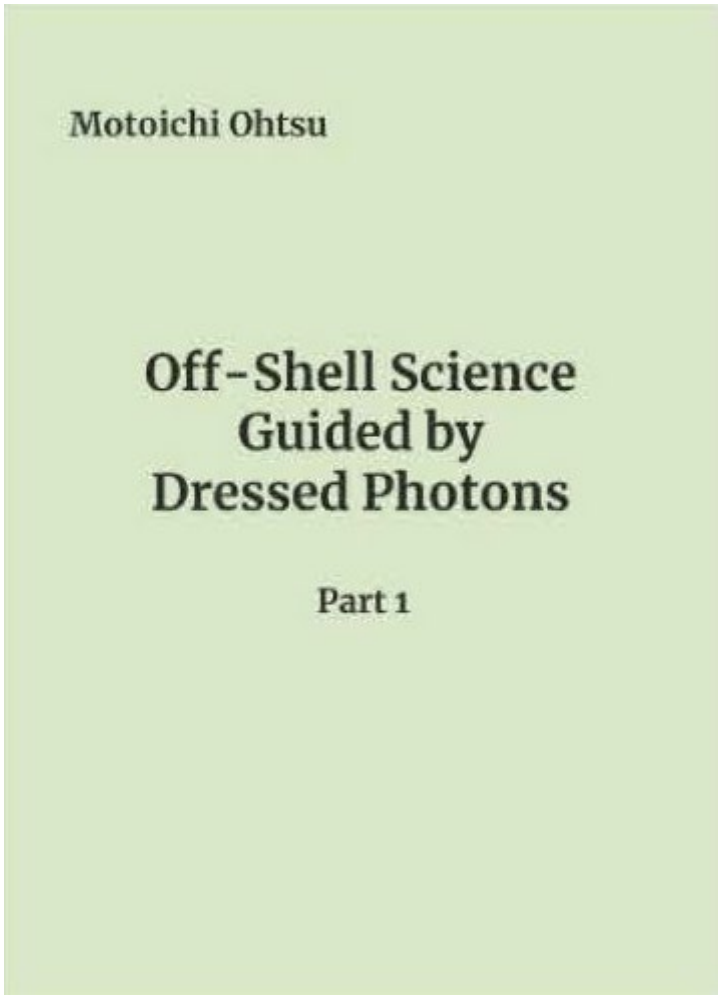

Off-Shell Science Guided by Dressed Photons, Pt.1

2025年11月3日初版第1刷発行

ISBN978-4-8150-4995-9
C0042 ¥2636E

デザインエッグ株式会社

価格：本体2,636円＋税
本書は書店などでの販売価格を拘束していません。

9 784815 049959

1 920042 026365

著　者　大津　元一
制　作　MyISBN
発行所　デザインエッグ株式会社

ISBN978-4-8150-4995-9

Author biography

Motoichi Ohtsu, Dr. Eng.
*Director-in-chief, (General Incorporated Association) Research Origin for Dressed Photon, Yokohama, Japan
*Professor Emeritus, the University of Tokyo, Tokyo, Japan
*Professor Emeritus, the Tokyo Institute of Technology, Tokyo, Japan

Motoichi Ohtsu received his Dr. Eng. Degree from the Tokyo Institute of Technology, Tokyo, in 1978.He was first appointed as a research associate, then an associate professor in 1982. From 1986 to 1987, while on leave from the Tokyo Institute of Technology, he joined the Crawford Hill Laboratory, AT&T Bell Laboratories, Holmdel, New Jersey, United States. In 1991 he became a professor at the Tokyo Inst. of Technol. In 2004 he moved to the University of Tokyo as a professor. He has been the leader of the "Photon Control" project (1993–98: the Kanagawa Academy of Science and Technology, Kanagawa, Jpn., the "Localized Photon" project (1998–2003: ERATO, JST, Japan), the "Terabyte Optical Storage Technology" project (2002–06: NEDO, Jpn.), the Near Field Optical Lithography System" project (2004–06): Ministry of Education, Jpn.), the "Nanophotonics" team (2003–09: SORST, JST, Jpn.), the "Innovative Nanophotonics Components Development" project (2006–11: NEDO, Jpn.), the "Nanophotonics Total Expansion: Industry-University Cooperation and Human Resource Development" project (2006–11: NEDO, Jpn.), and the "Development of a solar cell technology using dressed photons" project (2012–14, NEDO, Jpn.).

Dr. Ohtsu has written over 598 papers and received 83 patents. He is the author, coauthor, and editor of 87 books, including 46 in English. In 2000 he was appointed as President of the IEEE LEOS Japan Chapter. From 2000, he has been an executive director of the Japan Society of Applied Physics. His main fields of interests are off-shell science and dressed photon technology. He is a fellow of the Optical Society of America. He is also a fellow and life member of the Japan society of Applied Physics. He is a member of the American Physical Society and the Laser Society of Japan. He has been awarded 22 prizes from academic institutions and the Jpn. Government, including the Issac Koga Gold Medal of URSI in 1984; the Jpn. IBM Science Award in 1988; two awards from the Japan Society of Applied Physics in 1982 and 1990; the Inoue Science Foundation Award in 1999; the Japan Royal Medal with Purple Ribbon from the Jpn. Government in 2004; the H. Inoue Award From JST in 2005; the Distinguished Achievement Award from the Institute of Electronics, Information and Communication, Engineering of Jpn. in 2007; the Julius Springer Prize for Applied Physics in 2009; the Okawa Publications Prize in 2016; the IAAM Medal from the International Association of Advanced Materials in 2018; and the Order of the Sacred Treasure, Gold Rays with Neck Ribbon, from the Jpn. Government in 2024.

He served as the committee member of 18 international conferences, including the Chair of the Executive Committee, the German-Jpn. Symposium on Nanophotonics; the Chair of the Executive Committee, The US-Jpn. Symposium on Nanophotonics; the Chair of the Program Committee, the International Near-Field Optics Conference; the Chair of the Organizing Committee, the Asia-Pacific Near Field Optics Workshop; and the Chair of the Program Committee, the Pacific Rim Conference on Lasers and Electro-Optics.

Preface

This book collects original papers on off-shell science, written by M. Ohtsu. They have been published in “Off-shell Archive”, the preprint depository in the Web site of the (General Incorporated Association) Research Origin for Dressed Photon. The DOI, URL, and the date of publication are written at the beginning of each paper. Co-authors’ names and their affiliations are:

Name	Affiliation (At the point in time of publication)
Motoichi Ohtsu	Research Origin for Dressed Photon, 3-13-19 Moriya-cho, Kanagawa-ku, Yokohama, Kanagawa 221-0022, Japan
Etsuo Segawa	Yokohama National University, 79-8 Tokiwadai, Hodogaya-ku, Yokohama, Kanagawa 240-8501, Japan
Kenta Yuki	Middenii, 3-3-13 Nishi-shinjuku, Sinjuku-ku, Tokyo 160-0023, Japan
Seiken Saito	Kogakuin University, 2665-1, Nakano-machi, Hachioji, Tokyo 192-0015, Japan
Tadashi Kawazoe	Tokyo Denki University, 5 Senju-Asahi-cho, Adachi-ku, Tokyo 120-8551, Japan

August 2025

Yokohama, Japan

Motoichi Ohtsu
Director-in-chief
Research Origin for Dressed Photon

Contents

Part 1

Motoichi Ohtsu

Off-Shell Science Guided by Dressed Photons

Part 2

Off-Shell Science Guided by Dressed Photons, Pt.2

2025年11月17日 初版 第 1 刷発行

ISBN978-4-8150-4996-6
C0242 ¥2418E

デザインエッグ株式会社

価格：本体 2,418 円＋税
本書は書店などでの販売価格を拘束していません。

9 784815 049966

1 920242 024185

著　者　大津　元一
制　作　MyISBN
発行所　デザインエッグ株式会社

ISBN978-4-8150-4996-6

Author biography

Motoichi Ohtsu, Dr. Eng.
*Director-in-chief, (General Incorporated Association) Research Origin for Dressed Photon, Yokohama, Japan
*Professor Emeritus, the University of Tokyo, Tokyo, Japan
*Professor Emeritus, the Tokyo Institute of Technology, Tokyo, Japan

Motoichi Ohtsu received his Dr. Eng. Degree from the Tokyo Institute of Technology, Tokyo, in 1978.He was first appointed as a research associate, then an associate professor in 1982. From 1986 to 1987, while on leave from the Tokyo Institute of Technology, he joined the Crawford Hill Laboratory, AT&T Bell Laboratories, Holmdel, New Jersey, United States. In 1991 he became a professor at the Tokyo Inst. of Technol. In 2004 he moved to the University of Tokyo as a professor. He has been the leader of the "Photon Control" project (1993–98: the Kanagawa Academy of Science and Technology, Kanagawa, Jpn., the "Localized Photon" project (1998–2003: ERATO, JST, Japan), the "Terabyte Optical Storage Technology" project (2002–06: NEDO, Jpn.), the Near Field Optical Lithography System" project (2004–06): Ministry of Education, Jpn.), the "Nanophotonics" team (2003–09: SORST, JST, Jpn.), the "Innovative Nanophotonics Components Development" project (2006–11: NEDO, Jpn.), the "Nanophotonics Total Expansion: Industry-University Cooperation and Human Resource Development" project (2006–11: NEDO, Jpn.), and the "Development of a solar cell technology using dressed photons" project (2012–14, NEDO, Jpn.).

Dr. Ohtsu has written over 598 papers and received 83 patents. He is the author, coauthor, and editor of 87 books, including 46 in English. In 2000 he was appointed as President of the IEEE LEOS Japan Chapter. From 2000, he has been an executive director of the Japan Society of Applied Physics. His main fields of interests are off-shell science and dressed photon technology. He is a fellow of the Optical Society of America. He is also a fellow and life member of the Japan society of Applied Physics. He is a member of the American Physical Society and the Laser Society of Japan. He has been awarded 22 prizes from academic institutions and the Jpn. Government, including the Issac Koga Gold Medal of URSI in 1984; the Jpn. IBM Science Award in 1988; two awards from the Japan Society of Applied Physics in 1982 and 1990; the Inoue Science Foundation Award in 1999; the Japan Royal Medal with Purple Ribbon from the Jpn. Government in 2004; the H. Inoue Award From JST in 2005; the Distinguished Achievement Award from the Institute of Electronics, Information and Communication, Engineering of Jpn. in 2007; the Julius Springer Prize for Applied Physics in 2009; the Okawa Publications Prize in 2016; the IAAM Medal from the International Association of Advanced Materials in 2018; and the Order of the Sacred Treasure, Gold Rays with Neck Ribbon, from the Jpn. Government in 2024.

He served as the committee member of 18 international conferences, including the Chair of the Executive Committee, the German-Jpn. Symposium on Nanophotonics; the Chair of the Executive Committee, The US-Jpn. Symposium on Nanophotonics; the Chair of the Program Committee, the International Near-Field Optics Conference; the Chair of the Organizing Committee, the Asia-Pacific Near Field Optics Workshop; and the Chair of the Program Committee, the Pacific Rim Conference on Lasers and Electro-Optics.

Preface

This book collects original papers on off-shell science, written by M. Ohtsu. They have been published in “Off-shell Archive”, the preprint depository in the Web site of the (General Incorporated Association) Research Origin for Dressed Photon. The DOI, URL, and the date of publication are written at the beginning of each paper. Co-authors’ names and their affiliations are:

Name	Affiliation (At the point in time of publication)
Motoichi Ohtsu	Research Origin for Dressed Photon, 3-13-19 Moriya-cho, Kanagawa-ku, Yokohama, Kanagawa 221-0022, Japan
Etsuo Segawa	Yokohama National University, 79-8 Tokiwadai, Hodogaya-ku, Yokohama, Kanagawa 240-8501, Japan
Kenta Yuki	Middenii, 3-3-13 Nishi-shinjuku, Sinjuku-ku, Tokyo 160-0023, Japan
Seiken Saito	Kogakuin University, 2665-1, Nakano-machi, Hachioji, Tokyo 192-0015, Japan
Tadashi Kawazoe	Tokyo Denki University, 5 Senju-Asahi-cho, Adachi-ku, Tokyo 120-8551, Japan

August 2025

Yokohama, Japan

Motoichi Ohtsu
Director-in-chief
Research Origin for Dressed Photon

Contents

Part 2

ドレスト光子の数理

―オフシェル科学への展開―

大津元一
〔著〕

ドレスト光子の数理
―オフシェル科学への展開―

2025年10月20日 初版第 1 刷発行

ISBN978-4-8150-4934-8
C0042 ¥2870E

デザインエッグ株式会社

価格：本体 2,870 円＋税
本書は書店などでの販売価格を拘束していません。

9 784815 049348

1 920042 028703

著　者　大津　元一
制　作　MyISBN
発行所　デザインエッグ株式会社

ISBN978-4-8150-4934-8

まえがき

ドレスト光子（Dressed photon: DP）とは光子と電子または励起子がナノメートル寸法の微粒子の中で相互作用して生成される量子場である。本書の著者の大津は 1980 年代初めにそれを着想し、1990 年代初めに実験による検証に成功した。その後は大津と共同研究者によって実験研究が大きく進展し、DP の独特な性質を明らかにするとともに、計測、デバイス、加工、システム、エネルギー変換などの革新的応用技術を生み出した。以上は世界に先駆けて行われた独創研究である。

これらの成果は実験を繰り返し行うことにより蓄積され、2016 年初頭まで継続して大きく進展した。その歩みに合わせ、大津は DP を扱う科学技術を近接場光学、ナノフォトニクスと順次呼び変えてきた。現在では以下に記す理由からこれをオフシェル科学と称している。

大津は 2016 年 3 月に東京大学を定年退職したのを機に、DP の理論的基礎を確立するため（一般社団法人）ドレスト光子研究起点(RODreP)を設立し、活動を開始した。これまでの実験研究から理論研究に舵を切ったのである。その後、現在までに DP とは何か？その生成過程は？と言った根本的な疑問に答える研究が進み、宇宙論との繋がりなどの新しい知見が得られるなど、飛躍的な進展が見られた。

以上の経緯をふり返ると、DP はオフシェル場であり、したがって従来の電磁場（オンシェル場）とは相互補完的であることが改めて認識される。過去にはこのような補完的な場は研究されていなかったので、その理論的基礎が未発達だったのは当然である。

このような未発達の科学分野をさらに深く研究するため、次に解決しなければならないのは、DP がナノメートル寸法微粒子の間をどのように移動するか？そしてどのようにして外部の巨視系にエネルギーを放出し測定されるか？などの問題である。これらはもちろん従来のオンシェル科学に基づく理論研究では解決できない。それを解決するのがオフシェル科学であり、そこでは非可換代数の一つである量子ウォーク（Quantum walk: QW）の数理科学モデルが新たに採用され、問題解決に向けた研究が進展している。

本書はこのような数理科学モデルによる DP の移動の特性の解析について解説する。この理論研究は現在活発に行われており、日々進展がみられることから本書は研究の現状紹介の性質をもつ。しかし同時にその基礎となる QW モデルから始めて紹介しているので、学生・若手研究者向けの参考書としても有用であろう。

本書は 10 章からなるが、各々の役割に基づき分類すると四部に分かれる。各部では

【第Ⅰ部　導入編】 DP とは何か？その生成機構は？（第 1 章）、DP の移動と測定の記述のためになぜ QW が必要か？（第 2 章）の疑問に答える。

【第Ⅱ部　準備編】 QW モデルを定式化する（第 3 章）。

【第Ⅲ部　実践編】 物質の形状の特異点（第 4 章）での、および物質の構造の特異点（第 5～7 章）での DP の生成と移動を解析する。

【第Ⅳ部　発展編】 自律性の考察のための解析を行う（第 8～10 章）。

第 1 章は大津元一、「ドレスト光子の深わかり」―異次元の光の科学と技術を味わう―　アドスリー、（2022 年 6 月）の第 7 章を修正加筆して執筆している。第 2 章～第 10 章は当法人のホームページに掲載している Off-shell Archive に掲載した原著論文、解説論文の preprint を素材とし、それを和訳したうえで適宜修正加筆して執筆している。また、応用物理学会講演会でもこれらの内容を発表しているので、それらを巻末の「執筆の素材となった文献」に示す。なお、Off-shell Archive の英文論文は論文集として別途出版する予定である。

DP およびオフシェル科学の理論研究は長きにわたり大津がお世話になる多くの優れた研究者の方々のご指導、ご協力により推進された。次の方々に深くお礼申し上げます：小嶋泉氏（（一般社団法人）ドレスト光子研究起点）、佐久間弘文氏（（一般社団法人）ドレスト光子研究起点）、西郷甲矢人氏（ZEN 大学）、岡村和弥氏（中部大学）、瀬川悦生氏（横浜国立大学）、齋藤正顕氏（工学院大学）、坂野斎氏（埼玉大学）、三宮俊氏（（株）リコー）、結城謙太氏（Middenii）

2025 年 7 月

大津　元一

目次

Nano-Optics and Nanophotonics

Motoichi Ohtsu
Hirofumi Sakuma

Dressed Photons to Revolutionize Modern Physics

Exploring Longitudinal Electromagnetic Waves and Off-Shell Quantum Fields

Springer

Nano-Optics and Nanophotonics

The Springer Series in Nano-Optics and Nanophotonics provides an expanding selection of research monographs in the area of nano-optics and nanophotonics, science- and technology-based on optical interactions of matter in the nanoscale and related topics of contemporary interest. With this broad coverage of topics, the series is of use to all research scientists, engineers, and graduate students who need up-to-date reference books. The editors encourage prospective authors to correspond with them in advance of submitting a manuscript. Submission of manuscripts should be made to the editor-in-chief, one of the editors, or to Springer.

Motoichi Ohtsu · Hirofumi Sakuma

Dressed Photons to Revolutionize Modern Physics

Exploring Longitudinal Electromagnetic Waves and Off-Shell Quantum Fields

Springer

Motoichi Ohtsu
Department of Research
Research Origin for Dressed Photon
Yokohama, Japan

Hirofumi Sakuma
Department of Research
Research Origin for Dressed Photon
Yokohama, Japan

ISSN 2192-1970 ISSN 2192-1989 (electronic)
Nano-Optics and Nanophotonics
ISBN 978-3-031-77943-5 ISBN 978-3-031-77944-2 (eBook)
https://doi.org/10.1007/978-3-031-77944-2

This Springer imprint is published by the registered company Springer Nature Switzerland AG
The registered company address is: Gewerbestrasse 11, 6330 Cham, Switzerland

Preface

Dressed photon (DP) is a quantum field that mediates the interaction between nanometer-sized particles (NPs). It localizes at an NP and its size is much smaller than the wavelength of a propagating light (a free photon). That is, DP is not an entity directly observed by conventional methods in optics and it should not be confused with a special type of linear evanescent light field, because, through previous research on *optical near field*, it has been found that DP is generated by nonlinear field interactions between matter and incident light field, for which quantum off-shell momentum field plays an important role. DP has unique features that are complimentary to those of the free photon (on-shell field), and a variety of novel phenomena originate from DP. Since they are analogous to some physical, chemical, and biological phenomena, we conjecture that those similarities are the manifestation of underlying mathematical universality represented by nonlinear off-shell field interactions.

By the authors' previous publications, the results of experimental studies and their application to innovative technologies have been reviewed. Although some theories were also introduced, they were prototypes built by modifying conventional on-shell scientific theories. Even though this introduction seemed to be successful in analyzing some experimental results, the problem was that these theories did not deal with the concept of "field interaction" mentioned above in a satisfactory fashion.

However, in the last few years, theoretical studies on off-shell science have rapidly progressed to solve this problem. Based on this progress, this book reviews the theories of DP creation and relevant phenomena. The first half of this book introduces the results of experimental studies, application technologies, prototype theories, and their problems: Chap. 1 presents fifteen novel phenomena originating from DP and reviews the history of DP studies. Chapter 2 demonstrates application technologies based on unique features of DP. These technologies are complimentary to those of the conventional ones. Chapter 3 reviews the experimental grounds of the unique phenomena of DP energy transfer. Numerical simulation is also reviewed that was carried out by prototype methods modifying on-shell scientific approaches, and their problems are pointed out. Chapter 4 describes numerical simulation based on a quantum walk model that was developed to solve these problems.

The second half of this book deals with the recent theoretical progress on off-shell field study focusing on DP dynamics. In the first half of this Preface, we have emphasized the important role played by nonlinear field interactions between matter and light fields in DP dynamics. As Einstein's theories of special and general relativity clearly show, light field as free electromagnetic one is closely related to what we call "physical space-time". From such a viewpoint, "matter and light field" interactions may be formally regarded as "matter and physical space-time" interactions just like matter and gravitational field interactions. As we know, the notions of space and time were originally introduced into a given physical system under consideration as purely mathematical quantities called coordinates. Although the above-mentioned Einstein's theory had revolutionized the situation, we can safely say that the present status of "physical space-time" is not complete, as is typically shown by the presence of cosmological term $\Lambda g_{\mu\nu}$ in Einstein's field equation. Occasionally as has been ridiculed by the term *Einstein's mollusk*, metric tensor $g_{\mu\nu}$ itself is not a physical quantity.

The most important aspect of our accomplishment we are going to explain in the second half is that we have succeeded in formulating a complete theory on "physical space-time" which covers not only timelike but also spacelike components of it by utilizing Greenberg-Robinson theorem in the axiomatic quantum field theory. Presumably, we can say that the problems of the unification of four forces, dark energy, and dark matter stand as big three enigmas in the contemporary theoretical physics. We believe that the reason why we cannot understand dark energy and matter is because we do not have a relevant theory on "physical space-time".

The second half starts from Chap. 5, which gives introductory remarks on the following Chaps. 6–10. Since the knowledge on Hamiltonian structure of the classical physics plays a quite important role in formulating our notion of "physical space-time", Chap. 6 is reserved for the explanation of it. In Chap. 7, we discuss several cutting-edge topics including dark energy, which are related to the spacelike part of "physical space-time". By combining the notions of conformal gravity and of the timelike part of "physical space-time", we are going to solve the mystery of dark matter in Chap. 8. The noticeable advantage of our new form of conformal gravity is the fact that it naturally bears the characteristics of spin-network as well as an entropy field different from the one in thermodynamics.

Based on the important outcomes explained in Chaps. 7 and 8, we will discuss novel cosmology in Chap. 9, and in the final Chap. 10, we will touch on a certain aspect of hierarchy problem in elementary particle physics relating to the unification of four forces, together with a couple of intriguing implications noticed on the relation between our novel cosmology and remarkable predictions of superstring theory made by Witten and Maldacena.

The first half was mainly written by M. O., the first author. The second half was mainly by H. S. However, they completed the manuscript in close cooperation with one another. The authors hope that this article will stimulate readers to gain an interest in off-shell science and to expand the routes available for reaching new studies of modern science.

Yokohama, Japan

Motoichi Ohtsu
Hirofumi Sakuma

Contents

[VI] PRESENTATIONS

IN DOMESTIC CONFERENCES

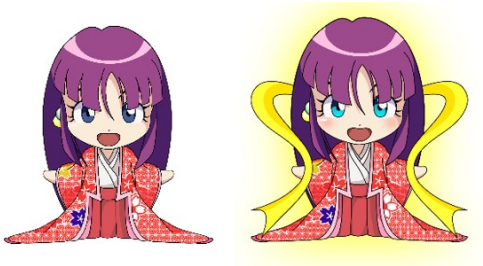

11aC2

光電誘起ドーパントドリフト現象に基づくリライタブル偏光回転効果
Rewritable polarization rotation effect based on the photoelectrically-induced dopant drift phenomenon

°杜昊澤[1]*，門脇拓也[2]，竪直也[1]，興雄司[1]，林健司[1]，大津元一[3]

° Haoze Du[1], Takuya Kadowaki[2], Naoya Tate[1], Yuji Oki[1], Kenshi Hayashi[1], Motoichi Ohtsu[3]

[1]九州大学大学院システム情報科学府，[2]日亜化学工業株式会社，[3]ドレスト光子研究起点−

[1]Graduate School and Faculty of Information Science and Electrical Engineering, Kyushu University,
[2]Nichia Co., [3]Research Origin for Dressed Photon
*duhaoze@laserlab.ed.kyushu-u.ac.jp

By applying annealing with an electric field applied simultaneously with laser irradiation to Al doped 4H-SiC, polarization modulation is enhanced near the wavelength of the annealing light. The effect was experimentally demonstrated to be wavelength-dependent and rewritable.

1. はじめに

一般的な磁気光学デバイスにおいては，偏光回転に際しての線形性・制御性・非相反性が特徴とされる一方，回転量を増大させるには強い磁場または長い伝搬光路を必要とするため，デバイス全体としての消費電力と光学損失に課題があるとされている．その一方で，Al イオンをドープした 4H-SiC 結晶に対し，レーザー照射と電界印加の併用により内在するドーパント分布を調整することで，高透過率ながら，高い Verdet 定数を実現した偏光回転デバイスの開発が報告されている [1]．また，このデバイスにおいては，偏光回転効果の波長特性が加工時に用いたレーザー光の波長近傍でのみ顕著に増幅することがわかっている [2]．今回，レーザー照射と電界印加の条件を調整することで当該偏光回転効果の波長特性を自在に書き換えることができることを実証したので，その内容について報告する．

2. 実験・結果

今回行った実験では，4H-SiC 結晶(Al イオン注入濃度: 1×10^{20} cm^{-3})に対し，まず波長 532 nm のレーザー照射と 500 mA の定電流印加を 3 時間施した．Verdet 定数は磁場を印加した電磁石に対するクロスニコル系における透過光を測定した結果を元に算出した．その結果，Verdet 定数の波長特性は初期状態(Fig.1(a))から波長 510 nm 近傍で増幅が検出された(Fig.1(b))．続いて，レーザー照射を行わず 500 mA 定電流印加のみを 12 時間施すと，初期状態へ同等の波長特性(Fig.1(c))へと変化した．さらに，波長 457 nm のレーザー照射と 500mA の定電流印加を 0.5 時間施すと，波長 443 nm 近傍にて Verdet 定数の増幅を示した(Fig.1(d)).

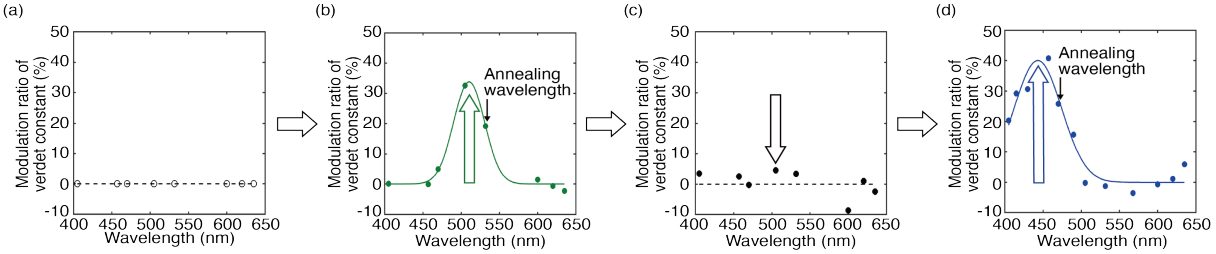

Fig. 1 Reset and rewrite of wavelength dependency of the Verdet constant, (a) the default property, (b) after the 1st processing with irradiation of λ=532 nm laser, (c) after the reset processing, and (d) after the 2nd annealing with irradiation of λ=457 nm laser.

3. 考察

実験の結果，同一のデバイスで，ドーパントドリフトを促すレーザー光の波長に応じて，Verdet 定数の増大が現れる波長帯が変化すること，さらには定電流のみの印加によりそれらの特性が消失することを実証した．この結果は，光電誘起により変動するドーパント分布が制御可能であり，その結果として偏光回転効果の波長特性の書き換えが可能であることを示している．発表では，レーザー光の条件に加えて，電界条件を調整した場合の変化についてより詳細な検証結果を報告する．

本研究は科研費基盤 S (22H04952)，科研費挑戦的研究(萌芽) (25K22229)，光科学技術研究振興財団，JST 次世代研究者挑戦的研究プログラム(JPMJSP2136) の助成を受けたものです．

参考文献

1) T. Kadowaki, et al. : Sci. Rep., **10** (2020) 12967.
2) H. Du, et al. : Opt. Lett., **50**(19) (2025) 6237-6240.

内在電磁場はどのような因果律に従うのか？

What Causal Laws does the Internal Electromagnetic Field Follow?

○ 坂野　斎　(山梨大院)

○Itsuki Banno　(Univ. of Yamanashi)

E-mail: banno@yamanashi.ac.jp

ミクロの世界で「原因の後に結果が現れる」という通常の因果律が有効なのか？[1] を議論したい．この疑問は量子電磁力学の作用積分を最適化する 2 つの方法の比較から生じた：

(a) 始めにマクスウェル方程式を解き電磁ポテンシャルを最適化した後，電子の場を最適化する，

(b) 始めにハイゼンベルグ方程式を解いて電子の場を最適化し，次に電磁ポテンシャルを最適化する．ここで，電子の場の最適化は感受率を求めることに対応する．

(a) の作用積分の最適化の最初の過程で，内在電磁場であるスカラーポテンシャルについて解き消去することで電荷密度間相互作用；クーロン相互作用となる．この電荷密度間相互作用の積分核は 2 箇所の電荷密度間の距離の逆数に比例し，時間遅れなくその影響が伝わり通常の因果律に従わない．同じ段取りで作用積分中の横ベクトルポテンシャル（横 VP）について解いて消去すると，横電流密度間相互作用となり，その積分核は波動方程式の遅延グリーン関数と先進グリーン関数の平均となる．この導出過程では，横 VP の発信側・受信側の電流密度が同じ系内にある（孤立系である）という条件を使っており，内在 VP を扱っていることになる．この結果も通常の因果律に従わない．

(a) についてまとめると，孤立系の作用積分中の内在電磁ポテンシャルをマクスウェル方程式を使って消去して得た電荷密度間相互作用，横電流密度間相互作用において，その積分核は因果律と逆因果律に関して中立な形になる．

一方，(b) の手続きでハイゼンベルグ方程式より感受率（応答関数）を求めるとき，通常，私たちはマクロ世界の日常経験から推認した「通常の因果律」をミクロの世界に適用する．ここにおいて，(a) の電磁場の扱いと (b) の電子の場の扱いに齟齬があるように思われる．この発表では以下の問題点を論じる：

- 非相対論系においての時間発展を記述する際，数学的には通常の因果律，逆因果律，または，それらの混合された因果律は対等であること．
- 因果律に無関係である作用積分と，特定の因果律を考慮したオイラー方程式の解；線形・非線形感受率の関係と整合性．
- 逆に，感受率（構成方程式）から互換な変分原理をつくれるが，その場合，感受率に考慮した特定の因果律の依存性は作用積分に残るのか？
- 内在電磁場に対するミクロな応答を記述する感受率に考慮されるべき相応しい「因果律」は何か？実験から判定することはできるか？

謝辞

大津元一博士が主宰されるドレスト光子研究起点 (RODreP) での研究会のメンバーの方々に感謝いたします. この研究の一部はドレスト光子研究起点からの援助を受けています.

参考文献

[1] 坂野　斎,「逆因果律と内在電磁場」オフシェル科学フォーラム（2024 年 10 月 28 日）https://rodrep.or.jp/img/series/Banno/%E2%85%A6-9%20Banno.pdf

内在ベクトルポテンシャルの非線形非断熱効果とフォトンブリーディングデバイス

Nonlinear and Non-adiabatic Effect of the Internal Vector Potential and Photon-Breeding Devices

○ 坂野　斎　(山梨大院)

○**Itsuki Banno　(Univ. of Yamanashi)**

E-mail: banno@yamanashi.ac.jp

川添，大津らの開発したフォトンブリーディング（PB）[1] は直接遷移型．間接遷移型を問わず半導体から高効率発光デバイス作成を可能にする方法である．発光波長を決めるのはプロセス中の照射光波長であり，従前の物質のバンドギャップ選択ではなく，仕組みの詳細は未解明である．PB で作成されたデバイスは高効率発光だけでなく，巨大磁気光学効果 [2] や強磁性 [3] を発現し，光学フォノンの関与 [4] の実験的証拠がある．現象の強さとフォノンの関与は大きなコヒーレント長の振電系の存在を，磁気的現象は内在ベクトルポテンシャル（内在 VP）の関与を示唆する．

本理論研究は PB で作成されたデバイスの動作原理の探求である．前回 [5]，電子系をバートリーフォック（HF）近似をして，非相対論系に遍在する VP の非線形効果による光学応答の増強の記述を目指したが及ばなかった．今回は，さらに TO 格子振動（TO フォノン）に付随する VP の時間変化；横電場による HF 軌道の変形として非断熱効果：振電相互作用系を記述し，直接遷移型半導体の発光波長の変化，フォノンとの多重相互作用を論じる．

PB デバイスの動作状態は基底状態から遠いと想定され，量子電磁力学の作用積分の変分法による最適化が必要である．物理的近似と親和性の高いハイゼンベルグ描像で以下の段取りを取る：**(1)** 線形・非線形感受率を作用積分の電磁ポテンシャルによる汎関数微分としてハイゼンベルグ演算子の形で求める．これは４元誘導電流密度を結果，ゲージフリーの電磁ポテンシャルを原因とし，電荷保存則，ゲージ不変性を保証する．**(2)** 非断熱効果を内在 VP から導かれる横電場による HF 軌道の変形として考慮する．**(3)** 電磁ポテンシャルと非線形感受率の変換を導入することにより非線形応答の系統的な扱いを可能にし，非相対論系に遍在する電荷密度と VP の２次の結合を (2) の非断熱効果とともに系統的に誘導電流密度に取り込む．**(4)** 無限次まで (3) の非断熱非線形効果を考慮する．その際，電子系の励起・脱励起の演算子の空間に相応しい基底を導入し表現行列を用いる．**(5)** 構成方程式 (上記で構成された誘導電流密度) と整合する変分原理を電磁ポテンシャルの振幅のパラメータ積分によりつくる．**(6)** 相応しい電子状態で期待値をとり，作用積分を最適化し，最適化した電流密度演算子の振動数スペクトル：発光の振動数，格子振動によるサイドバンドを考察する．

謝辞

大津元一博士が主宰されるドレスト光子研究起点 (RODreP) での研究会のメンバーの方々に感謝いたします. この研究の一部はドレスト光子研究起点からの援助を受けています.

参考文献

[1] T. Kawazoe and M. A. Mueed and M. Ohtsu, Appl. Phys. B, **104** p.747–754(2011); M. A. Tran, T. Kawazoe, and M . Ohtsu. Appl. Phys. A, **115** p.105-111(2014); M. Ohtsu, "Silicon Light-Emitting Diodes and Lasers" (Springer International Publishing, Swit- sland, 2016).

[2] N. Tate, T. Kawazoe, W. Nomura, and M. Ohtsu, Scientific Reports **5** p.12762-1-7 (2015); M. Ohtsu,

[3] 門脇 拓也, 川添 忠, 大津 元一, 佐野 雅彦, 向井 孝志.「ドレスト光子による誘導放出を利用した波長 1.3~1.9 μ m 帯の非冷却型 Si 受光素子], 応用物理学会 2021 年春期学術講演会, 17p-Z14-8.

[4] N. Wada, M. A. Tran, T Kawazoe, M. Ohtsu, Appl Phys A**115** p.113-118(2014).

[5] 坂野　斎,「流れが誘導する平衡から遠い量子構造 V」2025 年春季学術講演会，16p-K508-1.

ここ数年で構築されたドレスト光子新理論の振り返り

Overview on the newly developed theory of dressed photon

ドレスト光子研究起点、佐久間弘文
RODreP, Hirofumi Sakuma
E-mail: hsakuma1@gmail.com

ドレスト光子（以下 DP）は、光励起した半導体上で生成される（未解明の）特異な場で、当初は近接場光学の分野でその研究が開始され、20 世紀の末から 21 世紀の初頭において応用研究が大きく進展し、その後、数年前から先端的量子場理論に基づく新たな理論構築の試みが始まり、現在に至っている。本発表は、その新理論の概要と光学分野における意義を簡潔に説明するものである。

物性物理においては、そのBohr半径が10nm程度である「励起子」と呼ばれる電子正孔対が重要な役割を果たすという事実は、例えば、電子正孔対は “物性物理の縮図” と言われる程の多様性を示すという指摘に裏打ちされている。DP の新理論によれば、DP の大きさは量子化されていて、その最大値は、大津 [1] の実験によれば (40 ~ 50)nm 程度である。これは、DP が物性物理において励起子と同様な重要な働きを担う事を示唆しているものである。

新理論の特徴は、これまでの発表で繰り返し説明して来た様に、小嶋のミクロ・マクロ双対理論 (MMD)[2]、公理論的量子場理論の帰結である Greenberg-Robinson 定理、及び宇宙を生み出した “始原の光の場”[3] の共形不変性の破れから導かれる対称空間 [4] の出現という複数の理論を結び付け、物理的時空の創発とそれに伴う、ダークエネルギー場、ダークマター場及び DP 場を総括的に説明するというものである。特に DP 場について一言付け加えると、量子化された DP の最大長は、MMD が取り扱う量子的領域と古典的領域を距離的に分離する Heisenberg cut を与えていると同時に、それは、電磁場と重力場が同時に関与する量子的領域と古典的領域との相互作用に深く関わる事も示される。

DP の重要性という事に関して、本発表の導入部分では「励起子」を例に挙げたが、それは負電荷を持つ電子と hole として正電荷と見做される正孔との「対」としての存在である。DP の新理論では、DP の最大長の逆数で定義される波数 ($\pm\kappa_0$) を用いて導入される (+) timelike 及び (-) spacelike Klein Gordon 方程式

$$[\nabla^\nu\nabla_\nu \pm (\kappa_0)^2]\phi = 0 \qquad (1)$$

で記述さる二つの場の存在が重要になり、その場を基にして二つの時空領域 [+, -] のハミルトニアン (H) 構造が導かれる。

通常の光の場が二つの時空領域の境界に存在する様に、重力相互作用に付随すると想像されているスピン量子数２を持つ “gauge graviton” (gg) に対応する存在も新モデルの中で定義可能である。特に重要な点は、gg は二つの時空領域 [+] と [-] との相互作用に関与できる形で定義されているという事である。この事は、多分に比喩的ではあるが、正負の電荷の “結合体” として定義される「励起子」の構造と類似する特性を持っていると言えよう。物性物理における励起子の重要性については既に触れたが、 量子場理論における二つの時空領域 [+] と [-] との相互作用は、公理論的量子場理論における Greenberg-Robinson (GR) 定理 [2] により正当化されているものであるが、その表現の数学的抽象性の為に、物理の分野では殆ど省みられる事がなったと言える。DP 研究が nanophotonics を超えて、物理学全体に少なからぬ影響を及ぼしたとすれば、それは、GR 定理が示す内容を具体的に “応用物理光学” の分野で示す事ができたという事ではないかと、ここ数年の研究を総括している。

参考文献

[1]H. Sakuma et al. *Symmetry* **2020**, 12(8), 1244.
[2] ここからはじまる量子場、大津元一、小嶋泉（編著）朝倉書店、**2020**。
[3] R. Penrose, *Proceeding of EPAC*, **2006**.
[4] S. Helgason, *Differential Geometry, Lie Groups, and symmetric spaces*, **1978**, Acad. Press,

オンシェル科学の圏化としてのオフシェル科学

Off-shell Sciences as Categorification of On-shell Sciences

○ 西郷 甲矢人 (ZEN 大学)
○Hayato Saigo (ZEN University)
E-mail: h_saigoh@nagahama-i-bio.ac.jp

「圏化」とは、数学において近年用いられる（明確な定義を持たない）用語であるが、簡単に言えば、「集合」について定義されているような諸概念を「圏」（およびその高次の一般化）に拡張することをいう。圏は、対象とよばれるものたちとそれをつなぐ射とよばれるものたちからなるシステムであって、いくつかの公理をみたすものであるが、直感的には「（ある条件をみたす）可能な過程の全体」のようなものと思うとよい。そこでは、対象は「恒等射」という特殊な射（「何もしない射」）と同一視され、射の合成可能性の担い手という重要な役割を果たすものの、主人公の座はむしろ一般の射に譲られる。集合は対象／恒等射のみからなる圏（離散圏）と考えることができるので、圏は集合の一般化であるとといえる。圏化とは、この特殊な圏について定義された概念を一般の圏について意味のあるように拡張しようという営みなのである。

さて、以上は数学の話であるが、実はこの数年間の応用物理学会での講演において取り上げたすべてのことが、一言でいえば「オフシェル科学はオンシェル科学の圏化である」とまとめられるのである。具体的には、[2, 3] に基づき、量子場とその状態を「（部分的な）対合構造をもつ圏上の圏代数とその上の状態」として定義することにより、圏構造としての相対論的構造と非可換確率構造としての量子論的構造を直接に統合できることを示し、代数的量子場理論や位相的量子場理論などの先行するアプローチとの概念的関係についても論じた。またこれらを踏まえてオンシェル・オフシェルの概念を見直し、時空を「（構造づけられた）点集合」としてではなく「圏」—より詳細にいえば「（部分的な）対合構造を持つ因果的圏」[3]—として見直すことが、ドレスト光子研究 [1] に端を発するオフシェル科学にとって核心的であるという見方を提示した。さらに、2025年春の講演においては、この「因果的圏」として物理学的にどのようなものを考えるべきか明らかにした。

本講演においては、これまでのオフシェル科学の基礎に関する研究を「圏化」という観点からまとめあげ、「オフシェル科学とは何か」についてのひとつの回答を与え、今後のオフシェル科学の進展の方向性を展望したい。

参考文献

[1] M. Ohtsu: *Dressed Photons* (Springer, Berlin Heidelberg 2014)

[2] Saigo, H. Category Algebras and States on Categories. *Symmetry* **2021**, *13* 7, 1172. https://doi.org/10.3390/sym13071172

[3] Saigo, H. Quantum Fields as Category Algebras. *Symmetry* **2021**, *13* 9, 1727. https://doi.org/10.3390/sym13091727

ボーアの相補性と量子測定理論

Bohr's complementarity and quantum measurement theory

中部大工 [1]，　○ 岡村 和弥 [1]

Chubu Univ.[1], ○Kauzya Okamura[1]

E-mail: k.okamura.renormalizable@gmail.com

本講演では，ボーアの相補性原理と量子測定理論の相互への貢献について数理的な観点から発表を行う。特に，前回の講演（第 72 回春季学術講演会 16p-K508-4）の時点より明確になった点について詳しく議論する。

ボーアの**相補性原理**（complementarity principle）[1] とは，革新的な「科学的な分析と綜合のあり方」のことであり，分析パートと綜合パートからなる：

分析パート　物理系である量子系に対する実験結果の分析および説明における「制約」を認めなければならない。加えて，現象という言葉の使用を改めなければならない。

綜合パート　分析パートを前提として，量子系とは，異なる実験設定相互の排他関係があっても諸現象の全体が互いに補い合う対象のことである。特に，対象の振る舞いと，その現象の発生で関わる測定装置との相互作用の明確な分離は不可能である。

ボーアは 1920 年代後半に相補性原理を提唱し，アインシュタインとの論争の中で洗練していった経緯があるが，提唱から洗練の過程でもボーアの主張は一貫している。

相補性原理の分析パートと綜合パートがともに数理的表現をもつことを示す。このために必要な概念を，**代数的量子論**の枠組みと，**量子インストルメント**に基づく量子測定理論 [2, 3] が供給する。綜合パートは量子論の公理的アプローチと整合的であり，代数的量子論の概念が数理的表現と対応する。一方の分析パートでは，代数的量子論を前提として，量子インストルメントをもちいて「量子現象」が定義される。

代数的量子論とは，ある $*$-代数（行列の随伴の一般化にあたる対合 $A \mapsto A^*$ をもつ代数）$\mathcal{X}$ の自己共役元を物理量とし，$\mathcal{X}$ 上の期待値汎函数 $\omega : \mathcal{X} \to \mathbb{C}$ として状態を定め，これらに基づいて量子系を記述する体系である。また，量子測定理論の中心概念である量子インストルメントは物理的に実現可能な測定に対応しており，測定装置の出力のなす確率分布および出力に応じた系の状態変化を記述するために用いられる。

科学哲学的な観点からハルボソンとクリフトンにより定義された**存在可能量代数**（beable subalgebra）[4] は，考察する測定状況において値をもつ物理量の集まりに対応する。講演者は存在可能量代数を量子インストルメントを用いる状況に定義を改良し，アインシュタインとボーアの論争での論点を明確にする。

参考文献

[1] 山本 義隆 編,『ニールス・ボーア論文集 1 因果性と相補性』,（岩波書店，1999）.

[2] M. Ozawa, J. Math. Phys. **25** (1984), 79–87.

[3] K. Okamura and M. Ozawa, J. Math. Phys. **57** (2016), 015209.

[4] H. Halvorson and R. Clifton, Int. J. Theor. Phys. **38** (1999), 2441–2484.

正則木上の量子ウォークの波動関数

The wave function of a quantum walk on the regular tree

工学院大学
○ 齋藤正顕
Kogakuin University
○Seiken Saito

ドレスト光子（DP）を説明するモデルとして, 大津–瀬川 [3] によって 3 状態の量子ウォーク (QW) モデル（ドレスト光子の量子ウォークモデル）が提案され, その挙動の数値的あるいは理論的な解析が進められている [4]. 関連する 1 次元 3 状態の量子ウォークモデルの研究として [6] がある. 本研究では, 昨年の発表 [7] に続いて, グラフ上の量子ウォークを扱う. 具体的には, グラフ $G = (V, E)$ の隣接行列を A とするとき, 時間発展行列を $U(t) = e^{itA/2}$ とし, 初期状態を $\Psi(0) \in \mathbf{C}(V)$ とするとき, 時刻 $t \geq 0$ における状態が

$$\Psi(t) = U(t)\Psi(0)$$

によって定められる連続時間量子ウォークについて考察する. このような量子ウォークモデルについての先行研究として, グラフ G が 1 次元格子 $\mathbf{Z}$, サイクルグラフ C_N, 正則木 T_{q+1} の場合については, [2] などがある. 詳しくは,[1], [2], [5], [8] 等を参照のこと. 本研究では, 正則木の時間発展行列の幾何的な量による具体的表示を用いて, 波動関数, 密度行列, 関連する特殊関数の性質等について考察する.

謝辞 この研究の一部はドレスト光子研究起点の支援を受けています.

参考文献

[1] C. Godsil and H. Zhan, Hanmeng Discrete quantum walks on graphs and digraphs, London Math. Soc. Lecture Note Ser., 484 Cambridge University Press, Cambridge, 2023, xii+138 pp.

[2] 今野紀雄, 量子ウォークの数理, 産業図書, 2008.

[3] M. Ohtsu, A Quantum Walk Model for Describing the Energy Transfer of a Dressed Photon, Preprint, 2021, Offshell: 10.14939/2109R.001.v1.

[4] 大津元一, 瀬川悦生, 結城謙太, 量子ウォークモデルによるドレスト光子エネルギー移動のシミュレーション, 2022 年第 83 回応用物理学会秋季学術講演会 (講演番号 22a-A101-6).

[5] R. Portugal, Quantum walks and search algorithms, Quantum Sci. Technol., Springer, New York, 2013, xii+222 pp.

[6] 齋藤正顕, ドレスト光子の量子ウォークモデル: 1 次元の場合, 2022 年第 83 回応用物理学会秋季学術講演会 (講演番号 22a-A101-4).

[7] 齋藤正顕, 正則グラフ上の量子ウォークの波動関数について, 2024 年第 85 回応用物理学会秋季学術講演会 (講演番号 18p-A33-16).

[8] S. E. Venegas-Andraca, Quantum walks: a comprehensive review, Quantum Inf. Process.11(2012), no.5, 1015–1106.

量子ウォークとローテーションによるグラフの辺彩色

Quantum walks and edge coloring of graphs by rotation

横浜国大 [1]，○ 掛川 拓巳 [1], 瀬川 悦生 [1]

Yokohama ntnl. Univ.[1], ○Takumi Kakegawa[1], Etsuo Segawa[1]

E-mail: kakegawa-takumi-bc@ynu.jp

【はじめに】 エネルギーの蓄積効率と量子ウォークの快適度には関連性が見いだされている [1], [2]. 本研究では量子ウォークの快適度と, グラフの辺彩色の問題の関係を探る. グラフの辺彩色問題を考えるにあたり, ローテーションを用いるのが有効である. 特に 3 正則グラフにおいては, 辺の彩色と各頂点周りのローテーションとの間に自然な対応が生じる. そのため今回は, 簡単な 3 正則グラフとして, 同じ大きさのサイクルグラフ C_n を 2 つ用意し, それぞれの対応する頂点を 1 本の辺で結ぶことで得られるグラフ, R_n を考察の対象とする (図 1). さらに, R_n に対して図 1 から図 3 に示すような操作を行い, [3] で与えられている時間発展で考察する.

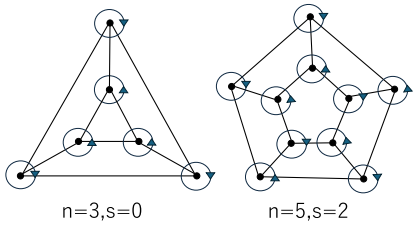

図 1: グラフ R_n

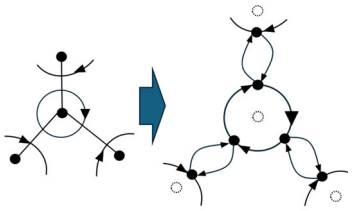

図 2: 頂点の膨張

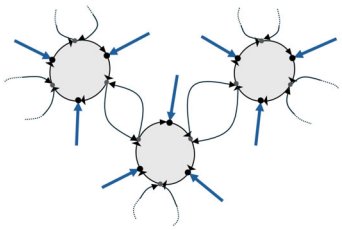

図 3: テールの接続

【主結果】 R_n を球面上に埋め込んだとき, 外周に現れる頂点の周囲における反時計回りのローテーションの総数を s と定義する. このとき, ローテーションとグラフとの彩色に関する以下の命題が導かれる.

命題 1. *R_n が彩色可能であることと, n と s が以下の合同式を満たすことは同値である：$n \equiv 2s \ (mod\ 3)$*

さらに, [3] による一般的な快適度の公式を今回のローテーショングラフの族に当てはめると次の命題のように, (n, s) が決まれば量子ウォークの快適度が埋め込み方によらず一意に定まることが分かった. ここで快適度は定常状態 Ψ_∞ に対し, $\mathcal{E} = \frac{1}{2}\sum_{a\in G}|\Psi_\infty(a)|^2$ とする.

命題 2. *$a > 0, \omega = 1$ を仮定すると, 量子ウォークの快適度の期待値は以下のようになる.*

$$E(\mathcal{E}) = \begin{cases} \frac{2+|b|^2}{6n|b|^2}\left(2(n+s)\frac{1+a^{2(n+s)}}{1-a^{2(n+s)}} + 2(2n-s)\frac{1+a^{2(2n-s)}}{1-a^{2(2n-s)}}\right) - \frac{2a}{3n|b|^2}\left(\frac{sa^{n+s}}{1-a^{n+s}} + \frac{(n-s)a^{2n-s}}{1-a^{2n-s}}\right) & : n \equiv 1, n-s \equiv 1 (mod\ 2) \\ \frac{2+|b|^2}{6n|b|^2}\left(2(n+s)\frac{1+a^{2(n+s)}}{1-a^{2(n+s)}} + 2(2n-s)\frac{1+a^{2n-s}}{1-a^{2n-s}}\right) - \frac{2a}{3n|b|^2}\left(\frac{sa^{n+s}}{1-a^{n+s}}\right) & : n \equiv 1, n-s \equiv 0 (mod\ 2) \\ \frac{2+|b|^2}{6n|b|^2}\left(2(n+s)\frac{1+a^{n+s}}{1-a^{n+s}} + 2(2n-s)\frac{1+a^{2(2n-s)}}{1-a^{2(2n-s)}}\right) - \frac{2a}{3n|b|^2}\left(\frac{(n-s)a^{2n-s}}{1-a^{2n-s}}\right) & : n \equiv 0, n-s \equiv 1 (mod\ 2) \\ \frac{2+|b|^2}{6n|b|^2}\left(2(n+s)\frac{1+a^{n+s}}{1-a^{n+s}} + 2(2n-s)\frac{1+a^{2n-s}}{1-a^{2n-s}}\right) & : n \equiv 0, n-s \equiv 0 (mod\ 2) \end{cases}$$

【今後の展望】 命題 1 と命題 2 を組み合わせて, R_n の彩色可能性と量子ウォークの快適度に関する, より明確な関係性を見出すことが期待できる.

【参考文献】

[1] M. Naruse et al., Nano Communication Networks 2 189–195 (2011).

[2] M. Ohtsu et al., Off -shell archive: 2304O.001.v1 (2023).

[3] Yu. Higuchi and E. Segawa, arXiv:2501.06765 (2025).

膨張グラフ上の量子ウォークと散乱

Scattering of Quantum Walk in Blowup Graph

横国 [1] ○(M1) 飯田佳之 [1], 瀬川悦生 [1]

Yokohama National Univ.[1] ○Yoshiyuki Iida[1], Etsuo Segawa[1]

E-mail: iida-yoshiyuki-fj@ynu.jp

【はじめに】入出力のある量子ウォークとドレスト光子のエネルギー輸送問題との関係が研究されている. ローテーション付きグラフ上の量子ウォークはこの物理現象の数理モデルとしての活用が期待できる. [1, 2] ローテーション付きグラフに対して膨張と呼ぶ変形を施した. 変形後のグラフの頂点に量子コインとして 2×2 のユニタリ行列 C を割り当てることで, 自然にユニタリな時間発展を構成することができる. このグラフに外部からの入出力を与える半無限パス tail を挿入する. グラフ上のある tail から出力を得るために, これ以外の tail から毎時刻 1 の入力を与えることを考える. このときの時刻無限大での出力, その散乱を考察する. また与えられた条件下で出力が大きくなるグラフを構成したい.

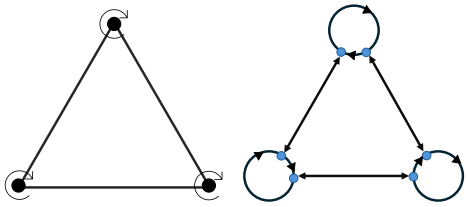

図 1: 膨張変形: 膨張は次のような変形である
頂点 v を v に接続する辺で置き換え新たな頂点とする. 置き換えた頂点同士をローテーションに従って有向辺で接続する. もとのグラフの隣接関係が保たれるように頂点を対称有向辺で結ぶ

【方法】先行研究 [3] によって散乱行列 S の具体的な表示が与えられている. S はローテーション付きグラフの沿側閉歩道に依存する行列であり, 量子ウォーカーは与えられた入力が接続する沿側閉歩道内にしか存在しない. したがってグラフ構造のうち, 沿側閉歩道内の構造について考察する.

【結果】量子ウォークの出力 τ を沿側閉歩道 f, 量子コイン C の関数で表した.

Proposition 1. 沿側閉歩道上で出力 *tail* 以外の *tail* から時刻毎に 1 を入力する. 時刻無限大で出力 τ は, 行列 C の 1,1 成分 a, C の行列式に -1 をかけた ω, f の長さ $|f|$, *tail* の数 k, 沿側閉歩道上での *tail* 同士の距離 *dist* を用いて以下のように表すことができる.

$$\tau = \frac{(1-|a|^2)^2}{|1-a^k\omega^{|f|}|^2}\left|\sum_{l=0}^{k-1} a^l w^{dist\{-(l+1),0\}}\right|^2$$

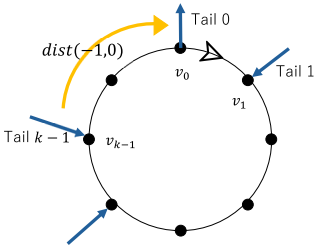

図 2: 沿側閉歩道 f の構造: dist$(-l, 0)$ は v_{k-l} から v_0 の f に沿った距離を表し, dist$(0, 0) = |f|$ と定義する

【考察とまとめ】この表示によって, 量子コイン C と沿側閉歩道 f が出力に与える影響が分かった. 量子コイン C が与えられたとき, 出力を最大にするような f の構造を考える. あるいは C と f の組み合わせによって, 達成可能な出力最大値を考える, といったことができる. 現在 k を固定したときの具体的な例について研究を進めている.

参考文献

[1] M. Naruse et al. Nano communication networks 2. p. 189–195, 2011.

[2] M. Ohtsu et al. *Offshell archive: 2304O.001.v1*, 2013.

[3] Yu. Higuchi and E. Segawa. Quantum walks on graphs embedded in orientable surfaces. *arXiv:2402.00360*, 2024.

ドレスト光子フォノンの移動チャンネル間の相関

Correlation among channels of dressed-photon-phonon transfer

ドレスト光子[1]，横浜国大[2]，Middenii[3]，工学院大[4]，（株）リコー[5]

○大津元一[1]，瀬川悦生[2]，結城謙太[3,4]，齋藤正顕[4]，三宮俊[5]

Res. Origin Dressed Photon[1], Yokohama Ntnl. Univ[2], Middenii[3], Kogakuin Univ.[4], Ricoh Co., Ltd.[5]

°Motoichi Ohtsu[1], Etsuo Segawa[2], Kenta Yuki[3,4], Seiken Saito[4], Suguru Sangu[5]

E-mail: ohtsu@rodrep.or.jp

【まえがき】ドレスト光子フォノン（DPP）が入力端子としての複数の小型ナノ寸法粒子（NP:NP_I）から、その中心の出力端子としての大型 NP（NP_O）へと移動する際（図 1a）、移動経路には明歩道と暗歩道があることをこれ迄に量子ウォーク（QW）モデルにより指摘した[1,2]。今回はその時間変化の動特性から DPP 移動経路チャンネル（Ch）間の相関を評価した。

【方法】上記の明歩道、暗歩道は定常状態の特性を議論するための分類であり、動特性では両者は混在する。これに留意して DPP の移動流量の時間変化を数値計算し（図 1b）、次の値を求めた：(1) 各入力 Ch の DPP 移動流量の間の相関。(2) 各入力 Ch の DPP 移動流量と出力 Ch からの流出流量の間の相関。

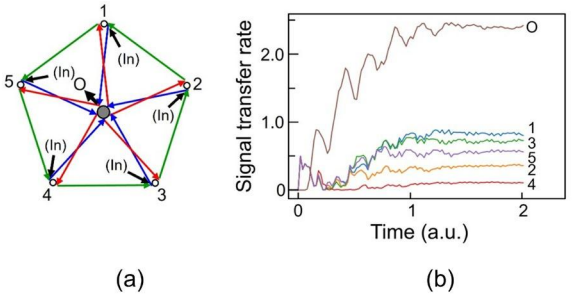

図 1　配置と時間変化の例

【結果】図 2（a）、（b）は各々連結スポーク数 n_{con} が奇数、偶数の場合、入力 Ch I とそれ以外の 4 つの入力 Ch i（=1-5, $\neq I$）の間の相互相関の平均値 C_{Ii} である。この横軸は入出力 Ch 間の距離 d_{io} である。

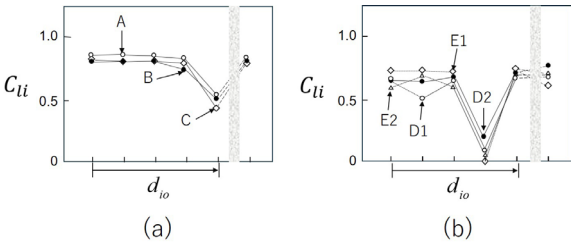

図 2　入力 Ch 間の相関の平均値 C_{Ii}。

（a）n_{con}=5（A）、3（B）、1（C）。（b）n_{con}=4（D）、2（E）。

右端：入出力 Ch 間の相関。d_{io} は入出力間距離。

【考察】出口から遠い入力 Ch は他の入力 Ch との相関が小さい。これは図 2a、b に共通する。図 2b 中の E1、E2 では入力 Ch4 は他の Ch との相関が小さい。これは暗歩道に含まれる入力信号が 4 つに達していることによる。図 2b は暗歩道を含むが、それに含まれる入力 Ch は明歩道に含まれる入力 Ch とも DPP 信号を授受し、相関を生じる。即ちこれらの歩道は混在して動特性を決め、自律性を発揮すると考えられる。

【まとめ】DPP 移動の動特性に関するチャンネル間の相関を解析し、複雑系システムとしての DPP の流れの特性と出力信号値を提示した。

【文献】1) M.Ohtsu, et al, in *Off—shell Archive* Offshell: 2501O.001.v1 (January 2025).

DOI 10.14939/2501O.001.v1

2）大津他,「ドレスト光子フォノンの移動の明歩道と暗歩道」、第 72 回応物講演会（2025 年 3 月）講演番号 16p-K508-5

ドレスト光子高励起状態の時空間ダイナミクスの可視化

Visualization of Spatiotemporal Dynamics of Highly-Excited States of Dressed Photons

(株) リコー[1]　○三宮 俊[1]

Ricoh Co., Ltd.[1]

E-mail: suguru.sangu@jp.ricoh.com

1. はじめに

ドレスト光子を介在した幾つかの興味深い物理現象が報告されている。間接型半導体であるシリコンによる発光素子の作製では，アニール処理を光照射下で行うことによりドーパントであるボロンの自律的な構造形成が実験的に観測されている[1]。この自律性に代表される特異な物理現象では，ドレスト光子の物質系内への閉じ込め機構と外部への散逸機構が重要な役割を担っている。著者らは複数のドレスト光子を物質系内にもつ高励起状態が外部とのエネルギーのやり取りを活性化させる起源ではないかとの予測のもと，散逸過程を顕わに表現し得る方法を探求し，最近は特にドレスト光子の過渡応答特性に注目し解析を進めている。本発表では，ドレスト光子の個数で分類した基底状態[2]について，空間分布の動的挙動を可視化する方法を検討した結果について報告する。

2. ドレスト光子空間分布の可視化

量子密度行列を用いた数値シミュレーションにより，離散ノード間のドレスト光子の過渡応答を算出し，各ノードにおけるドレスト光子個数すなわち生成・消滅演算子の行列積の動的変化を可視化した。計算結果の一例として，Fig. 1 に 6 個のノードを直線的に配置した系におけるドレスト光子個数をカラーマップとして表示した。Fig. 1(a)および(b)はドレスト光子個数の立上りのある瞬間の状態であり，エネルギーの差異により表現した不純物（中央の一対のノード）の位置において 4 つのドレスト光子を有する基底状態が強く励起されている様子を確認できる。Fig. 1(c)は左から 4 つ目のノードにおけるドレスト光子個数の時間発展をグラフ化したものであり，ドレスト光子の個数を変える，すなわち散逸をともなう遷移が幾つかのノードにおいて相関をもって発言していることが推察される。講演では，高励起状態の空間分布と散逸過程の関係性について解析を深め，エネルギー散逸を担う基底状態の顕在化を試みるとともに，不純物の自律的構造形成との因果について言及したい。

参考文献

[1] M. Ohtsu, *Silicon Light-Emitting Diodes and Lasers: Photon Breeding Devices Using Dressed Photons (Nano-Optics and Nanophotonics)* (Springer, 2016).
[2] M. Gross and S. Haroche, Phys. Rep. 93 (1982) 301.

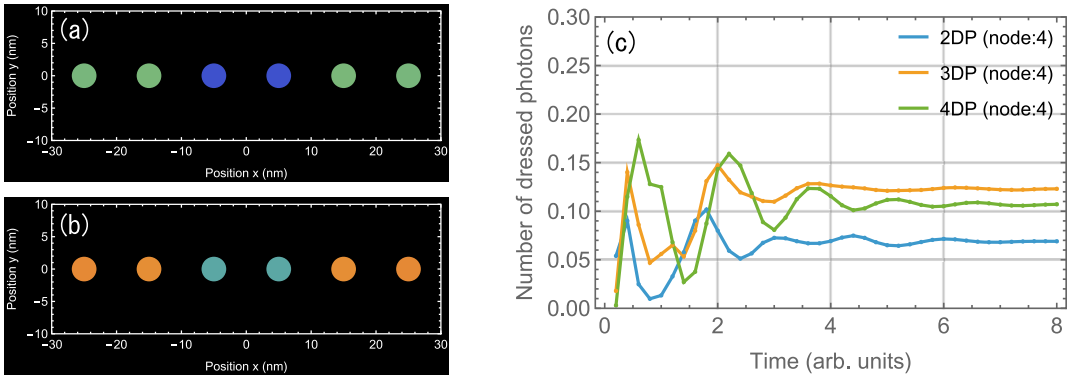

Fig. 1: ドレスト光子個数の空間分布：(a)DP2 個の状態，(b)DP3 個の状態、および時間発展（4 番目のノード）

流れが誘導する平衡から遠い量子構造 V

Current-induced Non-equlibrium Structure V

○ 坂野　斎　(山梨大院)

○Itsuki Banno　(Univ. of Yamanashi)

E-mail: banno@yamanashi.ac.jp

川添，大津らの開発したフォトンブリーディング（PB）[1] は間接遷移型半導体から高効率発光デバイス作成を可能にする方法で，その発光波長を決めるのは物質のバンドギャップではなくプロセス中の照射光波長である；このような発光波長制御方法は従前の物質選択によるものと全く異なり，光学のエポックメイキングである．

PB で作成されたデバイスは間接遷移型半導体からの高効率発光だけでなく，同時に巨大磁気光学効果 [2] や強磁性 [3] を発現する．現象の強さは大きなコヒーレント長の電子系の存在を，また，磁気的現象は内在ベクトルポテンシャル（内在 VP）の関与を示唆する．この考えの下，前回までに内在 VP を原因とする間接遷移型半導体の発光増強，及び，巨大磁気光学効果のトイモデルを提案した [4]．２つのトイモデルは，VP に対する物質の非線型応答を非摂動論的に考慮してマクスウェル方程式を導く変分原理によるもので，達成される状態は内在 VP が存在する流れがある動的状態；基底状態から遠く，摂動論では辿りつけない状態であった．

これらのトイモデル；非線形マクスウェル方程式を導く変分原理は，非相対論系の量子電磁力学の作用積分を以下の処方ののち，簡単化したものである；(1) ４元誘導電流密度を結果，ゲージフリーの電磁ポテンシャルを原因とする線形・非線形感受率を物質の作用の電磁ポテンシャルによる汎関数微分としてハイゼンベルグ演算子の形で求める．この感受率は相反性をもち，電荷保存則を保証し，ゲージ関数を核とする．(2) 非相対論系において電荷密度（４元電流密度の第０成分）と VP の２次が結合することを系統的に考慮するため，電磁ポテンシャルと非線形感受率の変換を導入する．変換後の非線形感受率演算子は簡単な漸化式を満たす．(3) 線形・非線形感受率により，電磁ポテンシャルの汎関数として記述された誘導電流密度を電子系を最適化済みものとして変分原理に取り込むために，電磁ポテンシャルの振幅のパラメータ積分を導入する．(4) 非線形応答のうち，電荷密度と VP の結合を無限次まで考慮する．(5) 相応しい電子状態で期待値をとる．

この発表では，主に (5) の電子状態について議論する．望ましい状態は電子-正孔対が存在する状態で電荷密度演算子に対して再帰的なものである．ハイゼンベルグ表示から相互作用表示に書き直せれば，作用積分の期待値を通常の量子電磁力学の手法で評価できる．

謝辞

大津元一博士が主宰されるドレスト光子研究起点 (RODreP) での研究会のメンバーの方々に感謝いたします. この研究の一部はドレスト光子研究起点からの援助を受けています.

参考文献

[1] T. Kawazoe and M. A. Mueed and M. Ohtsu, Appl. Phys. B, **104** p.747–754(2011); M. A. Tran, T. Kawazoe, and M . Ohtsu. Appl. Phys. A, **115** p.105-111(2014); M. Ohtsu, ”Silicon Light-Emitting Diodes and Lasers” (Springer International Publishing, Swit- sland, 2016).

[2] N. Tate, T. Kawazoe, W. Nomura, and M. Ohtsu, Scientific Reports **5** p.12762-1-7 (2015); M. Ohtsu,

[3] 門脇 拓也, 川添 忠, 大津 元一, 佐野 雅彦, 向井 孝志.「ドレスト光子による誘導放出を利用した波長 1.3~1.9 μ m 帯の非冷却型 Si 受光素子], 応用物理学会 2021 年春期学術講演会, 17p-Z14-8.

[4] 坂野　斎,「流れが誘導する平衡から遠い量子構造 III」2024 年春季学術講演会，24a-11F-1; 坂野　斎,「流れが誘導する平衡から遠い量子構造 IV」2024 年秋季学術講演会，18p-A33-13.

ミクロ・マクロ双対理論と一般相対論を繋げるドレスト光子場について

On the dressed photon field connecting micro-macro duality and general relativity theories

ドレスト光子研究起点、佐久間弘文
RODreP, Hirofumi Sakuma
E-mail: sakuma@rodrep.or.jp

ドレスト光子（DP）研究は、言うまでもなく「光の場」に基づく研究であり、「光の場」は共形不変性（scale free）を持つ故に、DP 研究から思いがけずに宇宙論に繋がる研究が花開いた事はこれまでにも説明を行った。宇宙論は量子物理と古典物理の 2 分野の知見が必須な膨大な未解明分野であり、その理解には、先端的加速器の実験結果に基づき大きく進展した素粒子論の知見と一般相対論の知見が必須となっている。発表者は、DP に関しての大津等の多くの実験結果と、公理論的アプローチに基づく代数的量子場理論である小嶋のミクロ・マクロ双対理論（MMD）[1] を組み合わせると、宇宙論において未だ手つかずに残っている「時空の物理」について興味深い知見（ダークエネルギーやマター等）が得られる事を、これまで段階的に示して来た [2,3] 。何故「時空の物理」かと言えば、それは相対論が示す様に、「光の場」と「時空」は密接に関係しているからである。

本発表は、これまで示して来た複数の知見を、MMD の内部構造と一般相対論の内部構造が持つ共通性を重要な手がかりとして、現在、更に発展している研究の現状を簡単に紹介するものである。研究の大局的方針を確かにする為に、素粒子論に関する複雑な数値スキームは横に置いて、MMD により数学的にも裏打ちされた「量子ー古典対応」という発見的問題手法により得られつつある興味深い知見の核心的部分を簡単に紹介する。

古典物理としての相対論には “光速の壁” が存在する為に、timelike な時空領域のみが対象となるが、Greenberg-Robinson 定理 [1] が示す様に、量子場理論に於いては、（波動の位相速度が）超光速となる spacelike な時空も重要な “物理空間” となる。また、その様な拡張された視点から見た timelike な “物理空間” とは如何なるものかという事は、これまでの一連の研究で明らかにして来た（以下、「新時空モデル」と呼ぶ）。では、「その量子論的構造とは如何なるものか?」が今回のテーマであり、これはもちろん量子重力場と深く関係する先端的テーマである。

昨年、低温物性物理の分野では chiral graviton [4] と呼ばれるスピン 2 の粒子の存在が報告されたが、「新時空モデル」では、まず重力を介在する gauge graviton (GG) と呼ぶべき光速のスピン 2 のボゾン場の存在を容易に示す事ができる。

通常のスピン 1 の光子と異なる点は、プラズマ粒子が磁力線に絡みついて進む様に、GG は測地線を絡む様に進み、その構造は光渦と同じで軌道角運動量を持つ為、スピン角運動量と併せてそのスピンは 2 となっている。また、その様な GG に対して、おそらくヒッグス機構に似たメカニズムにより、亜光速のスピン 2 の粒子が生成され、それがダークマターの様に振る舞う事を示す事ができる。物性物理で示された chiral graviton は、定性的にはこのダークマターに対応する。この様な理論の発展は、DP モデルの更なる深化へと繋がり、DP が介在する磁気光学効果 [5] にも関係すると思われる。

参考文献
[1] ここからはじまる量子場、大津元一、小嶋泉（編著）朝倉書店、**2020**。
[2] H. Sakuma and I. Ojima, *Symmetry* **13**, issue 4, (2021).
[3] H. Sakuma, I. Ojima, H. Saigo and K. Okamura, *Int. J. Mod. Phys. A* **37** No. 22, 2250155 (2022).
[4] J. Liang et al, Nature **628**, 78-83 (2024)
[5] T. Kadowaki, T. Kawazoe & M. Ohtsu, *Scientific Reports* (2020) 10:12967.

過程・因果・非可換確率：圏構造からオフシェル科学へ

Process, Causality and Noncommutative Probability: From Categorical Structures to Off-shell Sciences

○ 西郷 甲矢人 (長浜バイオ大学)

○Hayato Saigo (Nagahama Institute of Bio-Science and Technology)

E-mail: h_saigoh@nagahama-i-bio.ac.jp

これまでの本学会における講演では、[2, 3] に基づき、量子場とその状態を「(部分的な) 対合構造をもつ圏上の圏代数とその上の状態」として定義することにより、圏構造としての相対論的構造と非可換確率構造としての量子論的構造を直接に統合できることを示し、代数的量子場理論や位相的量子場理論などの先行するアプローチとの概念的関係についても論じた。またこれらを踏まえてオンシェル・オフシェルの概念を見直し、時空を「(構造づけられた) 点集合」としてではなく「圏」—より詳細にいえば「(部分的な) 対合構造を持つ因果的圏」[3]—として見直すことが、ドレスト光子研究 [1] に端を発するオフシェル科学にとって核心的であるという見方を提示した。

本講演においては、これまで抽象的に扱われてきたこの「因果的圏」として物理学的にどのようなものを考えるべきか明らかにする。

出発点は系、環境、それらの合成系、その合成系の環境＝「メタ環境」といった基本概念を踏まえて、「可能な過程のなす圏」を考えることである。この圏からは「因果性の圏」が定まる。因果性の圏は、「これがないとき、これがない」という関係性を、「因果的条件」とでもいうべき「媒介」をなす過程の集まりを通して定式化した「因果性」を射とする圏である。一般に圏は、「ダガー圏」とよばれる対合構造を持つ圏の部分圏として考えられ、この「因果性の圏」とそれをつつむダガー圏の対は「因果的圏」となる。このような因果的圏を、オフシェル科学にとっての時空として捉えることを提案したい。

Acknowledgments

本研究は（社）ドレスト光子研究起点の助成を得た。

参考文献

[1] M. Ohtsu: *Dressed Photons* (Springer, Berlin Heidelberg 2014)

[2] Saigo, H. Category Algebras and States on Categories. *Symmetry* **2021**, *13* 7, 1172. https://doi.org/10.3390/sym13071172

[3] Saigo, H. Quantum Fields as Category Algebras. *Symmetry* **2021**, *13* 9, 1727. https://doi.org/10.3390/sym13091727

ボーアの相補性と量子インストルメントについて

On Bohr's complementarity and quantum instrument

中部大工[1], ○岡村 和弥[1]

Chubu Univ.[1], ○Kauzya Okamura[1]

E-mail: k.okamura.renormalizable@gmail.com

実験結果の解析および理解に不可欠な，ボーアの相補性と量子インストルメントについて講演する。量子系に対する実験結果の説明には測定対象と測定装置の間の区別および相互作用が不可欠であり且つ古典物理学の用語で行われなければならないという制約を認め，そして，異なる実験設定相互の排他関係がありながらもそれらがつながる**全体性**（wholeness）を量子系は有しているとする「科学的な分析と綜合のあり方の更新・革新」が，ボーアの**相補性原理**（complementarity principle）である。1920 年代後半に提唱されアインシュタインとの論争の中で洗練されてきた経緯がある [1, 2]。

現在がボーアの時代と大きく異なる点は，**代数的量子論**により概念が洗練され，**量子インストルメント**に基づく量子測定理論が確立していることである [3, 4, 5]。代数的量子論とは，ある $*$-代数（行列の随伴の一般化にあたる対合 $A \mapsto A^*$ をもつ代数）$\mathcal{X}$ の自己共役元を物理量とし，$\mathcal{X}$ 上の期待値汎函数 $\omega : \mathcal{X} \to \mathbb{C}$ として状態を定め，これらに基づいて量子系を記述する体系である。そして，量子インストルメントは物理的に実現可能な測定に対応しており，測定装置の出力のなす確率分布およびそれに従う系の状態変化を記述するために用いられる。厳密には，C^*-L^1 空間の間の完全正値写像に値を取る確率測度を量子インストルメントと呼ぶ。小澤の不等式などの，測定誤差と擾乱の間の不確定性関係の導出は量子インストルメントの理論に基づいている。

本講演では，相補性原理の数学的表現が量子確率論および量子インストルメントによって与えられることを示す。ハルボソンとクリフトンは，考察する状況において値をもつ物理量の集まりに対応する**存在可能量代数**（beable subalgebra）[6] を定めた。彼らはこれを用い考察する状況における古典物理学での用語が通用する範囲を定め，アインシュタイン・ボーア論争でのボーアの返答を再考した [7]。今回，量子インストルメントを用いて存在可能量代数を定め，これにより先行研究よりも整合的な相補性原理の数学的表現が得られることをみる。

参考文献

[1] N. Bohr, Phys. Rev. **48** (1935), 696–702.

[2] N. Bohr, Discussion with Einstein on epistemological problems in atomic physics. In: *The Philosophical Writings of Niels Bohr*, Vol. II, (Ox Bow Press, 1987). [Originally published at *Albert Einstein: Philosopher-Scientist. The Library of Living Philosophers*, Vol. VII, edited by P.A. Schilpp, (Northwestern Univ., Evanston, 1949).]

[3] M. Ozawa, J. Math. Phys. **25** (1984), 79–87.

[4] K. Okamura and M. Ozawa, J. Math. Phys. **57** (2016), 015209.

[5] K. Okamura, Symmetry **13** (2021), 1183.

[6] H. Halvorson and R. Clifton, Int. J. Theor. Phys. **38** (1999), 2441–2484.

[7] H. Halvorson and R. Clifton, Reconsidering Bohr's reply to EPR. In: *Non-locality and Modality*, edited by T. Placek and J. Butterfield, pp. 3–18, (Kluwer, Dordrecht, 2002).

ドレスト光子フォノンの移動の明歩道と暗歩道

Bright and dark walks for dressed-photon-phonon transfer

ドレスト光子 [1]，横浜国大 [2]，Middenii[3]，工学院大 [4]
○大津元一 [1]，瀬川悦生 [2]，結城謙太 [3,4]，齋藤正顕 [4]
Res. Origin Dressed Photon[1], Yokohama Ntnl. Univ[2], Middenii[3], Kogakuin Univ.[4]
°Motoichi Ohtsu[1], Etsuo Segawa[2], Kenta Yuki[3,4], Seiken Saito[4]
E-mail: ohtsu@rodrep.or.jp

【まえがき】ドレスト光子フォノン（DPP）のエネルギーは入力端子としての複数の小型ナノ寸法粒子（NP:NP_I）から、それらの中心に設置された出力端子としての大型 NP（NP_0）へと移動する[1]。この現象に関し、本講演では量子ウォーク（QW）モデルに基づく数値計算により明歩道と暗歩道があることを指摘する。

【方法】QW モデルに沿側閉歩道の概念を導入する[2]。解析モデルとして 5 つの NP_I が配列された五角形の中心に NP_0 を設置する。五角形の全スポークが連結された場合（図 1(a)）、いくつかのスポークが切断された場合（図 1(b)）を考える。各 NP_I に入力信号を注入し DPP エネルギーが五角形外周の経路とスポークを移動して NP_0 に達し、エネルギー散逸・放出の結果生成する出力の信号強度を数値計算で求める。

【結果】スポーク切断後に残る連結スポーク数 n_{con} と出力信号強度との関係を図 1(c) に示す。この関係の特性は次の二要件によって決まる。(1) n_{con} が奇数（=1, 3）の場合、全スポークが連結される場合（n_{con} =5）と等しい出力信号を生ずる。これらは三重縮退した明歩道である。(2) n_{con} が偶数（=2, 4）の場合、エネルギー移動経路は明歩道と暗歩道とに分かれる。明歩道に注入された入力信号は出力端子に到達し出力信号を生ずる。しかしそれに寄与する入力信号の数は n_{con} =5 の場合に比べ少ないので、出力信号は減少する。一方、暗歩道に注入された入力信号はその中に閉じ込められ出力信号を生じない。両歩道は分子中の電子エネルギーの明状態、暗状態に相当する。上記の特性は多角形の角数には依らず、n_{con} のみに依存する。

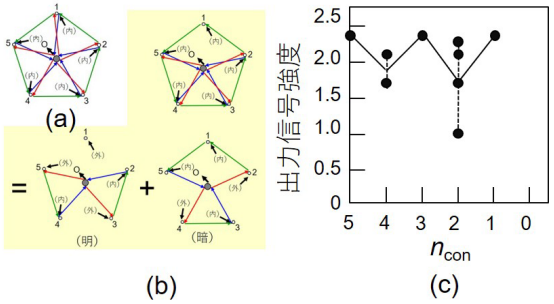

図 1 連結スポーク数 n_{con} と出力値との関係。(a) 全スポークが連結。(b) スポーク 1 が切断。明歩道と暗歩道。(c) 数値計算結果。

【まとめ】 DPP エネルギー移動は連結スポーク数に依存し、明歩道のみを取る場合、及び明歩道と暗歩道からなる場合があることを見出した。前者は縮退し、スポークのいくつかが切断していても出力信号は減少しない。後者では一部が暗歩道に閉じ込められる。これらは実験結果、予備的解析結果と整合した。

【文献】[1] Naruse, et al, *Nano Commun. Networks* **2**, (2011) pp.189-195.
[2] M. Ohtsu, et al., *Off-shell Archive* (July,2024) Offshell: 2407O.001.v1. **DOI** 10.14939/2407O.001.v1
https://rodrep.or.jp/en/off-shell/original_2407O.001.v1.html

エネルギー離調によるドレスト光子の停留および散逸制御

Retention and Dissipation Control of Dressed Photons by Energy Detuning

(株) リコー　○三宮 俊

Ricoh Co., Ltd., ○Suguru Sangu

E-mail: suguru.sangu@jp.ricoh.com

1. はじめに

ドレスト光子のエネルギー移動の特性理解および制御について、これまで量子密度行列を用いた数値シミュレーションによる検討を進めてきた。本シミュレーションは、ドレスト光子を(格子振動まで含めた)物質系と光子場が混成した離散ノードの束縛状態と見なすことで、局在性や弾性的なエネルギー移動といったドレスト光子の特徴を定性的によく説明している。前回の応用物理学会では、空間的に自由に配置した複数ノードにおけるドレスト光子の集団励起状態を調べ、複数ノードの凝集にともない特定の高励起状態が選択的に励起されることを確認した一方で、系外へのエネルギー取出しに高励起状態を援用できるかといった問いには解を得ていない[1]。

上述内容を受け、本研究では物質系内のドレスト光子の状態を制御し、効率的に外部へエネルギーを取り出す(散逸させる)機構を導き出すことを目的とし、そのためにエネルギー散逸機構としてエネルギー移動に選択制をもたせる意味でノード対を配置し、ノード対のエネルギー離調がもたらす効果について数値解析を行った。なお、エネルギー離調に注目した背景には、少数ノードの空間対称性を起源とするドレスト光子の機能動作の先行知見がある[2]。

2. 数値シミュレーション例

Fig. 1 に、本稿に例示する数値シミュレーションモデルを示す。4 個の対称配置されたノード(二準位系)と、その中央に配置したノード対(出力)による構成を考え、ノード対のエネルギーを正負に調整し、数値シミュレーションを実施した。Fig. 2(a)および(b)は、各ノードにおけるドレスト光子占有の有無を基底状態とした占有確率であり、それぞれ離調量 0 と 1(隣接ノード間結合強さに対する相対値)の場合を示している。図中の数値列(「;」はノード対とその他ノードの分離記号)は基底状態の一部を示し、適切な正離調が出力ノード対へのエネルギー流入を抑制する様子を確認できる。

発表では、ドレスト光子の高励起状態を絡めたエネルギー散逸経路や散逸効率への影響についての議論を行う予定である。

参考文献

[1] 三宮，2024 年第 85 回応用物理学会秋季学術講演会 講演予稿集(2024) 18p-A33-19.

[2] M. Ohtsu (Ed.), Progress in Nano-Electro-Optics V (Springer-Verlag Berlin Heidelberg, 2006) 1-62.

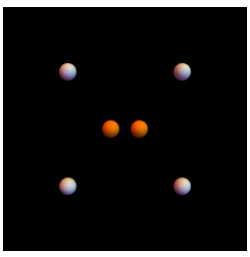

Fig. 1: 数値シミュレーションモデル

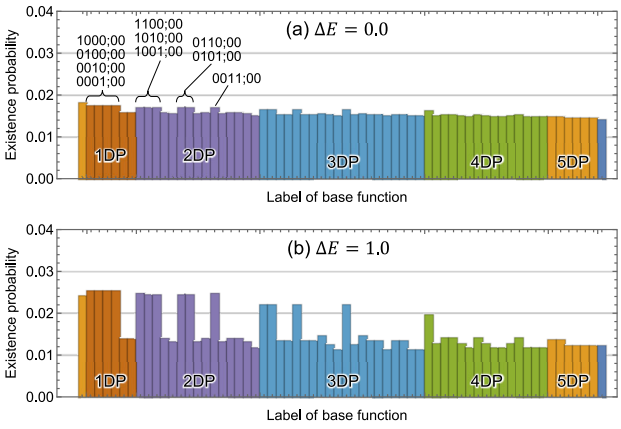

Fig. 2: 基底状態の占有確率; (a)離調ゼロ, (b)正離調

シンポジウム

ドレスト光子の自律的移動とその原理

Autonomous transfer of dressed photons and its principle

○大津　元一（(一社)ドレスト光子研究起点）

Motoichi Ohtsu (Reserach Origin for Dressed Photon)

1.　はじめに

ナノ寸法粒子(NP)や原子に局在するドレスト光子（DP）の生成機構が最近の理論研究により明らかになり,宇宙論との繋がりなどへと大きく発展している [1]. 今後の問題は DP が局在フォノンと結合して生成されるドレスト光子フォノン（DDP）のエネルギー移動, 特にその自律性の機構を明らかにすることであり, その理論的手法として量子ウォーク（QW）が使われている. これが使用可能である根拠は非可換性, サイトと位置の同等性である. 最近では QW モデルに基づき多様な数値計算が行われ実験結果と合致する結果が得られている [2].

2.　DPP のエネルギー移動の自律性

[1]　自律性を顕著に発現する実験の代表例は DPP による光エネルギー伝送・出力取り出しである [3]. 図 1(a)において出力端子用の大型 NP(NP_L)から巨視系に放出される光のパワーPは図 1(b)に示すように DPP エネルギー伝送用の小型 NP(NP_S)の三次元配列の厚さ H とともに増加する. DPP の移動経路全体での NP の光吸収に起因する散逸は H とともに増加するので, この単調増加は従来の巨視系の光学現象（オンシェル科学）とは相反する.

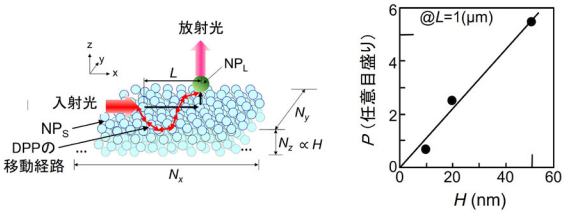

(a)　(b)

図 1 (a) 実験の配置(CdSe の NP を使用). (b) 厚さ H と放射光パワーPとの関係.

ここでは散逸を取り入れた QW モデル [4]を参照してこの実験結果を解析する. このモデルは B 原子対を含む Si 結晶中での DPP の局在確率に関するものであるが, 散逸係数 κ と局在確率は各々図 1(b)中 H と P に対応する. 解析の結果図 2 に示す特性が明らかになった: H が小さい場合（H_I）, 移動経路の選択自由度が少なく, また後述の最適経路も存在しないので P は小さい値を取る. H が増加し最適値 H_{opt} に達すると最適経路が実現し DPP はこの経路を選択して移動し P を最大（P_{max}）にする. $H>H_{opt}$ の場合（H_{II}）にはこの最適経路が必ず存在するので DPP は大きな選択自由度の中からこの経路を選んで移動し P を最大（P_{max}）にする. すなわち巨視系に放出される光パワーが最大になるよう, DPP はミクロ系の内部で最適経路を自律的に選んで移動するのである. この上記のように最適経路が自律的に選ばれることは DPP がオンシェル科学における最小作用の原理に従わないことを意味する.

なお、$H>H_{opt}$ の場合にも最適経路が選ばれることはナノ寸法光デバイスのための三次元構造の厚さ H を H_{opt} 以上にする必要がないことを示唆する.

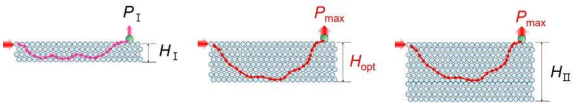

図 2　図 1(a)の断面, 及び H による P の変化の説明. 中図,右図の赤矢印のつながりが最適経路. $H_I<H_{opt}<H_{II}$.　$P_I<P_{max}$.

H に最適値 H_{opt} があること, そのとき P が最大値 P_{max} を取ることは平衡系から非平衡定常状態のへの脱離（散逸を介したミクロ系から巨視系へのエネルギー放出）が平均エントロピー生成極大の原理に従うことに他ならない [5]. 図 1(b)は 1988 年に理論的に見出されたこの原理に対応する実験結果を初めて見出したことを意味する. なお, 生成された平均エントロピーが極大となるのは図 1(a)中の小型 NP の寸法, 位置, 構造が揺らぐことに起因する [5].

[2]　自律性は DPP を用いた光電エネルギー変換でも発現する. すなわち図 1 と同様の NP が分散されたフィルムにより紫外の入射光が可視の放射光に変換されるので（図 3(a)）, これを太陽電池表面に設置すると光電変換効率 η が 25%増加する（$\eta \rightarrow \eta$ +25%: 図 3(b)の A）[6].

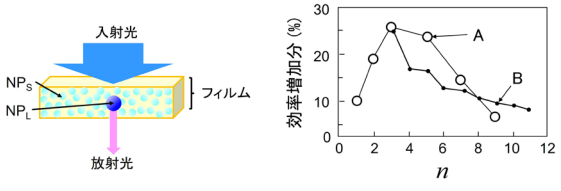

(a)　(b)

図 3(a) フィルムの構成. (b) 小型 NP の数 n と光電変換効率の増加分の関係. A, B は実験結果, 計算結果.

この増加は一つの大型 NP(NP_L)を取り囲む小型 NP(NP_S)の数 n が約 2-6 の場合に顕著であり, この特性は QW モデルにより再現されている（図

3(b)の B）[7].

ここでは n の値が小さいので沿側閉路を用いることにより各 NP における DPP の存在確率の時間的変化を詳しく計算することができる. n=5 の場合の結果を図 4 に示すが, NP_S の配置が回転対称性を有するにもかかわらず(図 4(a)), DPP の存在確率は沿側閉路上での NP_L までの距離が短い NP_S においてより大きな値をとることがわかる（図 4(b): 存在確率の大きさはサイト 1,3,5,2,4 の順）. このような存在確率値の非対称性は上記[1]に指摘したように NP_S の寸法, 位置, 構造が揺らいだ場合（すなわち配置の対称性が破れた場合）に DPP の自律的移動が発現する可能性を示唆している.

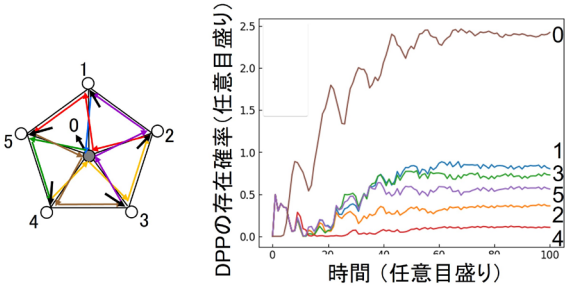

図 4 (a) n=5 の場合の QW モデル. 色付き矢印は沿側閉路の各要素. 黒矢印は入力と出力. (b) 各サイトでの DPP の存在確率.

NP_S の構造の揺らぎの例は図 4(a)の中で NP_S から NP_L への移動経路の欠落である(図 5). その予備的考察のために量子マスター方程式を用いて各 NP の中に生成される励起子の確率密度（ただしこれは DPP の確率密度ではない）が計算された[8]. その結果, 欠落数が 0 の場合（図 4(a)）よりも適度に欠落がある場合の方が, 出力サイトにおける励起子確率密度は 60%程度増加することが指摘された.

この増加は前節[1]に記したように巨視系に放出される光（出力信号）のパワーが最大になるよう, DPP はそのエネルギー移動経路を自律的に選ぶことに起因する. すなわちミクロ系の DPP はエネルギー移動の経路を自律的に設定することにより巨視系において観測されやすくなるよう振る舞うことを実証している. 現在, この予備的考察の結果の妥当性を検証し, より精度の高い評価を行うための数値計算が進んでいる.

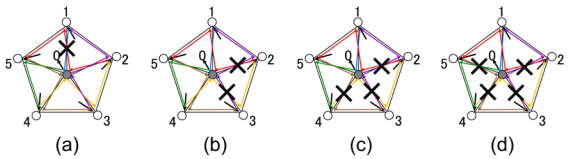

図 5 入力-出力間に欠落がある場合の沿側経路. n=5 の場合. 欠落数は各々1 (a), 2(b), 3(c), 4(d).

3. まとめと今後

ここではミクロ系内の DPP は巨視系に放出される光パワーを最大とする最適経路を自律的に選ぶことを示した. この自律性は小型 NP の温度の差異, 質的差異（これはミクロ的ゆらぎの運動・その環境との相互作用に連携）が平均エントロピー生成極大をもたらすこと, そして外部の巨視系への高次活動性を発現することに起因する[5]. この高次活動性はミクロ系から巨視系への「最高ギフト」と表現することができる. なお, 瀬川等は QW の理論の見地から自律性に関する基礎概念を提示している[9].

自律性を示す DPP 関連の現象のさらなる例として次を列挙する.

(a) 光ナノファウンテンデバイス[10]: 前節[2]を応用したナノ集光器. 紅色光合成細菌のアンテナ系における励起エネルギー伝達機構[11]に類似.

(b) Si 発光デバイス: B 原子対の空間分布が DPP により自律的に最適化された Si 結晶を使用. このデバイスは光子ブリーディング(PB)現象（デバイス製作用の照射光による発生光自己複製現象）を発現する. これは QW モデルにより記述されている[2,12]. この PB 現象は DNA の二重らせんの自己複製機能と類似.

(c) 物質表面の平坦化技術[13]: DPP を用いたドライエッチングを応用. 岩石の風化現象と類似.

以上に指摘した多数の類似性に注目すれば, DPP のエネルギー移動とその自律性の解析は多様な自然現象の起源の見極めに寄与すると期待される.

参考文献

1) H. Sakuma, et al., *JEOS-RP* **17** (2021) 28.
2) M. Ohtsu, et al., *Off-shell Archive* (January, 2023) Offshell: 2301O.001.v1.
3) W. Nomura, et al., *Appl. Phys. B*, **100** (2010) 181.
4) M. Ohtsu, et al., *Off-shell Archive* (April, 2023) Offshell: 2304O.001.v1.
5) 小嶋 泉, 物性研究, **51** (1988) 50.
6) M. Naruse, et al., Phys. Rev. B **80** (2009) 125325.
7) M. Ohtsu, et al., *Off-shell Archive* (July, 2024) Offshell: 2407O.001.v1.
8) M. Naruse, et al., Nano Commun. Networks **2** (2011) 189.
9) 瀬川悦生他, 第 85 回応物学会秋季講演会予稿 (2024) 新潟 18p-A33-18.
10) T. Kawazoe, et al., Appl. Phys Lett., **86** (2005) 103102.
11) 垣谷俊昭・三室 守編: 電子と生命 (共立出版, 2000) p.35.
12) M. Ohtsu, et al., *Off-shell Archive* (July, 2024) Offshell: 2311O.001.v1.
13) T. Yatsui, et al., Appl. Phys. **B93** (2008) 55.

シンポジウム

ドレスト光子の量子ウォークシミュレーションによる自律的移動経路とネットワークの幾何的構造の関係

Relation between autonomous paths of dressed photon and geometric structures of networks induced dressed quantum walk simulation

○瀬川　悦生，大津　元一[1] (横浜国立大学，[1]ドレスト光子研究起点)

Etsuo Segawa, Motoichi Ohtsu [1] (Yokohama Nat. Univ., [1] Research Origin for Dressed Photon)

1.　はじめに

ドレスト光子が自律的にある経路を選択している様子がうかがえる顕著な実験例として, 参考文献 1), 2)が挙げられる. この仕組みを理解するために, ドレスト光子の粗視化モデルとして, 量子ウォークが導入され, 実験結果との整合性が様々な数値計算で確認されている(例えば参考文献 3)). そこで本研究は, このドレスト光子シミュレーター―としての量子ウォークの数理的構造を通じて, ドレスト光子の不思議な挙動, 特に自律的経路の選択について, 考察をする.

2.　量子ウォークモデルの説明

与えられたネットワークは連結な有向グラフ G=(V, A)で, 全ての頂点の入次数と出次数が 2 であるとする. この設定は一見すると, かなり限られたネットワークのクラスに限定されたものに見えるが, 実は, 与えられた任意の連結無向グラフの各頂点をあるローテーションにしたがった有向サイクルに置き換えた膨張グラフを考えることによって, この条件が満たされつつ, オリジナルの隣接関係も保存されたものとして構成できることが知られている.

それぞれの有向辺に対して, 赤と青のどちらか 2 色で塗り分けて, どの頂点に対しても, それを終点に持つ 2 つの有向辺の色も, 始点に持つ 2 つの有向辺の色も, 必ず 1 色ずつになるようにとる. (つまり, 同じ色で塗られた有向辺が同時に入ってこないし, また出ていかない.) 赤く塗られた有向辺の集合を A_1, 青く塗られたものを A_2 とする. すると A_1, A_2 は閉路の族になっている. そして全ての頂点に自己ループをつけ, その集合を A_O とおく. これは, ドレスト光子の各頂点で 2 種類の局所的な赤と青のルートへの跳躍と, フォノンによるその跳躍の抑止を表現している. そして, 各頂点に 3 次元のユニタリ行列

$$C=\begin{bmatrix} h_{11} & h_{1O} & h_{12} \\ h_{O1} & h_{OO} & h_{O2} \\ h_{21} & h_{2O} & h_{23} \end{bmatrix}$$

を割り当てると, 2 種類の跳躍を持つドレスト光子とその跳躍を抑止するフォノンの相互作用を反映するダイナミクスが記述されることになる. ここで, h_{ij} はドレスト光子が現在いる A_j の有向辺から次のステップで A_i のルートに乗り換えるときに付随する複素の重みを与えている.

3.　大域的挙動の解析結果

定常状態を得るために, 入出力を与える頂点を定め, そこから常に一定値のドレスト光子が流入している状況を考える. このダイナミクスの定常状態への収束は保証されているため, その定常状態について考察する.

解析を簡単にするため, 現在考えている全空間である有向辺でその標準基底が記述される一様有界関数の集合$\ell^\infty(A_1 \vee A_2 \vee A_0)$上の時間発展作用素を$\ell^\infty(A_1 \vee A_2)$上の時間発展作用素に縮約ができる. より具体的には, 次のようになる.

Lemma $\ell^\infty(A_1 \vee A_2 \vee A_0)$上の量子ウォークの定常状態は次のような$\ell^\infty(A_1 \vee A_2)$上の量子ウォークの量子コインで時間発展する定常状態によって再現される.

$$\tilde{C}=\begin{bmatrix} \tilde{h}_{11} & \tilde{h}_{12} \\ \tilde{h}_{21} & \tilde{h}_{22} \end{bmatrix}$$

ここで

$$\tilde{h}_{ij}=\frac{1}{1-h_{OO}}\left(h_{ij}-(-1)^{i+j}Det(C)\bar{h}_{\neg i,\neg j}\right)$$

この Lemma と文献 4)の結果から以下の結果を得る.

Theorem (量子ウォーク粗視化モデルに基づくドレスト光子の大域的挙動)

(1) 条件 $\boldsymbol{h_{12}=-Det(C)\bar{h}_{21}}$ を満たすとき, 入力箇所を適切に選べば, ドレスト光子は定常状態で同じ色の有向辺で塗られた経路を選択し, 条件 $\boldsymbol{h_{11}=Det(C)\bar{h}_{22}}$ を満たせば, ドレスト光子は定常状態で交互に二つの色の有向辺を渡り歩く経路を選択する.

(2) $\boldsymbol{(h_{22}-Det(C)\bar{h}_{11})/(1-h_{OO})^{-1}\in\mathbb{R}}$ のとき, ドレスト光子は定常状態で, 膨張グラフにおいて, ローテーションに従った閉曲面埋め込みの各面の境界に沿った経路を選択する.

参考文献

1) W. Nomura, et al., Appl. Phys. B, 100 (2010) 181..
2) M. Naruse, et al., Phys. Rev. B 80 (2009) 125325.. **40** (2012) 100.
3) M. Ohtsu, et al., Off-shell Archive (January, 2023)Offshell: 2301O.001.v1..
4) Yu. Higuchi, E. Segawa, arXiv:2402.00360.

シンポジウム

幾何学的構造によるドレスト光子励起状態の制御

Control of dressed-photon excited states by geometrical structures

○三宮　俊 (リコー)

Suguru Sangu (Ricoh Co., Ltd.)

1.　はじめに

ドレスト光子の介在に起因した数々の興味深い物理現象が確認されている. 例えば, 間接半型半導体であるシリコンの発光現象 [1]やナノ粒子集合体における長距離エネルギー移動 [2]などが報告されている. これらは, ドレスト光子の局在性や高速な (量子性を有した) エネルギー移動がもたらす効果であり，自律的な構造形成に寄与し，不均一なナノ粒子の空間位置に対する最適経路を自律的に探索する．いずれの場合においても，物質系の幾何学的な構造が背後にあると推察される.

近年，著者らは上述の物理現象の解釈としてドレスト光子の高励起状態すなわち多体効果に注目し，数値シミュレーションを基に基本原理の解明を進めている [3]. 何故なら, 自由光子の放出を熱浴への散逸と捉えた場合に，物質系内のドレスト光子個数の少ない低励起状態とドレスト光子個数の多い高励起状態とで状態の数が異なり, また, 遠方から見た基底状態の空間対称性が異なるため，ドレスト光子を自由光子へ取り出すモードの切り替えスイッチとして働くのではないか, と考えるためである．さらに, 欠陥構造近傍に局在するドレスト光子が高輝度発光のようなドラスティックな外部影響を引き起こすために，多体効果の介在は一つの解となり得ると考えるためである.

本講演では，数値シミュレーションモデルとしてドレスト光子を束縛する，複数ノードにより構成される系を考え，それらの幾何学的構造（配置）により, 前述したドレスト光子の高励起状態を制御できる可能性について考察を行う.

2.　数値シミュレーションの概略

ドレスト光子の振る舞いを，量子密度行列を用いて記述する．計算手法の詳細は既出版の文献に譲り [4], ここではその概略だけを述べる．ドレスト光子の運動方程式は量子密度行列$\hat{\rho}(t)$を用いて次式のように表すことができる.

$$\frac{d\hat{\rho}(t)}{dt} \approx -\frac{i}{\hbar}\left[\hat{H}_0 + \hat{H}_{\mathrm{int}} + \hat{H}_{\mathrm{exc}}, \hat{\rho}(t)\right] + \mathcal{L}^{(nr)}\,\hat{\rho}(t) + \mathcal{L}^{(r)}\,\hat{\rho}(t) \qquad (1)$$

$\hat{H}_0, \hat{H}_{\mathrm{exc}}$はそれぞれ，非摂動ハミルトニアンおよび外部励起を表わすハミルトニアンである．相互作用ハミルトニアン$\hat{H}_{\mathrm{int}}$はドレスト光子のノード間ホッピング移動であり次式にて与える.

$$\hat{H}_{\mathrm{int}} = \sum_{i\neq j} \hbar V\left(|\boldsymbol{r}_i - \boldsymbol{r}_j|\right)\left(\hat{a}_i^{\dagger}\hat{a}_j + \hat{a}_i\hat{a}_j^{\dagger}\right) \qquad (2)$$

i, jはノードのインデックスであり，相互作用の強さ$V(r)$には距離依存の関数として湯川関数を用いる．ノードの幾何学的配置は各ノードの重心座標から算出した$V(r)$の差異によって与えられる．(1)式の第一項の交換関係で与えられる項は Liouville 方程式と呼ばれる散逸のない場合の運動方程式に対応している．第二項および第三項はそれぞれ，非輻射および輻射をともなう散逸を表わす項であり，外部の熱浴との結合を一次近似で記述した Lindblad 型の演算子を$\mathcal{L}^{(nr,r)}$として表わしている [5]. ここで, 一次近似とは外部放出されるエネルギーについて逆流のない状況を意味している.

(1)式の微分方程式を解くには，量子密度行列の要素となるドレスト光子の取り得るエネルギー状態，すなわちノードを占有し得る全状態を書き出し，左右から作用させ期待値の連立微分方程式を得る. そして, 数値微分により十分に時間経過した後の準定常解または過渡応答を算出する. 次節で示す結果では, 準定常解のみ考察するが，発表時には過渡応答特性についても必要に応じて取り上げたい.

3.　幾何学的構造とドレスト光子励起状態

ノードの幾何学的配置を変化させる意図には次のようなものがある．(1)欠陥構造を作りドレスト光子を局在させる，(2)遠方から見た物質系の対称性(非対称性)を変化させ禁制・許容遷移を制御する，(3)物質系内の状態間遷移(緩和過程)を制御する.

図 1 は，ライン上に配列した 6 個のノードによる準定常状態の計算結果であり，量子密度行列の対角要素すなわち各エネルギー状態の占有確率をプロットしている．図中右上の挿入図はノード配置の概念モデルであり，(a)等間隔配置と(b)右端のノード間距離を狭めた配置についての計算結果を示している．赤字の数値は量子密度秒列の基底状態であり，数値 1 がドレスト光子の占有するノード位置に対応する．図 1(a)と(b)の比較から，欠陥構造に起因してドレスト光子二個を含む状態(2DP)の占有確率が高くなる様子が伺え, また僅かにではあるが, 3DP, 4DP の一部状態についても占有確率の増加が確認できる.

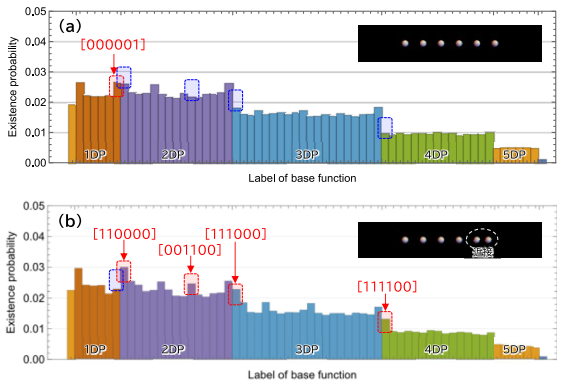

図 1 欠陥導入による占有確率の変化

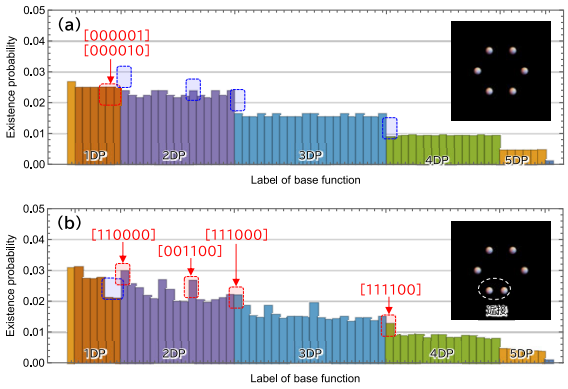

図 2 円周上ノードにおける占有確率の変化

図 2 は同様の計算を，円周上に配置したノードについて行った結果である．ここで，ノード間距離および欠陥部分のノード間距離はライン配置の場合と揃えている．図中の赤字で示すラベルは左端のノードから反時計回りで位置を付与した基底状態を表わしている．ライン配置と円周上ノード配置の場合とでおおよそ同等の傾向が見られる．細かな部分を確認すると，ライン上配置の場合に比べ円周上配置の場合では，真空状態(0DP)の確率が高くなり，物質系内にドレスト光子を停留し難い構造（対称性）であることがわかる．また，物質系内にドレスト光子を蓄えることができないために，遠方への自由光子の放出も効率が低くなる．

4. まとめ

以上の数値シミュレーション結果から，ノードの幾何学的構造の設定により，ドレスト光子の局在の強さが制御可能であること，欠陥位置やノード全体の配置に依存して外部への自由光子の取出し効率，換言するとドレスト光子と自由効率の変換効率を制御可能であることが示唆される．ただし，現時点で十分な最適化が為されてはおらず，ドラスティックな変化を誘発するには至っていない

物質系内の緩和過程の制御に関しては，超放射現象に見られるような集団運動における空間対称性に依存した外部への自由光子放出効果の表出を期待しているが，計算負荷によるノード数の制限もあり，そのような現象を顕わに確認するには至っていない．

ドレスト光子介在現象の将来応用に向けて，自由光子の取出し効率を高める最適構造の同定や設計に関わる知見を得るために，幾つかのモデル化や粗視化を検討中である．見通しが立てば本講演にて上記結果の進展と合わせて議論したい．

参考文献

1) M. Ohtsu, *Silicon Light-Emitting Diodes and Lasers: Photon Breeding Devices using Dressed Photons* (Springer, 2016).
2) M. Ohtsu, Off-shell Archive (2019) Offshell: 1906R.001.v1.
3) 三宮, 第 85 回応物学会秋季講演会予稿 (2024) 18p-A33-19.
4) S. Sangu, et al., Symmetry 13 (2021) 1768.
5) H. J. Carmichael, *Statistical Methods in Quantum Optics 1* (Springer: Berlin/Heidelberg, Germany, 1999).